

**UNCLASSIFIED**

---

**AD 296 984**

*Reproduced  
by the*

**ARMED SERVICES TECHNICAL INFORMATION AGENCY  
ARLINGTON HALL STATION  
ARLINGTON 12, VIRGINIA**



---

**UNCLASSIFIED**

NOTICE: When government or other drawings, specifications or other data are used for any purpose other than in connection with a definitely related government procurement operation, the U. S. Government thereby incurs no responsibility, nor any obligation whatsoever; and the fact that the Government may have formulated, furnished, or in any way supplied the said drawings, specifications, or other data is not to be regarded by implication or otherwise as in any manner licensing the holder or any other person or corporation, or conveying any rights or permission to manufacture, use or sell any patented invention that may in any way be related thereto.

63-2-4

**RESEARCH ON SOUND PROPAGATION  
IN SOUND-ABSORBENT DUCTS  
WITH SUPERIMPOSED AIR STREAMS**

**VOLUME III**

TECHNICAL DOCUMENTARY REPORT NO. AMRL-TDR-62-140 (III)

December 1962

Biomedical Laboratory  
6570th Aerospace Medical Research Laboratories  
Aerospace Medical Division  
Air Force Systems Command  
Wright-Patterson Air Force Base, Ohio

Contract Monitor: William C. Elrod, Captain, USAF  
Project No. 7231, Task No. 723104

[Prepared under Contract No. AF 61(052)-112  
by  
F. Mechel  
P. Mertens  
W. Schilz  
III. Physikalisches Institut der Universität Göttingen  
Göttingen, Germany]

29 0084

ASTIA  
AS  
AD 100

296 984

## NOTICES

When US Government drawings, specifications, or other data are used for any purpose other than a definitely related government procurement operation, the government thereby incurs no responsibility nor any obligation whatsoever; and the fact that the government may have formulated, furnished, or in any way supplied the said drawings, specifications, or other data is not to be regarded by implication or otherwise, as in any manner licensing the holder or any other person or corporation, or conveying any rights or permission to manufacture, use, or sell any patented invention that may in any way be related thereto.

Qualified requesters may obtain copies from ASTIA. Orders will be expedited if placed through the librarian or other person designated to request documents from ASTIA.

Do not return this copy. Retain or destroy.

Stock quantities available at Office of Technical Services, Department of Commerce, \$2.50.

## FOREWORD

This report is Volume III of a series of reports on sound propagation in sound-absorbent ducts with a superimposed air stream prepared by Göttingen University, Göttingen, Germany, for the Bioacoustics Branch, 6570th Aerospace Medical Research Laboratories, Aerospace Medical Division, under Contract AF 61(052)112. The work was performed under Project 7231, "Biomechanics of Aerospace Operations," Task 723104, "Biodynamic Environments of Aerospace Flight Operations." Principal Investigators for Göttingen University were Dr. Erwin Meyer and Dr. Fridolin Mechel. Technical and administrative personnel monitoring this effort have included Dr. H. von Gierke, Capt. W. Elrod, R. G. Powell, and J. N. Cole.

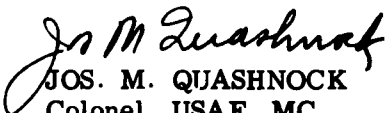
Initial research on this investigation commenced in June 1958.

## ABSTRACT

This report, Volume III, gives theoretical and experimental results on the interaction between sound and air flow in a duct for the following studies: (1) signal amplification as related to size, shape, and position of periodically spaced Helmholtz resonators mounted in the walls of a duct, (2) extension of flow velocity and signal frequency parameters (as employed in Vols. I and II) for a duct coated with a porous absorber, and (3) investigation of plate absorbers for their usefulness in wind tunnel applications. Results of these studies show, respectively, (1) the ratio of the Helmholtz resonator neck width to the spacing, for sound propagation in the flow direction, is an important factor; (2) the solution of a wave equation agrees with experimental measurements for frequencies having a wavelength greater than and comparable to the duct diameter; and (3) the attenuation is dependent on the type of plate absorber (pliable, rigid, or resilient) and the flow velocity. Also reported upon is the construction of a test duct for determining the sound field influence on the air flow boundary layer over a plate vibrating perpendicular to its surface.

## PUBLICATION REVIEW

This technical documentary report has been reviewed and is approved.

  
JOS. M. QUASHNOCK  
Colonel, USAF, MC  
Chief, Biomedical Laboratory

## Part A

### Investigation of Sound Propagation in Sound Absorbent Ducts with Superimposed Air Flow of Great Velocity (up to 200 m/sec).

<u>Contents</u>	<u>Page</u>
List of Symbols	4
Summary	6
1. Introduction	7
2. Experimental Set-Up and Measuring Methods	8
2.1 Measuring Duct	8
2.2 Measuring Equipment	9
2.3 Microphone with Low Self-Noise	9
2.4 Measurement of the Cross Distribution of the Sound Field	11
3. Attenuation Measurements with Reactive Absorbers	11
3.1 Resonators with Circular Necks	11
3.2 Slit Resonators	13
3.3 Dependence of Signal Amplification from Free Duct Height	14
3.4 Dependence of Signal Amplification from Resonator Dimensions	17
4. Measurements with Porous Absorbers	21
4.1 Attenuation Measurements	21
4.2 Measurement of the Cross Distribution of the Sound Field	25
4.3 Theory of Sound Attenuation in Absorbing Ducts with Superimposed Flow	27
4.31 Approximations for Low Frequencies	29
4.32 Approximation for High Frequencies	31
4.4 Influence of Flow on Wall Impedance	34
4.5 Experimental Verification of Theory	35
4.6 Conclusions	36
<u>Appendix</u>	
5. Solution of the wave Equation in Absorbing Ducts with Superimposed Flow.	37

### List of Symbols

$b$	free duct height
$c_o$	adiabatic sound velocity
$c_{oph}$	phase velocity in the duct without flow
$E$	sound energy
$f$	frequency
$f_o$	resonance frequency
$f_M$	center frequency of third-octave range
$f_{eq}$	equivalent frequency
$F$	velocity potential
$G$	amplification factor
$H$	height of the resonator volume
$I$	sound intensity
$I_o$	sound intensity without flow
$I_v$	sound intensity with flow of velocity $V$
$K_z$	complex longitudinal wave number
$K_{zo}$	longitudinal wave number without flow
$K_x$	complex transversal wave number
$K_{xo}$	transversal wave number without flow
$k_o$	free field acoustic wave number
$l'$	effective length of resonator neck
$m$	oscillating mass of resonator
$L$	spacing of resonators
$M = V/c_o$	Mach number
$M' = V/c_{oph}$	"Mach number" relative to phase velocity
$p$	sound pressure
$Q$	cross-sectional area of resonator volume
$S$	cross-sectional area of resonator neck



$t$	time
$v$	sound particle velocity
$V$	flow velocity or resonator volume
$\bar{V}$	mean flow velocity
$V_{loc}$	local flow velocity
$\bar{W}$	wall impedance
$x$	coordinate normal to flow and to absorber surface
$z$	coordinate parallel to duct axis
$Z = \rho c_0$	wave impedance of plane wave
$\alpha$	attenuation constant in dB per meter
$\bar{\alpha} = \alpha(1+M)$	reduced attenuation constant
$\alpha'$	attenuation constant without energetic coupling with flow
$\lambda_{zo}$	signal wavelength in duct without flow
$\lambda_{zv}$	signal wavelength in duct with flow
$\rho$	density of air
$\omega$	angular frequency
$\omega_0$	angular frequency at resonance

### Summary

In ducts coated with a spatially periodic arrangement of Helmholtz resonators amplification of the acoustic signal propagating in the direction of the flow occurs under certain circumstances of signal frequency and flow velocity. This dependence of signal frequency of amplification on flow velocity is known already [2]. The dependence of signal amplification on the dimensions and the shape of the resonators used is investigated. An important figure is the ratio of the neck width in the flow direction to the spacing of the resonators.

In ducts coated with porous absorbers the attenuation of the acoustic signal depends strongly on the flow velocity. The influence of the flow is in the opposite direction at low frequencies (wavelength great compared to duct diameter) and at high frequencies (wavelength comparable to duct diameter) where the acoustic energy concentrates near the duct axis ("acoustic ray formation"). Measurement of the cross-distribution of the acoustic field for high frequencies indicates two mutually opposite flow effects. For quantitative evaluation of flow effects on the attenuation constant in absorbing ducts the wave equation is solved under the assumption of unidimensional flow and of flow-independent wall impedance. The resulting determining equation is approximated for both low and high frequencies. As long as the assumptions are realised the approximate equations yield good agreement with measurement. The theory gives a clear insight in how at high frequencies the actual attenuation constant is a compromise between two concurring flow effects.

## 1. Introduction

The attenuation in sound-absorbing ducts is changed by superimposed air flow. This fact was studied by P. Mechel [1,2] for two types of absorbers. In the duct coated with Helmholtz resonators with low losses, the resonators arranged with constant spacing, the occurrence of signal amplification instead of signal attenuation was found for certain flow-dependent signal frequencies. The amplification could be put into a close analogy to the amplification in electronic traveling-wave tubes. In the duct coated with porous absorbers the attenuation constant decreases with increasing flow velocity for downstream propagation of the acoustic signal and increases with flow velocity for upstream propagation. For the frequencies used in those measurements (0.3 to 3 kc) the signal wavelength was great compared to the lateral dimensions of the duct. The flow velocity never exceeded 80 m/sec. Under the simplifying assumption of a purely dissipative attenuation it was tried in [2] to eliminate the influence of the flow. For the frequencies used there the convection of the signal wave by the flow was recognised as the predominant effect. The remaining influences were attributed by W. Schilz in [3] to nonlinearity of the absorber and to the influence of the flow profile. The signal amplification with reactive absorbers was explained by sound-induced synchronisation of the flow turbulence.

In the present work the measurements with resonator absorbers and with porous absorbers are continued. The dependence of signal amplification on the dimensions and on the shape of the resonators shall be studied. Resonators yielding amplification already for small flow velocities shall be designed. With dissipative absorbers the ranges of frequency and of flow velocity shall be enlarged (velocity up to 180 m/sec, frequency up to 6 kc). Former tentative conceptions for quantitative explanation of the change of attenuation by superimposed flow shall be based on an analytical theory.

## 2. Experimental Set-Up and Measuring Methods

### 2.1 Measuring Duct

The experimental set-up and the measuring methods are similar to those used in [1] and [2]. The air flow is generated by a five-stage centrifugal blower. The air heated up by compression passes a water cooler, then enters to a muffler. There the free cross-section is subdivided into four ducts. Two walls of each duct are coated with low-tuned slit resonators which guarantee the silencing of the low frequency noise components whereas the reduction of the high frequency noise is achieved by coating the two other walls of each duct with rockwool. Acoustic ray formation is avoided by sinusoidal curvature of the ducts. The insertion losses of the silencer are better than 45 dB for frequencies higher than 150 cps. Rubber insulators inhibit propagation of structure-borne sound into the test section of the duct. Behind the silencer the turbulence level of the flow is decreased by insertion of gauze screens. A succeeding contracting cone with great contraction ratio further decreases the turbulence of the flow. The turbulence level at the entrance of the test section is for a wide velocity range smaller than 0.5 per cent. The flow profile is nearly even. At this station the flow velocity is measured with the help of a Pitot probe.

The acoustic signal is fed into the test section either at the entrance or at the exit. The signal is generated by 200 Watt pressure-chamber loudspeakers. Behind the test section an eight degree diffuser 3.5 m long follows. Its walls are coated with rock wool covered by a perforated sheet. Thus flow separation at the exit of the test section is avoided, acoustic reflection at the end is reduced and signal irradiation from the outer measuring room into the test section is inhibited.

## 2.2 Measuring Equipment

A cross-sectional view of the test section is shown in Fig.1. The free duct area is  $100 \times 35 \text{ mm}^2$ . The upper wall of the duct is formed by the respective absorber to be investigated. The wooden housing around the absorber avoids air outlet through the absorber. The sound field is picked up by a microphone probe. It can be drawn along the duct axis by the steel band gliding in a groove in the bottom of the duct. The band is perforated along its sides and is driven by a toothed wheel. The driving wheels and the band return are enclosed in an air-tight housing below the test section. Propagation of structure-borne sound along the band is damped by rubber glued on the band.

The microphone output is fed to a logarithmic level recorder via a heterodyne filter of 6 cps bandwidth. The attenuation along the duct is read from the slope of the curves on the level recorder when the microphone is moved through the duct.

## 2.3 Microphone with Low Self-Noise

The registration of sound fields in flows with high velocities demands a sound pick-up with small self-noise. Pulsations of the flow velocity meeting the microphone probe are transformed into pressure pulsations. The conversion factor is greatest in the stagnation point of the probe and smallest on the probe walls parallel to the flow. Since these pressure fluctuations are registered as if they were sound pressure, the pick-up of the probe must be at a position with low conversion factor. Furthermore the pick-up must not lie in the turbulent wake of the probe. The dimensions of the probe must be small to keep the distortions of the sound field small and to make the flow resistance of the duct independent of the probe position.

The cited conditions are thought to be best realised by the probe microphone shown in Fig.2. The microphone has a maximum diameter of 8 mm and a length of 80 mm. The profile of the body of revolution is a so-called laminar profile [4]. Flow separation takes place near the point with maximum diameter. The sound-sensitive section is on the upstream cone of the body. It is designed as a condenser microphone. The foil 20  $\mu$ m thick, metallised on its outer side is glued smoothly to the body of the probe. The performance of this probe is compared in Fig.3 with the probe of the dynamic microphone used in [1]. The signal-to-noise ratio in a rigid duct is plotted vs. frequency for an electrical loudspeaker input of 50 Watts and the two flow velocities of 50 m/sec and 200 m/sec. The unbroken curve is for the condenser microphone, the dashed curve is for the reference microphone. Actually the laminar profile leads to an improvement of the signal-to-noise ratio. It must be stated, however, that already the reference probe was designed for a low turbulence-to-pressure conversion factor. The condenser probe microphone is mounted on the steel band with a mechanical low pass filter inserted for insulation of structure-borne sound.

The overall signal-to-noise ratio of the measuring equipment without flow is determined by the level of structure-borne sound. Its value is greater than 45 dB. with high flow velocities (greater than 80 m/sec) the flow noise determines the perturbation level. The signal-to-noise ratio is greater than 30 dB for flow velocities up to 180 m/sec. The attenuation of the test section with a rigid upper wall without flow is smaller than 5 dB/m the waviness due to reflections at the end of the duct is smaller than 4 dB. The accuracy of the evaluation of the attenuation depends on the deviations of the registered level records from a straight line. It is best (5 per cent) for medium slopes of the records and decreases for greater (80 dB/m) and smaller (10 dB/m) figures of attenuation.

## 2.4 Measurement of the Cross Distribution of the Sound Field.

With porous absorbers the profiles of the sound pressure and of the phase of the signal are measured. The boring of the microphone probe was 1 mm in diameter with a resulting high spatial resolution. The probe can be moved parallel to and normal to the duct axis. A second fixed probe is at the entrance into the test section. Its out-put controls the signal level at the entrance to the test section via an automatic-volume-control amplifier. Moreover this microphone delivers the reference phase for the phase profile measurements. For these measurements of the phase profiles the outputs of the fixed monitoring microphone and of the movable probe microphone are filtered and fed to the inputs of a lock-in amplifier which is used as a phase-sensitive demodulator. The output of the lock-in amplifier is zero for uncorrelated input signals. The output is zero moreover if the phase lag between the two input signals is  $(2n+1)\pi/2$ , independent from the signal amplitudes. During the measurement of the phase profile the probe microphone was moved in such a way that this phase lag was preserved, the position of the probe microphone thus tracing immediately the phase profile. This null method operates very accurate and insensible to amplitude variations.

## 3. Attenuation Measurements with Reactive Absorbers

### 3.1 Resonators with Circular Necks

First, Helmholtz resonators with circular necks in a periodic arrangement are used. These resonators are the same as used in [2]. The diameter of the necks is 8 mm, the neck length is 3 mm, the spacing  $L = 33$  mm, the resonance frequency without flow is 0.8 kc. The other dimensions can be seen from Fig.4. There the attenuation in dB per meter is plotted vs. signal frequency  $f$  in kcps. Parameter is the mean flow velocity  $V$ . In all measurements with resonance absorbers the signal propagation is in the direction of the flow.

The curves depict the high attenuation at resonance. with increasing flow velocity the maximum is shifted towards higher frequencies altogether with a decrease of the maximum attenuation. The shift of the resonance frequency is caused by a flow-induced reduction of the oscillating mass. The relative change of the resonance frequency and the according reduction of the oscillating mass are plotted in Fig.5 vs. flow velocity. Resonance frequency and mass reach saturation values at a flow velocity of about 120 m/sec. The mass reduction there is 63 per cent. For comparison, the oscillating mass due to the end corrections of the neck length is 50 per cent of the total mass. The reduction of the oscillating mass must be thought to be caused by irreversible turbulent movements at the resonator necks. The loss of kinetic energy due to this turbulence changes the reactive component of the resonator impedance in the sense of a mass reduction but at the same time the losses of the resonator are increased which is depicted by a greater width of the resonance curves.

Above the resonance and with flow velocities greater than 40 m/sec regions of negative attenuation, i.e. signal amplification, are formed. Up to high signal levels the value of the amplification exponent is independent from the signal level. The frequency  $f$  of maximum amplification increases with increasing flow velocity  $V$  according to [2]

$$V = \frac{1}{2} c_{\text{oph}} \left( -1 + \sqrt{1 + \frac{4L \cdot f}{c_{\text{oph}} \cdot n}} \right) \quad (1)$$

where  $c_{\text{oph}}$  is the phase velocity in the duct without flow and  $n$  is a total number. In the case of Fig.5:  $n = 1$ . Equation (1) is derived from the condition that the phase velocity of the  $n$ -th Hartree harmonic in the duct be equal to the propagation velocity of the turbulence which is synchronised by the oscillation of the air in the resonator necks. The floating velocity



of these flow pulsations which we may call pseudo-sound is assumed to be  $V$ . From the measurements in [3], for  $V$  must be taken the local flow velocity at about 5 mm distant from the wall containing the resonators. In a first approximation  $V$  can be taken equal to the mean flow velocity.

### 3.2 Slit Resonators

The number  $n$  of the Hartree harmonic coupling with the flow was  $n = 1$  in all experiments up to now. The other Hartree harmonics are of smaller amplitude. Therefore it is expected that signal amplification with Hartree harmonics other than the first will occur rather seldom. In connection with this statement the following measurements are of some importance. Fig.6 shows the attenuation curves for a slit resonator. The dimensions of the resonators are indicated in the graph. The slits are  $5 \times 62 \text{ mm}^2$  wide. The resonance frequency without flow is 0.8 kc. There are important differences as compared to Fig.4.

The attenuation in resonance is greater with slits than with circular necks. This can be understood from the fact that now the pressure release openings extend nearly over whole the width of the duct. The frequencies of amplification are quite different from one another for the two measurements. First, the associate flow velocities now are much smaller, then the frequency range between 1.3 kc and 3.0 kc is covered by a much smaller interval of associate flow velocities. The frequency band of the individual zones of amplification is about  $2/3$  of an octave. The phase velocity in the duct with the slit resonators measured without flow reveals only small differences as compared to the resonators with circular necks. The dispersion curves for the Hartree harmonics with  $n = 1$  and  $n = 2$  are calculated from (1) with the measured phase velocity  $c_{\text{oph}}$ . They are plotted in Fig.7. The open circles (connected by the dashed line) are the values of frequency and associate mean

flow velocity of maximum amplification. They are close to the dispersion curve for the second Hartree harmonic. As mentioned above the relevant flow velocity for the energy exchange between the sound signal and the sound-stabilised flow turbulence is the local flow velocity at a wall distance of about 5 mm. In Fig.8 profiles of the flow velocity are plotted as they are measured in the duct with the slit resonators. The center of the layer active in the sound amplification is marked by the dashed line. with the flow velocities of this layer instead of the mean flow velocities the points of maximum amplification in Fig.7 are the full circles. They coincide with the dispersion curve of the second Hartree harmonic. Thus signal amplification is also possible by energetic coupling of the flow with the second Hartree harmonic.

### 3.3 Dependence of Signal Amplification from Free Duct Height.

The fact that the energy exchange between the flow and the acoustic signal in the case of signal amplification takes place only in a thin layer near the wall containing the resonators can be used in order to increase the amplification.

For small signal levels the signal amplitude at the entrance of the duct is proportional to the signal amplitude at each other point of the duct. From this it follows that the gain of acoustic energy from one resonator to the next is proportional to the acoustic energy density at the necks of the resonators. Since the amplitude ratio of the Hartree harmonics is determined only by the boundary conditions of the duct the energy increase distributes over all Hartree harmonics, i.e. over the whole cross-section of the duct. The energy increase must remain the same if the free height of the duct is varied as long as it remains greater than the thickness of the active layer near the resonators. If the

height is decreased the increment in energy between two resonators distributes over a smaller area, therefore the energy density at the next resonator will become greater, thus leading to a greater gain at this resonator.

These statements in a more quantitative formulation will read as follows: In a duct with unity lateral width and the free height  $b$  the attenuation  $\alpha'$  without the influence of the active layer is defined by the decrease of the acoustic intensity along the axis of the duct in the  $z$ -direction:

$$d_1 I = -\alpha' \cdot I dz . \quad (2)$$

The gain of acoustic energy  $dE$  along the path  $dz$  will be

$$dE = g I dz \quad (3)$$

with  $g$  as an "amplification factor". The corresponding increase of the sound intensity will be

$$dzI = \frac{dE}{b} = \frac{g}{b} I dz \quad (4)$$

From (2) and (4) the total change of the sound intensity along  $dz$  will be

$$dI = \left(\frac{g}{b} - \alpha'\right) I dz = -\alpha I dz \quad (5)$$

where  $\alpha$  is the attenuation constant as it will be measured. The decrease of the attenuation constant due to the active layer:

$$(\alpha' - \alpha) = \frac{g}{b} \quad (6)$$

is inversely proportional to the free duct height  $b$ . It shall be indicated that this dependence from the duct height is the same as with the attenuation in ducts caused by the viscous boundary layer [5]. In both of these cases acoustic energy is transformed within a boundary layer at the boundaries of the duct. The other area of the duct cross-section serves only for transportation of the acoustic energy. In the case of sound amplification the acoustic boundary layer is an active one instead of a dissipative one.

For an experimental examination of equation (6) the free duct height was decreased from 35 mm to 16 mm. Fig.9 shows the results of the measurements with the resonators of Fig.4. Because of the small height the measurements could be extended beyond the frequency limit of 3 kc in the wide duct up to 5,4 kc. For this frequency the spacing between the resonators becomes equal to half a signal wavelength. According to the theory of transmission lines these sections of half a wavelength act as parallel resonant circuits. According to the Q-value of these circuits in series the attenuation in the duct increases. Beyond this frequency the graphs of the level recorder could not be evaluated. They became wavy by the signal reflections at the individual resonators.

Without flow the attenuation in the flat duct is greater than in the wide duct, especially above resonance. Nevertheless the absolute value of the amplification is greater. The difference ( $\alpha - \alpha'$ ) has increased inversely proportional to the height of the duct. Deattenuation is still found at the flow velocity 110 m/sec. The frequencies of maximum amplification are the same as in Fig.4. The energy exchange takes place with the first Hartree harmonic. For flow velocities below 60 m/sec the duct showed strong self-excitation. Therefore attenuation measurements for these flow velocities were impossible.

### 3.4 Dependence of Signal Amplification from Resonator Dimensions.

It is to be expected that the dimensions of the necks of the resonators and the distance between the resonators will be the most important figures governing the signal amplification. The area of the resonator necks is easily changed by partial or by complete masking with an adhesive foil which must be thin enough not to disturb the flow but heavy enough to have a sufficiently high acoustic impedance. If the neck area  $S$  is reduced the resonance frequency  $f_0$  decreases according to

$$\omega_0^2 = \frac{c_0^2 S}{l' V} \quad \omega_0 = 2\pi f_0 \quad (7)$$

There  $V$  is the resilient volume of the resonator,  $l'$  the effective length of the neck and  $c_0$  the adiabatic sound velocity.

Resonators with different resonance frequencies can be compared with one another. This follows from equation (1) for the phase velocity of the Hartree harmonics, which reads with the wavelength  $\lambda_{z0}$  of the signal in the duct without flow:

$$V = \frac{1}{2} c_{oph} \left( -1 + \sqrt{1 + \frac{4L}{n \cdot \lambda_{z0}}} \right) \quad (8)$$

With all resonators tested up to now deattenuation was present only above resonance. Therefore it is sufficient in the following to confine ourselves to these frequencies. Fig.10 shows the frequency curves of the wavelength  $\lambda_{z0}$  and of the phase velocity  $c_{oph}$  without flow of the signal wave in the duct with the slit resonators. Above resonance (marked by the strong dispersion) the wavelength and the phase velocity are greater than in the free field. Near the resonance the wavelength is great

compared to  $4L/n$ . Neglecting quantities small of the second order equation (8) there becomes, therefore

$$v = \frac{Lf}{n} \quad (9)$$

It is independent of the wavelength and indicates the upper limit of the phase velocity of the  $n$ -th Hartree harmonic. With increasing frequency the wavelength and the phase velocity in the duct approach the free field wavelength  $\lambda_0$  and the sound velocity  $c_0$ . With these the equation (8) becomes

$$v = \frac{1}{2} c_0 \left( -1 + \sqrt{1 + \frac{4fL}{n c_0}} \right) \quad (10)$$

which is at the same time the lower limit of the phase velocity of the Hartree harmonic. This equation too is independent from the qualities of a specific resonator. The two equations (9) and (10) are plotted in Fig.11 for the integers  $n = 1$  and  $n = 2$ . The zone wherein the second Hartree harmonic must lie is very narrow. That means that the dispersion curve for this Hartree harmonic has nearly the same form independent of the specific resonator. For  $n = 1$  the zone becomes broader for high frequencies. But, as the resonators tested below have their resonances below 1 kc, the signal wavelength in the duct is practically equal to the free field wavelength for frequencies greater than 2 kc. Therefore the dispersion curve for  $n = 1$  will practically coincide with the lower limit (dashed curve) for these higher frequencies. From Fig.11 it can be seen furthermore, that already for small flow velocities amplification will be possible if low-tuned resonators are used and the coupling takes place with the second Hartree harmonic.

How much the points of maximum amplification are independent from the resonance frequencies of different resonators can be seen from the measured points in Fig.11 which belong

to different absorbers. It shall be mentioned however that in Fig.11 the mean flow velocities for the measured points are used instead of the local velocities in the boundary layers. Therefore the points partially fall beyond the dispersion zones.

Now the influence of the dimensions of the resonator necks on the amplification shall be examined. In a first series of measurements it was started with slit resonators with the slit dimensions  $5 \times 65 \text{ mm}^2$ . The resonance frequency was kept low (0.6 kc) by a great resilient volume. In a second step the center part of the slits was covered over a width of 20 mm leaving two slits of 45 mm total length per resonator. Finally the total length was reduced to 20 mm by masking from the sides. The attenuation curves of the latter resonators are plotted in Fig.12. The dimensions of the resonators there are indicated. The original length of the slits is indicated by the broken lines. The resonator distance is as before  $L = 33 \text{ mm}$ .

In Fig.12, by the rigorous masking, the resonance frequency has shifted to 0.45 kc. The first deattenuation is at a flow velocity of 15 m/sec. The points of maximum amplification for these masked resonators of Fig.12 are represented in Fig.11 by the upright triangles. The triangles upside down are for the resonators with the middle of the slits covered. The squares are for the completely unmasked resonators. Taking into account that for these points the mean flow velocity was used it can be stated that they all belong to the second Hartree harmonic. The difference between the three types of resonators is rather small.

The rise of the attenuation curves in Fig.12 for  $f = 2.8 \text{ kc}$  comes from that the height of the resonator volumes there is no longer small to the wavelength. The input impedance of the resonator then is

$$W = j(\omega q l' - \frac{Z \cdot S}{Q} \text{ctg } \frac{\omega H}{c_0}) \quad Z = \rho c_0 \quad (11)$$

The condition  $W = 0$  of resonance therefore can be realised for more than one frequency. A second resonance for the resonators of Fig.12 is at about 2.8 kc.

In contrast to the masking of the slits in the lateral direction the amplification reacts sensitively on masking in the longitudinal direction, i.e. in the direction of the flow. For instance, if the circular necks of the resonators of the Fig.4 are covered so that only lunate apertures remain free, as indicated in Fig.13 for the necks of 8 mm diameter, the attenuation curves reveal clear differences from those of Fig.4. The frequencies of deattenuation for equal flow velocities are shifted to higher frequencies. They are the same values as for a coupling with the second Hartree harmonic. By comparison with the dispersion curves in Fig.11 this is confirmed. The small masking was sufficient to replace the first Hartree harmonic as the coupling mode by the second Hartree harmonic. In Fig.14 this transition can be followed up. There the masking was increased for the constant flow velocity of 40 m/sec. It can be seen how the frequency of maximum amplification is shifted in a step when increasing the masked segment from 1.5 mm in height to 3 mm in height. Since the energy exchange is a strictly nonlinear effect it must be supposed that coupling with only one mode at the same time will be possible. The exchange of the coupling mode will occur suddenly.

Evidently the crucial quantity is not so much the neck width itself but the ratio of the neck width to the resonator spacing. This is confirmed by the results obtained when each second row of the resonators is completely covered. The positions of the amplification frequencies remain the same as in Fig.4. But now  $L$  is twice the original value. For equal frequency and flow velocity of maximum amplification in both cases the number  $n$  in (1) must be doubled too. Actually all the resonators for which amplification with the second Hartree harmonic takes place have about the same ratio of neck width to resonator spacing. The importance of the neck width-to-spacing



ratio comes out as follows: For a unidirectional energy exchange between the sound wave and the flow pulsation, which takes place only at the necks of the resonators, a certain flow pulsation must meet with the sound wave at the necks of the resonators always in the same phase. Therefore the wavelength  $\lambda_p$  which can be associated to the flow pulsation,

$$\lambda_p = \frac{V}{f} \quad (12)$$

must be great compared to the neck width. In the case of synchronism with the coupling Hartree harmonic, i.e. in the case of amplification, it must be equal to the wavelength  $\lambda_n$  of the Hartree harmonic which is approximately

$$\lambda_n = \frac{L}{n} \quad \text{for } \lambda_{zo} \gg L. \quad (13)$$

Therefore

$$a/L = \frac{1}{n} \frac{a}{\lambda_n} = \frac{1}{n} \frac{af}{V} \quad (13')$$

If the ratio  $a/\lambda_n$  shall be near to the optimum value of this ratio for maximum energy exchange the number  $n$  must increase if  $a/L$  is decreased either by a decrease in  $a$  or by an increase in  $L$ .

#### 4. Measurements with Porous Absorbers

##### 4.1 Attenuation Measurements

If the duct is coated with a porous absorber the mechanism of the attenuation is not a continuous reflection of the wave as with the reactive resonance absorbers but predominantly a dissipation of acoustic energy into heat. In most technical applications porous absorbers are used because of their

broadband absorption. As an example of these absorbers a layer of rockwool 75 mm thick ("Sillan", Grünzweig und Hartmann) was tested. The layer was backed by a rigid plate and was covered on its front side with a perforated 1 mm metal sheet. The holes in the sheet were 1.5 mm in diameter and the perforation was 31 per cent of the total area. The use of the perforated sheet was without acoustic significance as the small flow resistance of the holes can be neglected vs. the flow resistance of the layer. The metal sheet was used for mechanical stability of the layer.

The results of the attenuation measurements with this absorber are plotted in Fig.15 and Fig.16. There again the attenuation in dB per meter is plotted vs. frequency  $f$  in kc. Parameter is the mean flow velocity  $V$ . Positive values of  $V$  stand for downstream propagation, negative values of  $V$  mean upstream propagation of the signal.

The attenuation curve without flow shows maximum attenuation for medium frequencies. The drop of the curve for low frequencies is caused by the rigid backing of the layer and the large wavelength compared to the thickness of the layer. The decrease of attenuation for the high frequencies is caused by the "acoustic ray formation". This term stands for the fact that for high frequencies where the free duct height becomes comparable to the signal wavelength the acoustic energy concentrates near the center of the duct or near rigid walls whereas in front of the absorber an acoustic depletion layer is formed. In the present duct ray formation becomes perceivable at about 2.5 kc.

The attenuation curves with superimposed flow show - for downstream propagation of the signal - a decrease of attenuation with increasing flow velocity for the low and the medium frequencies. For high frequencies the attenuation increases with the flow velocity. Contrary - for upstream propagation - the attenuation increases with increasing flow velocity at the low and the medium frequencies whereas it decreases at high frequencies.

Up to now in all measurements the signal was a sine wave. In technical applications nearly everytime broadband noise must be damped. Eventually nonlinear performance of the absorber, the nonlinearity could be caused by the turbulent flow, could make the attenuation different for noise bands and for pure tones resp. For a check of this objection measurements with third-octave noise bands were performed. Fig.17 and Fig.18 show the results. Abscissa are the band center frequencies. By comparison with the curves of Fig. 15 and Fig.16 no important differences can be found. Therefore our pure tone measurements can give satisfactory information about the performance of the absorber with broadband noise.

In the papers [2] and [3] the change of the attenuation by the superimposed flow with velocities up to 80 m/sec and for low and medium frequencies was ascribed to the change of the acoustic intensity in the duct caused by the flow. For plane waves, starting from the relation

$$p = \rho c_0 v \quad (14)$$

between sound pressure  $p$  and acoustic particle velocity  $v$ , Pridmore-Brown [6] has calculated the acoustic intensity  $I_v$  in a flow from the intensity  $I_0$  without flow.

$$I_v = I_0 \left(1 + \frac{v}{c_0}\right) = I_0(1 + M) \quad (15)$$

$$I_0 = \frac{p^2}{\rho c_0} \quad M = \frac{v}{c_0}$$

In [2] and [3] for a first approach to a quantitative treatment of the flow influence upon attenuation equation (15) was used. Since the waves in the duct are not plane, even not at low frequencies, because of the finite wall impedance of the absorber, (15) was replaced by

$$I_v = I_0 \left(1 + \frac{V}{c_{oph}}\right) = I_0 (1 + M') \quad (16)$$

A purely dissipative attenuation supposed, equ. (16) leads to a flow dependence of the attenuation as  $(1 + M')^{-1}$ . This means for example a decrease of attenuation for downstream propagation. If it is further assumed that the phase velocity with flow is the algebraic sum of the phase velocity without flow plus the flow velocity, i.e. the wavelength  $\lambda_{zv}$  with flow is connected with the wavelength  $\lambda_{z0}$  without flow by

$$\lambda_{zv} = \lambda_0 (1 + M') \quad (17)$$

then the product of the attenuation times the wavelength should be flow-independent. Measurements at medium values of flow velocity and of frequency did not fully satisfy this requirement. Measurements at great values of flow velocity and of frequency could not satisfy this requirement at all.

Actually this simple treatment suffers from the following limitations. First, the condition of plane waves in the duct will be violated for pressure release absorbers and the curvature of the wavefronts cannot be compensated fully by use of  $M'$  instead of  $M$ . Second, the condition of plane waves will be violated at high frequencies with acoustic ray formation. Third, the condition of purely dissipative attenuation will not be met with at those frequencies for which the thickness of the porous layer is small to or comparable with the signal wavelength. This can be seen from the dispersion of the phase velocity in the duct with the porous absorber for low frequencies. The measured phase velocity is shown in Fig.19.

#### 4.2 Measurement of the Cross Distribution of the Sound Field.

It is mainly the change of attenuation at high frequencies which cannot be described by the above elimination of the flow influence. Certainly the change of the acoustic intensity will be effective at high frequencies too but it is masked by an opposite flow effect. It suggests itself that it will be the acoustic ray formation at the high frequencies which causes the opposite direction of the flow influence compared to that at low frequencies. It was stated above that the ray formation is characterised by a depletion of acoustic energy near the absorber surface. The cross distribution of the sound intensity, i.e. of the sound pressure amplitude, is governed by a lateral wavenumber.

With superimposed flow the longitudinal wavenumber is changed. The lateral wavenumber in the duct is connected with the longitudinal wavenumber by the wave equation. It is changed whenever the longitudinal wavenumber is altered. For low frequencies where the wavelength is great compared to the free duct height the sound intensity is distributed uniformly over the cross section, the lateral wavenumber being very small. Therefore, changes of the lateral wavenumber do scarcely change the distribution of the sound intensity. For high frequencies, however, the attenuation depends critically from the lateral wavenumber.

The following measurements of the profiles of the sound pressure and of the phase in the frequency range between 3.0 and 5.5 kc and for flow velocities between -100 and +100 m/sec shall give an insight into the manner in which the cross distribution of the sound field in the duct is influenced by the superimposed flow.

Before entering into the absorbing test section the signal wave propagates in a rigid duct section 50 cm in length. Thus the wave at the entrance of the absorbing duct is plane. The measuring station is about 30 cm distant from the entrance to the absorbing section. There the cross distribution is already stationary. The results of the measurements are shown

in Fig.20 for downstream propagation of the signal and in Fig.21 for upstream propagation of the signal. Each graph in these figures represents a schematic longitudinal sectional view of the duct. The full circles give the relative sound pressure amplitudes over the duct height. The sound pressure at the rigid wall corresponds to 100 per cent. The open circles represent the phase profiles, i.e. sectional curves of the surfaces of equal phase. The scale of the abscissa is indicated at the first graph of the first row. The rows belong to measurements with constant signal frequency, the columns belong to constant flow velocity. The equivalent frequency  $f_{eq}$  of the graphs is that frequency to which in the duct without flow would belong the same wavelength as it is actually with the indicated values of frequency and of flow velocity. The wavelength is calculated from (17).

The sound pressure profiles without flow give an evident explanation for the decrease of the attenuation with increasing frequency. Whereas the sound pressure at 3 kc is still nearly constant over the cross section it is, at 5.5 kc, reduced to 60 per cent in front of the absorber. For upstream propagation (see Fig.21) the variation of the profiles is qualitatively the same whether the frequency is increased for a constant flow velocity, or if at a constant frequency the flow velocity is increased. Roughly speaking in this case an increase of the flow velocity is equivalent to an increase of the frequency. An increase of the flow velocity therefore favors the ray formation thereby reducing the attenuation. By this the effect of the changed sound intensity which would lead to an increased attenuation can be eventually overcompensated. For downstream propagation (see Fig.20) an increase of the flow velocity inhibits the ray formation. The action of two mutually opposite flow effects, i.e. change of the total acoustic intensity and change of the cross distribution of the acoustic intensity, can be clearly seen.

For downstream propagation, high frequency and great flow velocity (5.5 kc; +100 m/sec) the ray formation can even be overcompensated with the result that the sound pressure near the absorber is even greater than near the rigid wall. This sound pressure distribution, impossible without flow, must be attributed to the gradient of the flow velocity. It shall be the subject of further investigation.

The phase profiles are only little affected by the flow for both directions of propagation. Small changes in the form of the profiles and of the glancing angle at the absorber surface can be explained by the shift of the equivalent frequency. In all cases the phase at the absorber is retarded behind the phase at the center of the duct. For upstream propagation of the signal the glancing angle never becomes greater than 90 degrees.

#### 4.3 Theory of Sound Attenuation in Absorbing Ducts with Superimposed Flow.

Experimental evidence exists for the following effects of flow influencing the sound attenuation in absorbing ducts:

- a. Convective change of the total sound intensity. It is predominant at low frequencies and for dissipative absorbers with great input impedance.
- b. Change of the cross distribution of the acoustic intensity by variation of the lateral wavenumber. It becomes important for high frequencies, for great velocities and for absorbers with low input impedance.
- c. Change of the cross distribution of the acoustic intensity in the gradient field of the flow profile. It is only effective for frequencies so high that the wavelength becomes comparable with the boundary layer thickness.
- d. Nonlinearity of the absorber. This is significant either for resonance absorbers near the resonance or for porous absorbers if they are penetrated by a stationary flow or by turbulent pulsations of great amplitude.

e. Scattering of the sound wave at the random inhomogeneities of the turbulent medium. In our measurements this effect proved to be of minor importance.

For the present measurements with porous absorbers the influences under a. and b. are the most important ones. As described above their action is opposite to one another. A theory comprising these two effects shall be developed.

For this purpose the wave equation for the signal wave in the absorbing duct with flow is solved in the appendix. For simplicity and in order to eliminate the effect under c. the flow profile there is assumed to be plane. Justification for this simplification is taken from the measurements.

The secular equation of the wave equation in the unidimensional flow is

$$K_x^2 + K_z^2 = (k_0 - K_z M)^2 \quad (18)$$

where

$$K_x = k_x + jg_x; K_z = k_z - jg_z; k_0 = \frac{\omega}{c_0}; k_z = \frac{2\pi}{\lambda_z}$$

It combines the longitudinal wavenumber  $K_z$  with the transversal wavenumber  $K_x$ . The z-axis is in the direction of the duct axis, the x-axis is normal to the absorber surface. The boundary condition at the absorber yield the second equation

$$\frac{\text{ctg } K_x b}{K_x} = -j \frac{\bar{W}}{Z} \cdot \frac{1}{k_0 - MK_z}; Z = \rho c_0 \quad (19)$$

$\bar{W}$  is the complex wall impedance of the absorber, the imaginary part of  $K_z$  is the attenuation  $\alpha$ , b is the free duct height, Z is the wave impedance.



A simple solution of the equations (18) and (19) for  $\bar{K}_z$  is not possible. Also the maps of MORSE cannot be used since  $\bar{K}_z$  stands in the denominator of the right side of equ.(19). A conformal mapping therefore is impossible. In their general form the equations must be solved by numerical approximate methods. However, for low frequencies and for high frequencies approximations to the general equations are possible.

#### 4.31 Approximation for Low Frequencies

For low frequencies the sound waves in the duct are quasi-plane. Then  $|\bar{K}_x b| \ll 1$ . The cotangent in eq.(19) can be replaced by the inverse of its argument. Together with eq.(18) a determining equation for  $\bar{K}_z$  is derived:

$$+j \frac{Z}{Wb} (k_o - M\bar{K}_z) = (k_o - M\bar{K}_z)^2 - \bar{K}_z^2 \quad (20)$$

The wall impedance  $\bar{W}$  in (20) can be eliminated if in (20)  $M = 0$  is inserted. This leads to:

$$+j \frac{Z}{Wb} = \frac{k_o^2 - \bar{K}_{zo}^2}{k_o} \quad (21)$$

Reinsertion of this into (20) leads to the quadratic equation:

$$\bar{K}_z^2 + \frac{M(k_o^2 - \bar{K}_{zo}^2)}{(1 - M^2) k_o} \bar{K}_z - \frac{\bar{K}_{zo}^2}{1 - M^2} = 0 \quad (22)$$

with the solution:

$$\bar{K}_z = - \frac{M(k_o^2 - \bar{K}_{zo}^2)}{2(1-M^2) k_o} + \sqrt{\frac{M^2(k_o^2 - \bar{K}_{zo}^2)^2}{4(1-M^2)^2 k_o^2} + \frac{\bar{K}_{zo}^2}{1-M^2}} \quad (23)$$

This elimination of  $\bar{w}$  presupposes that the wall impedance of the absorber is not changed by the flow.

The tentative elimination of the influence of the signal convection by the flow according to eq.(16) leads to:

$$g_z = \frac{1}{1+M} g_{zo} = \frac{1}{1+M \frac{k_{zo}}{k_o}} g_{zo} \quad (24)$$

for the imaginary part  $g_z$  of  $\bar{K}_z$ . By comparison with eq.(23) it follows, that equ.(24) becomes insufficient for great flow velocities and for frequencies with great dispersion of the phase velocity. Therefore eq.(23) must be used for low frequencies (see Fig.19). Furthermore eq.(23) shows that the phase velocity with superimposed flow is not simply the algebraic sum of the phase velocity without flow and of the flow velocity, as it was assumed in eq.(17). An obvious explanation therefore is seen in eq.(19). There the Mach number  $M$  in the denominator of the right side acts like a change of the wall impedance. For low frequencies, however, the phase velocity depends strongly on the wall impedance. Since the imaginary part of  $\bar{K}_z$  is negative one sees from eq.(19) that the "effective wall impedance" becomes more and more capacitive with increasing  $M > 0$  (downstream propagation) and more and more inductive for  $M < 0$  (upstream propagation). The tendency of the effective wall impedance is to cancel the convective change of the flow velocity.

#### 4.32 Approximation for High Frequencies

In order to derive an approximate equation for the attenuation at high frequencies it is convenient to separate (18) into the real and into the imaginary part:

$$k_z^2 - g_z^2 + \frac{2 k_0 M}{1 - M^2} k_z - \frac{k_0^2 - (k_x^2 - g_x^2)}{1 - M^2} = 0 \quad (25)$$

$$g_z = \frac{g_x k_x}{k_z (1 - M^2) + M k_0} \quad (26)$$

The measurements of the phase velocity without flow yield only small differences between the phase velocity and the free field velocity for frequencies greater than about 2.5 kc. Therefore for the real part of the wavenumber can be put  $k_{zo} \approx k_0$ . Further, the measurements of the attenuation yield for this frequency range  $k_{zo} > 0.1 g_{zo}$ . Therefore, for  $M = 0$  in (25)  $g_{zo}^2$  can be neglected compared to  $k_{zo}$  and because of  $k_{zo} \approx k_0$  also  $(k_x - g_x^2)$  can be neglected. For flow velocities not too great these neglects will be valid. Then equ.(25) becomes:

$$k_z = \frac{k_0}{1 + M} \quad \lambda_{zv} = \lambda_0 (1 + M) \quad (27)$$

Thus equ.(27) simply states that the phase velocity is the sum of the phase velocity without flow and the flow velocity. From (26) and (27) the attenuation constant becomes:

$$g_z = \frac{g_x k_x}{k_0} = \frac{g_x k_x}{(1 + M) 2\pi} \lambda_{zv} \quad (28)$$

Here the unknown product  $g_x k_x$  can be determined from equation (19): It can be shown that the omission of the imaginary part of  $\bar{k}_z$  (possible because of  $k_z > 0.1 g_z$ ) in equation (19)

corresponds to a decrease of the phase angle of the complex wall impedance. The difference of the phase angle is of the order

$$M(1+M) \cdot g_{z0}/k_0 < 0.1 \quad M(1+M) \quad [\text{rad}] .$$

For  $M$  not too great  $g_z$  in (19) can therefore be neglected. Together with (27) equation (19) becomes:

$$\frac{\text{ctg } K_x b}{K_x} = -j \frac{\bar{W}}{Z(k_0 - k_z M)} = -j \frac{\bar{W}}{Z 2\pi} \lambda_{zv} \quad (29)$$

If the wall impedance is independent of frequency, equation (29) states that the transversal wavenumber  $K_x$  is constant for a constant wavelength. Therefore the product  $g_x k_x$  depends only from the wavelength  $\lambda_{zv}$ . The dependence of this product from the flow velocity is determined by the dependence of  $\lambda_{zv}$  from the flow velocity according to equ. (27).

Thus it is possible to eliminate the influence of the flow: If the approximations made ( $k_z > 0.1 g_z$ ;  $\bar{W} = \text{constant}$ ) are valid the measured attenuation constant multiplied by  $(1+M)$  plotted over the wavelength  $\lambda_{zv}$  in the duct must fall on one and the same curve independent from flow velocity.

How the attenuation with superimposed flow comes out from the attenuation without flow can be seen from the following: The equ.(29) can be written:

$$\frac{\text{ctg } K_x b}{K_x} = -j \frac{\bar{W}}{Z} \cdot \frac{c_0(1+M)}{2\pi f} = j \frac{\bar{W}}{Z} \cdot \frac{c_0}{2\pi f_{eq}} \quad (30)$$

There is put  $f = f_{eq} \cdot (1+M)$ . Equation (28) leads to:

$$g_z(f) = \frac{c_0 g_{zx} k_x}{2\pi f} = \frac{c_0 g_{zx} k_x}{2\pi f_{eq}(1+M)} = \frac{1}{1+M} g_{zo}(f_{eq}) \quad (31)$$

The attenuation with flow  $g_z(f)$  at the frequency  $f$  can be derived from the attenuation without flow  $g_{zo}(f_{eq})$  at the frequency  $f_{eq}$  through division by  $(1+M)$ . This shows clearly the influence of two effects. First, the transformation of the frequency  $f \rightarrow f_{eq}$  comes from the change of the cross distribution of the acoustic intensity, second, the division by  $(1+M)$  comes from the convective change of the total acoustic intensity.

If the attenuation without flow is plotted vs. the frequency in a double logarithmic scale the attenuation at medium frequencies is constant [7] and decreases at high frequencies with a final slope of  $-2$ . In this double logarithmic representation the above divisions through  $(1+M)$  are reduced to simple additions or subtractions of equal distances parallel to the coordinate axis. This geometric construction of the attenuation with superimposed flow from the attenuation without flow is shown in Fig.22 for downstream propagation ( $M > 0$ ) and in Fig.23 for upstream propagation ( $M < 0$ ). From that, the attenuation with  $M > 0$  is smaller than the attenuation without flow as long as the slope of the attenuation curve without flow is smaller than unity, whereas the attenuation with flow in the propagation direction of the signal is greater for frequencies with the slope greater than unity. For the other direction of propagation, i.e.  $M < 0$ , it is just vice versa. The point of intersection with the attenuation curve without flow depends on the special form of this curve and on the Mach number  $M$ . The decision which of the two flow effects at high frequencies is the predominant one thus is simply reduced to the slope of the attenuation curve without flow.

#### 4.4 Influence of Flow on wall Impedance

In the above approximations it was assumed that the wall impedance of the absorber be independent from the flow velocity and that at high frequencies it be independent from frequency too. Now it shall be examined how these conditions are met with the porous absorber.

Fig.24 shows the wall impedance of a thick layer of rock wool in the complex plane as it was measured in the impedance tube. For frequencies greater than 2.5 kc the real part of the wall impedance remains sensibly constant. The imaginary part too changes only little with frequency. The measurements in [3] showed a small flow-induced change of the internal flow resistance of the porous absorber which can principally change the wall impedance. The change of the flow resistance is a function of the flow velocity and of the frequency, being small for high frequencies. The dependence of the wall impedance of a porous absorber from the internal flow resistance  $r_1$  at high frequencies is given by [5]:

$$\bar{W} = \frac{Z}{\delta} \sqrt{1 - j \frac{r_1}{\omega \cdot \delta}} \quad (32)$$

$\delta$  = porosity

From this, a change in  $r_1$  is equivalent to a change of the frequency. Since the frequency dependence of  $\bar{W}$  is small for high frequencies (the second term in the square root is small compared to unity) the wall impedance there can be considered to be constant with a good approach.

For low frequencies the thickness of the porous layer is small compared to the wavelength. Equation (32) there is no longer valid. The wall impedance is capacitive because of the rigid backing. The energy penetrating into the absorber therefore is not determined by the flow resistance. Thus it can be expected that a flow-induced change of the flow resistance does not affect too much the wall impedance.

Another cause for a change of the attenuation not yet mentioned up to now comes from the dependence of the wall impedance from the angle of incidence of the sound wave if sound propagation within the absorber parallel to its surface is possible [5]. The angle within the absorber is determined by the matching of the wavelength at the surface. The wavelength in the duct is changed by the flow. Under unfavorable circumstances this results in a changed wall impedance. This can be avoided by thin rigid walls in the absorber perpendicular to its surface in a small distance from one another.

#### 4.5 Experimental Verification of Theory

With most porous absorbers internal wave propagation parallel to the surface is inhibited by the internal structure. With the rock wool used in our measurements, however, for low frequencies a lateral coupling takes place. In Fig.25 therefore the same absorber was used as in Fig.15 but now with partition walls 3 mm thick in a distance of 50 mm from one another. Now the attenuation curves at 0.8 kc show a maximum of attenuation in contrast to the Fig.15, which is caused by a damped quarter-wavelength resonance in the absorber. In a smaller scale the same is true when the layer thickness is equal to  $3\lambda/4$ . Above 2.5 kc the curves are equal to those of Fig.15. The full points are the values of the attenuation constant with superimposed flow calculated from the wavenumber without flow according to equ.(23). Between 0.3 kc and 0.6 kc the calculated values agree well with measurement. Above 0.6 kc the measured attenuation is smaller than the calculated values are. It was proved that these deviations do not result from the approximations made in the derivations of equ.(23). For this purpose the wavenumber with superimposed flow was calculated from the measured values without flow using the exact equations. These were solved with the

help of an electronic digital computer. The values from the exact equation agree well with the values from the approximate equation (23) up to 1.0 kc. The difference between the calculation and the measurement is caused by the flow dependence of the wall impedance near the resonance at 0.8 kc. Between 0.3 kc and 0.6 kc the approximate attenuation from equ.(23) shows good agreement with the measured values for upstream propagation too.

According to the results of section 4.32 for high frequencies in Fig.26 and Fig.27 the measured attenuation  $\alpha$  multiplied by  $(1 + M)$  is plotted as  $\bar{\alpha} = \alpha(1+M)$  as a function of the wavelength in the duct with superimposed flow. For the region of small dispersion (1.0 - 2.0 kc) this wavelength was calculated from equ.(17). The full curve is the corrected attenuation without flow. The triangles and the full circles are for the flow velocities  $\pm 60$  m/sec and  $\pm 100$  m/sec respectively. For both directions of signal propagation the points are in satisfactory agreement with the curves. Due to the small frequency dependence of the wall impedance the deviations for great velocities are greater than for small velocities.

For completeness it shall be mentioned: the influence of the matching of the wavelengths at the absorber surface is eliminated by the representation of Fig.26 and Fig.27 as  $\bar{\alpha}$  is always referred to a constant wavelength.

#### 4.6 Conclusions

The topic of the present investigations is the influence of a superimposed air flow on the sound attenuation in absorbing ducts. Already a theory neglecting the flow profile is in good agreement with the measurements. Especially the attenuation for frequencies with acoustic ray formation is described by a simple method. Differences between theory and measurement occur only where the wall impedance becomes



flow-dependent. From this it can be concluded that the flow profile is of minor importance as long as the wavelength is great compared to the boundary layer thickness. The influence of the flow profile could be determined if the exact equations of section 4.3 would be used with the wall impedance measured with flow present. The knowledge of the wall impedance without flow alone is not sufficient because by a changed wall impedance both attenuation and phase velocity in the duct are changed.

## Appendix

### 5. Solution of the Wave Equation in Absorbing Ducts with Superimposed Flow.

For the sake of simplicity it is assumed that the wall impedance of the absorber is independent from the flow and that the flow is unidimensional. For further simplicity the problem is considered in two dimensions.

With the flow velocity  $V$  in the  $z$ -direction the wave equation is

$$\Delta F = \frac{1}{c_0^2} \left( \frac{\partial^2 F}{\partial t^2} + 2V \frac{\partial^2 F}{\partial t \partial z} + V^2 \frac{\partial^2 F}{\partial z^2} \right) \quad (33)$$

$\Delta$  = Laplace operator

By the Gallilei transformation

$$x = x' \quad y = y' \quad z = z' + Vt' \quad t = t' \quad (34)$$

the wave equation in the moving coordinates (primed coordinates) assumes again the usual form

$$\Delta' F = \frac{1}{c_0^2} \frac{\partial^2 F}{\partial t'^2} \quad (35)$$

A solution of (35) is

$$F(x', z', t') = A \cos(\bar{K}_x x') e^{-j(\bar{K}_z z' - \bar{\omega}' t')} \quad (36)$$

Insertion of (36) into (35) yields the secular equation

$$\bar{K}_x^2 + \bar{K}_z^2 = \left(\frac{\bar{\omega}'}{c_0}\right)^2$$

$$\bar{K}_x = k_x + jg_x; \quad \bar{K}_z = k_z - jg_z; \quad \bar{\omega}' = \omega' - j\delta' \quad (37)$$

The bar over the symbols denotes complex quantities. Without flow the solutions of the wave equation must be stationary, i.e. the frequency must be real. For an observer moving with the flow the sound field in the duct with attenuation is not stationary however. Therefore in the solution (36) valid for the moving coordinates the angular frequency  $\bar{\omega}'$  must be allowed to be complex.

If  $F$  denotes the potential function of the sound field, the sound pressure and the  $x$ -component of the particle velocity are given by:

$$p = -\rho \frac{dF}{dt} = -\rho \left( \frac{\partial F}{\partial t} + v \frac{\partial F}{\partial z} \right) = -\rho \frac{\partial F}{\partial t'} \quad (38)$$

$$v_x = \frac{\partial F}{\partial x} = \frac{\partial F}{\partial x'}$$

Insertion of (36) into (38) yields:

$$p = -j\bar{\omega}'q A \cos \bar{k}_x x' \cdot e^{-j(\bar{k}_z z' - \bar{\omega}'t')} \quad (39)$$

$$v_x = -\bar{k}_x A \sin \bar{k}_x x' \cdot e^{-j(\bar{k}_z z' - \bar{\omega}'t')} \quad (40)$$

The boundary conditions are that the x-component of the particle velocity  $v_x$  be zero at the rigid wall, i.e. for  $x' = 0$  and that the ratio of the sound pressure to the particle velocity  $v_x$  at the absorber, i.e. for  $x' = b$  must be equal to the wall impedance  $\bar{W}$  of the absorber. The boundary condition for  $x' = 0$  is satisfied by the expression (36). For  $x' = b$  the condition is:

$$\bar{W} = \left( \frac{p}{v_x} \right)_{x'=b} = \frac{j\bar{\omega}'q}{\bar{k}_x} \operatorname{ctg} \bar{k}_x b \quad (41)$$

By this equation the transversal wavenumber  $\bar{k}_x$  is determined by the wall impedance. By back-transformation into the unprimed coordinates the solution in the fixed coordinate system is:

$$F(x, z, t) = A \cos \bar{k}_x x \cdot e^{-j(\bar{k}_z z - \bar{k}_x Vt - \bar{\omega}'t)} \quad (42)$$

The solution in the fixed coordinate system must be stationary again. The factor of  $t$  in the exponent must be real. From the form

$$-j[(k_z - jg_z)z - (\omega' + k_z V)t + j(\delta' + g_z V)t] \quad (43)$$

of the exponent it follows therefore:

$$\delta' + \varepsilon_z V = 0 \quad (44)$$

Then the final solution in the fixed coordinate system is:

$$F(x, z, t) = A \cos \bar{k}_x x \cdot e^{-j(\bar{k}_z z - \omega t)} \\ \omega = \omega' + k_z V \quad (45)$$

The secular equation and the boundary condition

$$\frac{\operatorname{ctg} \bar{k}_x b}{\bar{k}_x} = -j \frac{\bar{\omega}}{z} \cdot \frac{1}{k_0 - \bar{k}_z M} \quad M = \frac{V}{c_0} \\ k_0 = \frac{\omega}{c_0} \quad (46) \\ \bar{k}_x^2 + \bar{k}_z^2 - \left(\frac{\bar{\omega}'}{c_0}\right)^2 = (k_0 - \bar{k}_z M)^2 \quad Z = q c_0$$

are the determining equations for the wavenumber  $\bar{k}_z$  of which the imaginary part is the attenuation constant.

## Literature

- [1] E.Meyer,  
F. Mechel,  
G. Kurtze      Experiments on the Influence of Flow on  
Sound Attenuation in Absorbing Ducts.  
J. Acoust.Soc.Am. 30 (1958) 165
- [2] F. Mechel      Schalldämpfung und Schallverstärkung in  
Luftströmungen durch absorbierend aus-  
gekleidete Kanäle  
Acustica Vol.10. No.3 (1960) 133
- [3] W. Schilz      Untersuchungen zur Wechselwirkung  
zwischen Schallfeld und Strömung im  
Windkanal, der mit porösen Absorbern und  
Helmholtz-Resonatoren ausgekleidet ist  
Acustica Vol.11 No.1 (1961) 137
- [4] H.Schlichting      Grenzsicht-Theorie  
Verlag G.Braun, Karlsruhe 1958
- [5] L. Cremer      Die wissenschaftlichen Grundlagen der  
Raumakustik, Band III: wellentheoretische  
Raumakustik  
S.Hirzel Verlag, Leipzig 1950
- [6] D.C. Pridmore-  
Brown      Sound Propagation in a Fluid Flowing  
through an Attenuating Duct  
J.Fluid Mechanics 6 (1958) 393
- [7] L. Cremer      Theorie der Luftschalldämpfung im Recht-  
eckkanal mit schluckender Wand und das  
sich dabei ergebende höchste Dämpfungs-  
maß.  
Acustica Akust.Beihefte 2 (1954) 249

## Part B

### Sound Attenuation in Wind Tunnels by Plate Absorbers.

#### 1. General Considerations Concerning Plate Absorbers for Wind Tunnels.

In addition to porous absorbers (e.g. rockwool) and Helmholtz resonators plate absorbers are used in room acoustics to control the reverberation time of rooms. Plate absorbers are resonating systems consisting of the mass of the plate and of the compliance of the air volume behind the plate or of the stiffness of the plate or of both of them. The system can be damped by partial padding the volume with porous materials or by losses incorporated in the plates. By proper design the absorber can be matched to the acoustic wave yielding high absorption in a relatively large frequency range.

For the construction of the absorber either completely pliable plates (e.g. oilcloth) are used, in which case the compliance of the air volume behind the plate is the only mechanical capacitance, or stiff plates (e.g. wooden sheets) are used, in which case the bending strength of the plate itself must be added to the compliance of the air volume.

There are two promising properties of the plate absorber, which make it appropriate for use in wind tunnels, first its smooth and tight surface, second its small depth as compared to Helmholtz resonators and to porous absorbers used in the same frequency range. The first quality is important with respect to flow conditions in wind tunnels. For a selective attenuation of noise pikes Helmholtz resonators are sometimes unsuited because of their inherently rough surfaces generating strong turbulence. The plates of a plate absorber, however, can be manufactured as a continuous, smooth wall coating. Relative to porous absorbers it is a further advantage of plate absorbers that they do not change their performance as a consequence of contamination.

There are some differences however whether a plate absorber is used for attenuation in a wind tunnel or for absorption in room acoustics. They shall be briefly discussed in the following sections.

### 1.1 Bending Resilience of the Plate.

When constructing a resonant plate absorber with the resilient volume as the only capacitance care must be taken, that the clamping of the plate (completely pliable) along its rims does not influence the resonant frequency. In order to avoid diaphragm oscillations the tension of the plate must not be too great. A slack foil, however, will be excited by the flow to flutter movements, thereby generating turbulence and shifting the resonant frequency. Therefore pliable foils can be used, if ever, only as small elements under moderate tension with a resonant frequency determined by the resilient volume and the clamping.

Much more convenient for use in wind tunnels are plates resistant to bending, the resonant frequency being determined by the normal modes of the plate oscillation. The air volume behind the plate is only of inferior importance for the resonant frequency. It can be used, however, for an additive damping of the vibrations besides the losses incorporated in the plate itself.

### 1.2 Dimensions and Frequency Range.

The surface area of completely pliable plates does not enter into the resonant frequency of the absorber. With resilient plates however the scale and the form of the plate together with the manner of the clamping of the edges of the plate determine the normal frequencies of such a plate of a given material. This leads at once to a design condition for

plate absorbers for use in wind tunnels. Here the sound wave propagates parallel to the absorber surface. Since the plates are most effective when vibrating in their fundamental mode, the length of the plates in the direction of the tunnel axis must be smaller than a half of the sound wave, if annoying interferences between air-borne sound and bending oscillations are to be avoided. The duct used in the following measurements had a cross sectional area of  $30 \times 100 \text{ mm}^2$ . So the area of a plate element was limited to  $100 \times 100 \text{ mm}^2$  in the maximum. This in turn leads to relatively high resonant frequencies of resilient plates. Because of the small cross sectional area of the duct and of the high resonant frequencies the following measurements must be considered as model tests only.

### 1.3 Mechanism of Attenuation.

In room acoustics the absorptivity of an absorber is its essential characteristic. Only the energy absorbed by the system contributes to the final damping of the room. In contrast hereto a high attenuation in ducts can be achieved not only by dissipation of acoustic energy (dissipative attenuation) but also by reflection of the energy towards the source, which is a characteristic of the reactive attenuation achieved by mismatching the absorbers wall impedance. The high values of maximum attenuation with Helmholtz resonators as wall coating are caused by this reactive attenuation. High values of reactive attenuation achieved by undamped resonant systems has an inherently small bandwidth. Therefore attenuation over a broad frequency range mostly will be realised by a proper combination of reactive and as well as dissipative attenuation. This will be illustrated in the following by some measurements.



#### 1.4 Coupling by Structure-Borne Sound.

If a mechanical coupling of resilient plates with one another takes place at the clamping of the plate edges, a bending wave may be excited which propagates along the plates, being nearly undamped, if the attenuation of the air-borne sound is achieved predominantly by reactive attenuation. This bending wave can radiate sound into the duct. Thereby the resulting attenuation of the air-borne sound in the duct can be sharply decreased. Besides from this, interferences between the sound radiated from the plates and the sound propagating in the duct will inhibit an exact measurement of the attenuation in the duct. Therefore mechanical coupling between the single plate elements must be carefully avoided. This decoupling was guaranteed in the following measurements by gluing the plates on a grating of foamed rubber which transfers nearly no shear stresses. A smooth surface can be achieved by a thin, pliable foil connecting adjacent plates with one another.

### 2. Design and Measuring Results of Some Types of Plate Absorbers.

#### 2.1 Experimental Set-Up.

The duct used in these measurements was of a free cross sectional area of  $30 \times 100 \text{ mm}^2$ . At the entrance to the lined section of the duct a sine wave is added to the flow. The decrease of the sound level is registered continuously along the duct axis with the help of a probe microphone. The attenuation in decibels per meter is evaluated from the registered curves. Reflections at the end of the duct are suppressed by proper matching to the diffusor.

For some types of absorbers the phase velocity of the acoustic signal was measured as well (for flow velocity zero).

The factor

$$c_v/c_0 = (1 + M')$$

$c_0$  = phase velocity for air at rest

$$c_v = c_0 + \text{flow velocity } V$$

$$M' = V/c_0 = \text{Mach number}$$

allows for a correction of the attenuation, measured for different flow velocities, with regard to the convection of the signal by the flow. Thus a change of the acoustic energy density by the flow is eliminated.

## 2.2 Absorbers with Completely Pliable Plates.

The test section of the duct lined with the absorber had a length of 1.30 m. The pliable plate consisted of a synthetic foil 0.05 mm thick. Flutter movements of the foil were reduced by use of a supporting frame consisting of a troilite lattice with the lattice dimensions of  $31 \times 31 \text{ mm}^2$ . The foil was moderately prestressed. The resilient air volume was  $22.5 \text{ cm}^3$  per lattice element. This leads to a resonant frequency of 1.06 kc.

The unbroken lines in Fig.28 show the results of the attenuation measurements with this absorber. For flow velocity zero the resonant frequency is marked by a distinct maximum of attenuation (120 dB/m). With nonvanishing flow velocities the stress of the foil increases with increasing flow velocity due to the static excess pressure in the duct. As a consequence the resonant frequency is shifted. At the same time the resonance width becomes larger and larger and the maximum attenuation decreases. With increasing flow velocity the oscillation of the foil becomes more and more a diaphragm oscillation.

In the same graph are entered the results with the same absorber but now the foil perforated (about 1 mm diameter) at two opposite corners of each lattice element thus procuring a pressure compensation between duct and resilient volume. By

this perforation the resonant frequency is decreased to 0,97 kc. The influence of the flow on the attenuation remains nearly the same, the shift of the resonance frequency, however, has become distinctly smaller.

The attenuation with these two absorbers is a predominantly reactive one. In a further measurement the absorber was damped by a layer of rock wool 1 cm thick inserted into the resilient volume of each lattice element. Fig.29. By the losses due to the rock wool the resonance width has strongly increased. At the same time the maximum attenuation for air at rest has decreased to 105 dB/m. For a flow velocity of about 20 m/sec this absorber reveals a somewhat better attenuation than the preceding absorbers. For higher flow velocities however the attenuation decreases to very small values for this absorber as well. Therefore these absorbers with a thin foil as a vibrating plate can be used only for flow velocities up to 20 m/sec.

These measurements reveal the general behaviour of vibrating absorbers with reactive attenuation, namely that they react very sensitively upon disturbances due to flow and turbulence; the attenuation decreases from very high values with air at rest in the maximum of resonance down to only moderate values of attenuation if a turbulent flow is present.

### 2.3 Absorbers with Rigid Plates.

In order to achieve a mass-spring system with a rigid plate the plates must be unclamped. This was possible by combination with a solid spring. The absorber was realised by use of a plate of aluminium ( $50 \times 100 \times 0.5 \text{ mm}^3$ ) as the mass element and of a 5 mm thick layer of foamed rubber as the resilient element. Corresponding to the compliance of the foamed rubber a resonant frequency of 1.3 kc was measured. Due to the great internal losses in the resilient element the system is damped so much that it is strongly mismatched to the sound wave in the duct. As a consequence the frequency response of the absorber reaches a maximum attenuation of only 28 dB/m at the resonance frequency. The attenuation decreases only little with flow superimposed.

## 2.4 Absorbers with Resilient Plates.

A resilient plate vibrates in its normal modes, the normal frequencies of these modes being determined by the elastic properties of the plate, its dimensions and the manner in which the edges of the plate are clamped. With the following types of absorbers the single elements are glued on a lattice of foamed rubber for mechanical decoupling. The  $Q$  value of the plate oscillation is determined by the imaginary part of the shear modulus of the plate material, by the losses incorporated in the air space behind the plate and by eventual friction losses of the clamping.

The first absorber of this type was composed of plates of pertinax of  $100 \times 90 \times 1 \text{ mm}^3$ . Corresponding to the low losses of the pertinax plates the attenuation in the duct is a reactive one with a corresponding small bandwidth. Arrangement and results for this absorber are plotted in Fig.30. The maximum attenuation is 90 dB/m. In the same graph are entered the curves for the attenuation corrected with the factor  $(1 + M')^{-1}$  for flow velocities ranging from 50 m/sec for upstream propagation of the signal to 65 m/sec for downstream propagation of the signal. Besides the resonance frequency all these curves coincide with the curve for air at rest. In the neighbourhood of the resonance the corrected curves as well reveal a marked dependence from flow velocity leading to a variation of the corrected attenuation within the dashed region. The attenuation there decreases with increasing flow velocities, for both directions of sound propagation relative to the direction of flow. Nor can it be expected, from the discussion in Part A, section 4, that the simple multiplication by  $(1 + M')^{-1}$  will completely eliminate the influence of the flow for frequencies with predominantly reactive attenuation.

If losses are inserted in the volumes behind the plates the bandwidth of the attenuation is only little increased associated by a decrease of the maximum attenuation by about 20 dB/m.

In order to incorporate higher losses of the plate, vibration plates of verneer 0.6 mm thick were used. For mechanical decoupling of the single plates they are glued again on a lattice of foamed rubber with the lattice dimensions of  $80 \times 90 \text{ mm}^2$  and 15 mm height. Several tests showed that the results were best, when the shape of the plate was near to square.

The plates of verneer are anisotropic in their elastic properties due to their fibrous structure. As a consequence the stiffness is smaller for bending across the grain and corresponding to the deformation of the material the internal losses are greater for this direction of bending. In all measurements described below the grain of the sheets is along the axis of the duct. The lateral dimension across the grain is 90 mm.

Measured attenuation values for an absorber consisting of verneer sheets are plotted in Fig. 31 in their corrected form [by the factor  $(1+M')^{-1}$ ] for flow velocities up to 50 m/sec. The frequency response shows two frequencies of high attenuation, where the attenuation behaves quite different for flow superimposed. The half width of both peaks for air at rest differs as well. ( $4f/f_{\text{res}} = 0.027$  and  $0.018$  resp.) These two peaks can be associated to the resonances of vibration across the grain and along the grain. The relative values of the resonant frequencies and of the losses of the vibrations are in accordance with the above statements. As a consequence the second maximum for 2.15 kc would correspond to a more reactive attenuation due to a vibration with low losses, whereas the maximum for 1.85 kc would represent a more dissipative attenuation of a normal mode of the plate with higher losses. This classification is corroborated by the behaviour of the attenuation in the two peaks for superimposed flow. Only the peak of the reactive attenuation is strongly decreased whereas the corrected values

of the attenuation in the other peak coincide with the curve for air at rest within the indicated deviations. Another hint for the different quality of the two resonances can be drawn from the frequency response of the phase velocity in the duct revealing only a small dispersion for 1.85 kc compared with the great dispersion for 2.15 kc. A sketch of the frequency response of the measured phase velocity is entered in Fig.31.

By the two resonances the absorber shows a relatively great bandwidth exceeding by far the corresponding values of the foregoing absorbers. The possibility of a further increasing of the bandwidth of this absorber by additive losses in the air volume behind the plates was investigated according to Fig.32. A rock wool layer 1 cm thick was put behind the plates. In Fig.13 again the corrected values of attenuation are shown for flow velocities up to 65 m/sec. The lower peak now is at 1.7 kc. With an only small decrease of the maximum attenuation the bandwidth could be distinctly increased ( $\Delta f/f_{\text{res}} = 0.05$ ). The second (reactive) peak has decreased very much by the inserted losses. Only for air at rest it surpasses the average values of attenuation. The decrease of the maximum attenuation with this absorber to 75 dB/m as compared to 118 dB/m of the undamped absorber is "compensated" by a gain in bandwidth, the attenuation being almost independent from flow velocity.

## 2.5 Comparison of the Different Types of Absorbers.

The different absorbers are compared with one another in Fig.33. As functions of flow velocity there are plotted the following values:

Maximum attenuation,

Bandwidth (in octave ranges) of the frequencies, for which the attenuation is greater than 40 dB/m,

Half width of the attenuation maximum ( $\Delta f/f_{\text{res}}$ ).

As mentioned already above the absorbers with pliable foils can be used only for velocities up to 20 m/sec because of their strong decrease of the maximum attenuation. In contrast to this behaviour the absorbers with resilient plates show a relatively good constancy of the attenuation with respect to superimposed flow. The use of a low loss material (e.g. pertinax) leads to a selective absorber. By absorbers with verneer sheets and losses in the air space behind the plate frequency ranges of about one octave can be reached for which the attenuation is greater than 40 dB/m.

## Part C

### Experiments about the Influence of Sound Fields on the Boundary Layer of Flow.

#### Summary

The influence of the sound field in front of a vibrating plate upon the boundary layer of air flow is investigated. In a duct with low turbulence level ( $Tu < 10^{-3}$ ) the development of the boundary layer along the plate is measured for different strengths of the initial boundary layer disturbances at the leading edge and for different oscillation amplitudes of the plate vibrating at the constant frequency of 14 kcps. The initial disturbances could be varied at will from laminar boundary layer up to fully turbulent boundary layer by the suction rate at the leading edge of the plate. Already for moderate velocity amplitudes of the plate ( $v < 5 \cdot 10^{-3}$  cm/sec) the initial distortions are damped out as long as they are not fully turbulent. The attenuation is greatest for Tollmien-Schlichting-Waves (TSW). The shear stress of the flow is also reduced by the plate oscillations.

#### List of Symbols

$V$	central flow velocity
$\sqrt{v^2}$	r.m.s. velocity fluctuation
$\sqrt{v_{\max}^2}$	maximum r.m.s. velocity fluctuation
$x, y, z$	coordinates
$Tu = \sqrt{v^2}/V$	turbulence level
$\delta^*$	displacement thickness
$\phi = \int_0^y \sqrt{v^2} dy$	total distortion
$\tau = -\rho \overline{v_x v_y}$	shear stress
$w/s$	occurrence frequency of turbulent spots



In the past year investigations about the influence of strong sound fields on the boundary layer of flow over a flat plate were started. The experiments shall be performed in two steps:

- a. The boundary layer over a rigid plate vibrating perpendicularly to its surface and radiating sound into the boundary layer.
- b. The boundary layer over a porous plate with sound radiation through the plate.

The acoustic particle velocity normal to the surface of the porous plate acts like a periodic suction and blow-out. This is expected to control the development of the boundary layer and of the wall turbulence. In connection with these measurements also the influence of porous sound absorbers on the boundary layer shall be investigated.

The present report deals with the construction of the test duct for these measurements and with investigations to section b. For the present measurements only one frequency of oscillation of the plate was used. The measurements shall be continued with respect to the frequency dependence of the acoustic boundary layer control.

#### 1. Construction and Test of the Wind Tunnel.

The achievement of a low turbulence level was the most important design principle of the wind tunnel. For the investigation of the Tollmien-Schlichting waves (TSW) in the boundary layer a turbulence level  $Tu < 10^{-3}$  was a prerequisite. The flow is generated by a centrifugal blower. Through two acoustic silencers it is conducted to a wide-angle diffuser, Fig. 34. This leads to a smoothing duct with the lateral dimensions  $50 \times 50 \text{ cm}^2$  and the length 150 cm. The finemeshed screens  $G_1 - G_3$  avoid flow separation in the diffuser and procure an equal distribution of the flow over the smoothing

duct. The screen  $G_4$  before the contraction cone is for the same purpose.

Much care was used for the construction of the contraction cone. Its contraction ratio is 1:25. The profile of the cone is calculated according to G.S.Ram, who has found, that the best performance of the cone is for a profile given by a polynomial of the 9th degree the first three derivatives being zero at the inlet of the cone and the lowest five derivatives vanishing at the outlet of the cone.

The contraction cone is followed by the test section,  $10 \times 10 \text{ cm}^2$  wide and 2 meters long. The duct is terminated by an 8-degree diffuser which reduces reactions from the blow-out into the test section. The screens  $G_5$  and  $G_6$  again avoid stall in the diffuser. As the measuring probe a hot-wire probe is used. It can be moved by dovetails along the duct axis and perpendicular to it. The hot-wire probe is calibrated by a Pitot probe.

For a test of the duct performance the r.m.s. turbulent velocity on the duct axis was measured. The turbulence level  $Tu = \sqrt{v'^2}/V$  is plotted in Fig.35 as a function of the flow velocity  $V$  on the duct axis. In the interesting velocity range the turbulence level is about  $Tu \sim 0.8 \cdot 10^{-3}$ .

Profiles of the mean flow velocity and of the turbulence for two values of  $V$  are plotted in Fig.36 and Fig.37. For a wall distance  $h > 1 \text{ cm}$  ( $h/h_0 > 0.2$ ) the flow profile is plane with a turbulence level  $Tu < 10^{-3}$  over the full height of the duct. The leading edge of the plate over which the boundary layer is investigated is put into this wall distance.

## 2. Measuring Equipment.

A schematical view of the measuring equipment is given in Fig.38. The output signals from the hot-wire probe are analysed either by an oscilloscope or by an electronic counter or by a slow r.m.s. voltage meter indicating the r.m.s. value for statistical pulses too. The measuring object is a plate,

100 x 400 mm<sup>2</sup>, into which an aluminium transducer is inserted in such way that its surface of 70 mm diameter is in the plane of the plate surface. The transducer, an aluminium cylinder driven electro-dynamically in its first longitudinal resonance at 12.4 kc, oscillates freely in a ring slot 0.1 mm wide. The narrow slot, airtight towards the outside, does not disturb the boundary layer. The maximum oscillation velocity of the surface is about 1 cm/sec. The radiated sound field is nearly plane and has the diameter of the transducer. Towards the periphery the sound pressure decreases with a slope of about 7 dB/cm (measured at the distances 4 mm and 17.5 mm from the plate). By reflection at the opposite wall of the duct a standing wave is formed. The first pressure node is at 7 mm above the plate.

Below the leading edge of the plate borings in the duct wall are for the suction of the air choked by the transducer. By regulation of the suction rate the flow distortion at the leading edge, i.e. the turbulence level at the measuring station, can be varied from laminar flow to full turbulence.

The plate with the transducer is supported by three adjustment screws by which the angle between the plate and the flow can be controlled. For most measurements reported below the plate was parallel to the flow.

### 3. Measurements.

The measurements cover the whole range: from laminar flow to full turbulence. This range can be subdivided into three sections:

- a. Laminar boundary layer with superimposed Tollmien-Schlichting waves (TSW).
- b. Excitation of turbulent spots by great TSW-amplitudes.
- c. Fully turbulent flow.

With the arrangement used in our measurements the turbulence level for laminar flow without TSW is  $1.3 \cdot 10^{-3}$  in the boundary layer. This is, for a flow velocity  $V = 25$  m/sec, equivalent

to a r.m.s. turbulent velocity of 0.03 m/sec (all measurements are for the flow velocity  $V = 25$  m/sec unless otherwise specified).

The TSW are generated by an accidental disturbance, then increase during propagation with the velocity  $c_{TSW}$  in an exponential scale according to the equation for the velocity

$$v = A e^{\alpha x} e^{j\omega(t - \frac{x}{c_{TSW}})} .$$

The attenuation constant  $\alpha$  and the frequency  $\omega$  are determined by the properties of the boundary layer ([4] of Part A). The theory delivers a certain value of  $\alpha$  for each pair of frequency  $\omega$  and of Reynolds number. Thereby the stable waves ( $\alpha < 0$ ) are separated from the unstable, increasing, waves ( $\alpha > 0$ ) by the curve for the neutral waves ( $\alpha = 0$ ).

If the amplitudes of the TSW become greater than 0.13 m/sec they break up into statistical turbulent spots with velocity fluctuations greater by a factor 10. The frequency of these spots increases exponentially along the plate. At a frequency of about 400 to 500 spots per second ( $Tu \sim 8$  per cent) the individual spots penetrate one another and break up into full turbulence.

Fig.39 shows turbulence profiles for the different states of the boundary layer thickness and in the turbulence level the double-logarithmic scale was used.

The TSW too are formed by a rotational motion, of constant frequency and constant extension, however. Therefore the turbulence level at the core of these eddies is a minimum (in Fig.39 at 0.05 mm wall distance). Between the upper and the lower maximum is a phase lag of 180 degrees. The minimum of the turbulence level is yet visible in the profiles for the range of turbulent spots. Here it is at a wall distance of about 0.5 mm.

By the oscillation of the transducer a pressure fluctuation periodic in time is superimposed to the boundary layer. This fluctuation affects the amplitude of the TSW. The frequency

of the oscillation, 12.4 kc, is far beyond the region of unstable TSW [4]. As a function of the velocity amplitude of the sound field and of the path length along the plate the amplitude of the TSW was measured. The amplitude of the TSW without wall oscillation was adjusted by the plate angle. From these measurements the exponent  $\alpha$  was determined (the index  $i$  refers to the particle velocity of the sound field).

In all cases <sup>\*)</sup> the exponent  $\alpha$  became smaller with increasing oscillation amplitude. The picture in Fig.40 taken from the oscilloscope show the change of the amplitude of the TSW when the transducer is switched on and off. Two examples of the amplitude measurements are represented in Fig.41. The curve with  $\alpha_0 = 0.135$  is measured with the plate parallel to the flow. For the oscillation velocity amplitude  $v = 5 \cdot 10^{-3}$  cm/sec  $\alpha$  becomes negative. The second curve with  $\alpha_0 = -0.02$  is measured with a decrease of the static pressure along the plate. Here the favourable pressure gradient keeps the TSW stable. With superimposed sound however the exponent  $\alpha$  is further decreased. The third curve of Fig.8 refers to the attenuation of the spot frequency and is discussed below.

From these measurements it can be seen that the natural distortions of the boundary layer can be damped out by superposition of a sound field of appropriate frequency and amplitude, and the boundary layer can be kept laminar.

The exponent  $\alpha$  was measured by amplitude measurements of the TSW along the surface of the transducer. In the range of the turbulent spots the surface of the transducer is too small to allow for exact measurements over this short length, as the

---

<sup>\*)</sup> For very great oscillation amplitudes also an increase of the natural flow distortions was observed. This can be caused by imperfections of the experimental set-up. It was not studied in detail.

statistical occurrence of the spots there causes too great scattering of the measured values. Therefore the initial distortion of the flow at the leading edge of the plate was adjusted by the suction rate in such way that several measurements along the transducer surface fitted at its ends. By this method the increase of the spot frequency over a range from 0 to 500 spots per second could be measured. For the flow velocity of 25 m/sec this corresponds to an equivalent length of the measuring path of about 40 cm. In each section of this composed measuring path the spot frequency was measured as a function of the oscillation velocity and of the distance from the leading edge. The result of this measurement is plotted in Fig.42. The individual sections fit well to an exponential curve. The exponent  $\alpha$  was taken from the logarithmic representation of this curve.

The ordinate of this curve is not the maximum velocity fluctuation but the spot frequency. The spot frequency can be taken as a measure of the distortion of the boundary layer, as the intensity of the singular eddies only changes by about 5 per cent. For these measurements, therefore, an absolute calibration of the hot-wire probe is not necessary. For a spot frequency greater than 400 per second the individual spots could no longer be counted. The spatial separation between them is so small that they penetrate one another. In this case there are no longer TSW between the individual spots. The spots excite directly subsequent spots. This difference in the mechanism of excitation is important for the damping of boundary layer distortions by sound superposition.

The exponent of the spot excitation is also plotted in Fig.41 as a function of the oscillation velocity. The curve follows exactly the corresponding curve for the damping of the TSW measured under the same conditions. This indicates that the damping influence of the sound field is efficient directly only on the TSW and that the frequency of the turbulent spots

by this way is influenced indirectly. For this reason a suppression of the turbulent spots becomes impossible for great spot frequencies. This can be seen from the photos in Fig.43 where every time in the middle of the pictures the sound field was switched on.

The diameter of the turbulent spots is about 0.8 mm. The center of the spots is about 0.4 to 0.5 mm above the plate. As mentioned already the turbulence profile shows two maxima in the range of the turbulent spots too. The values of the lower maximum was used also for a determination of the boundary layer distortion since a clear relation exists between  $\sqrt{v_{\max}^2}$  and the spot frequency.

If the spot frequency exceeds 400 per second and the spots penetrate one another a rearrangement of the boundary layer takes place: The turbulence profile becomes broader and flat (Fig.39). The maximum velocity fluctuation  $\sqrt{v_{\max}^2}$  at first decreases whereas the total distortion

$$\delta = \int \sqrt{v^2} dy \quad \text{increases}$$

uniformly.

The following list contains some values of maximum velocity fluctuations  $\sqrt{v_{\max}^2}$ , spot frequency w/s, total distortion  $\delta$  and displacement thickness  $\delta^*$ .

		$\sqrt{v_{\max}^2}$	$\delta$	w/s	$\delta^*$
TSW	from	0,03	$2 \cdot 10^{-5}$	-	0.15
	to	0.15	$4 \cdot 10^{-5}$	-	0.2
spots	from	0.15	$4 \cdot 10^{-5}$	0	0.2
	to	1.30	$1.3 \cdot 10^{-3}$	500	1.2
full turb.	from	1.00	$1.3 \cdot 10^{-3}$	-	1.2
	to		$2.8 \cdot 10^{-3}$	-	
		m/sec	m <sup>2</sup> /sec	sec <sup>-1</sup>	mm

In the range of turbulent spots the total distortion  $\delta$  can be changed by sound irradiation by a factor of 35. This is far above the possible influencing of the fully developed turbulence.

As the complete suppression of the disturbances is impossible already for the turbulent spots as soon as they begin to penetrate one another, this possibility of reduction of the full turbulence must be excluded the more. The oscillation levels used in our measurements did not reveal an influence on the turbulence distribution. (Thereby it is assumed that the distance between the point of generation and the measuring station is held constant. It is clear that a shift of the point of generation by damping of the TSW results in a change of the turbulence level at the measuring station as the turbulence level increases with increasing distance).

A weak change of the intensity of the fully developed turbulence was observed for much higher oscillation amplitudes. Fig. 44 shows some measured turbulence profiles. Parameter is the acoustic particle velocity. The flow profile has a point of inflection according to the high turbulence level. From Fig. 44 it can be seen that the influence of the sound field is very weak. The relative change of the total distortion is about 12 per cent for oscillation velocities as great as 0.5 cm. The main influence is visible on the sides of the profiles. The maxima were decreased only by about 3 to 4 per cent.

For the different phases of the boundary layer development the shear stress  $\tau(y)$  was determined from the measured turbulence velocities  $\sqrt{v_x^2}$  and  $\sqrt{v_y^2}$  according to

$$\tau(y) = -\rho \overline{v_x v_y} = -\rho \cdot \psi \cdot \sqrt{v_x^2} \cdot \sqrt{v_y^2}.$$



The correlation factor  $\psi$  was taken from literature as 0.5. The approximate shear stress profile is plotted in Fig.45. With sound irradiated into the boundary layer the shear stress is reduced over the whole boundary layer thickness due to the damping of the components  $v_x$  and  $v_y$ .

The change of the fully developed turbulence by sound is most clearly expressed by the frequency analysis of the turbulence spectrum. These spectra are shown in Fig.46. The wall distance of the hot-wire probe for these measurements was that of the upper slope of the turbulence profile. The lower curve belongs to the measurement with the sound of 12.4 kc irradiated. The turbulence reduction takes place especially at the lower frequencies. Eventually this can be explained by breaking up of the large eddies, which contribute to the low frequencies of the spectrum, into smaller ones.

In a further series of measurements the dependence of the damping of the boundary layer distortions by the sound field on the initial turbulence level was investigated in greater detail. For this purpose the degree of the flow distortions at the leading edge was varied by regulation of the suction rate below the plate. The flow velocity and the distance between the leading edge of the plate and the measuring probe were held constant. As a measure of the distortion the maximum velocity fluctuation

$$\sqrt{v_{\max}^2}$$

in the turbulence profile at the upstream edge of the transducer was used. The distortion of the boundary layer at the center of the transducer is given by

$$\delta = \int_0^{2.5 \text{ mm}} \sqrt{v^2} dy.$$

This distortion level was measured as a function of the initial distortion level and of the oscillation amplitude of

the transducer. The results are represented in Fig.47. The parameter there is the acoustic particle velocity. Within the dashed region the boundary layer with singular spots converts into the fully turbulent boundary layer.

The optimum damping of the distortions is already achieved at the oscillation velocity of  $6.8 \cdot 10^{-3}$  cm/sec. Up to velocity fluctuations of the magnitude 0.38 m/sec the flow is kept laminar by the sound field. ( $\bar{a} = 0.02 \cdot 10^{-3}$  m<sup>2</sup>/sec). Without wall oscillation the value of  $\bar{a}$  is  $1.2 \cdot 10^{-3}$  m<sup>2</sup>/sec. That is the value for the transition to full turbulence. The individual spots penetrate one another and complete suppression of the distortion is no longer possible. (Fig.43). Regardless of sound irradiation the spot frequency further increases. If the curve with damping enters into the transition zone ( $\sqrt{v_{\max}^2} = 0.65$  m/sec;  $\bar{a} = 0.8 \cdot 10^{-3}$  m<sup>2</sup>/sec) the mechanism of damping breaks down and the transition to turbulence occurs suddenly if the distortion is only little increased.

With the other curves the superimposed acoustic particle velocity is smaller. The nature of the curves is similar. Only the onset of turbulence is earlier because of the smaller damping of the TSW.

Finally, the whole development of the boundary layer with different oscillation amplitudes is represented in Fig.48. The curves are composed from measuring results in the several phases of the development of the boundary layer. Abscissa of the graph is the distance along the plate, ordinate is the maximum r.m.s. velocity fluctuation  $\sqrt{v_{\max}^2}$  in a logarithmic scale.

The ordinate is subdivided into four zones:

1.  $\sqrt{v_{\max}^2} \leq 0.03$  m/sec : duct turbulence (pseudo-laminar)
2.  $0.03 < \sqrt{v_{\max}^2} \leq 0.12$  m/sec: Tollmien-Schlichting waves
3.  $0.15 < \sqrt{v_{\max}^2} \leq 1.00$  m/sec: turbulent spots
4.  $1.4 < \sqrt{v_{\max}^2}$  : full turbulence

The zones are separated from one another by transition zones where the change of the boundary layer takes place.

As the starting point of the TSW the origin of the abscissa was chosen. Without sound irradiation the boundary layer is fully turbulent after a traveling length of about 40 cm. With increasing sound level the exponent of the TSW and of the occurrence frequency of the turbulent spots is more and more decreased. (Parameter of the curves is the acoustic particle velocity in cm/sec). By this decrease the traveling path until transition to turbulence is more and more increased. By extrapolation, a traveling length of 220 cm with a sound amplitude of  $4.3 \cdot 10^{-3}$  cm/sec is achieved compared to the length of 40 cm without sound. Thus by a vibrating wall of sufficient spatial extension the flow can be kept laminar over long distances even for small oscillation amplitudes (for a relation between Reynolds number and frequency as in our experiments). This is especially true for oscillation amplitudes which make the amplitude exponent of the TSW negative.

The results reported here are valid for a plane plate and a frequency of wall oscillation of 12.4 kc. Systematic measurements as to the influence of the Reynolds number were not yet performed. Preliminary measurements showed that for greater flow velocities also greater oscillation amplitudes were necessary to achieve damping of the natural flow distortions. The frequency dependence of the damping effect shall be investigated. The frequency used up to now is much higher than the frequency of instability of the TSW. Other interactions between the oscillating wall and the boundary layer are to be expected if the oscillation frequency lies within the region of unstable TSW.

## List of Figures

### Part A

- Fig. 1 Cross-sectional view of the test section with a rockwool absorber under test.
- Fig. 2 Cross-sectional view of the probe microphone.
- Fig. 3 Signal-to-noise ratio obtained with the microphone from Fig.2 for 50 Watts loudspeaker input. Dashed curves are valid for the probe used in ref.[1] of Part A.
- Fig. 4 Attenuation  $\alpha$  vs. frequency  $f$  for undamped resonators with short circular necks. Parameter: Mean flow velocity  $\bar{V} \neq 0$ .
- Fig. 5 Relative shift of resonance frequency  $f_0$  and oscillating mass  $m$  of a resonator according to Fig.4 as a function of mean flow velocity.
- Fig. 6 Attenuation  $\alpha$  vs. frequency  $f$  for undamped slit resonators. Parameter: Mean flow velocity  $\bar{V} \neq 0$ .
- Fig. 7 Comparison of the values of frequency and flow velocity of maximum deattenuation with the dispersion curves of the first and second Hartree harmonic. o---o using the mean flow velocity, • • • using the local flow velocity near the wall.
- Fig. 8 Local flow velocity  $V_{loc}$  vs. wall distance for the resonators of Fig.4 for several mean flow velocities.
- Fig. 9 Attenuation  $\alpha$  vs. frequency  $f$  for undamped resonators with short circular necks at reduced duct height  $b = 1.6$  cm. Parameter: Mean flow velocity  $\bar{V} \neq 0$ .
- Fig.10 Wavelength  $\lambda_{zo}$  and phase velocity  $c_{ph}$  in the duct without flow covered with slit resonators with the resonance frequency at 1.0 kc.
- Fig.11 Limits for the position of the dispersion curves of the first and second Hartree harmonics at frequencies above resonance. Measuring points: values of mean flow velocity  $\bar{V}$  and frequency of maximum deattenuation for several resonators.
- Fig.12 Attenuation  $\alpha$  vs. frequency  $f$  for slit resonators with partially covered slits and low resonance frequency. Parameter: Mean flow velocity.

- Fig.13 Attenuation  $\alpha$  vs. frequency  $f$  for undamped resonators with short circular necks as in Fig.4, now partially covered. Parameter: Mean flow velocity  $\bar{V} \geq 0$ .
- Fig.14 Comparison of the attenuation curves of undamped resonators with short circular necks for different degrees of covering at a mean flow velocity  $\bar{V} = 40$  m/sec.
- Fig.15 Attenuation  $\alpha$  of a porous absorber (Fig.1) for downstream propagation.
- Fig.16 As in Fig.15 but for upstream propagation.
- Fig.17 Attenuation for third-octave noise propagating downstream.
- Fig.18 Attenuation for third-octave noise propagating upstream.
- Fig.19 Wavelength and phase velocity in the duct of Fig.1.
- Fig.20 Profiles of sound pressure and phase in the duct with a porous absorber for several values of signal frequency and flow velocity. Downstream propagation.
- Fig.21 Profiles of sound pressure and phase in the duct with a porous absorber for several values of signal frequency and flow velocity. Upstream propagation.
- Fig.22 Construction of the curve of frequency response of sound attenuation with superimposed flow from the attenuation curve without flow. Downstream propagation.
- Fig.23 Construction of the curve of frequency response of sound attenuation with superimposed flow from the attenuation curve without flow. Upstream propagation.
- Fig.24 Wall impedance of the porous sound absorber.
- Fig.25 Attenuation  $\alpha$  vs. frequency  $f$  for a porous absorber with partitions. Comparison of the measured values (open points) with the calculated values (full points). Parameter: Mean flow velocity.
- Fig.26 Measured values of sound attenuation in the sound absorbing duct with superimposed flow multiplied by  $(1 + M')$  vs. signal wavelength in the duct. Downstream propagation.

**Fig.27** Measured values of sound attenuation in the sound absorbing duct with superimposed flow multiplied by  $(1 + M')$  vs. wavelength in the duct. Upstream propagation.

### Part B

**Fig.28** Attenuation vs. frequency for the absorber with completely pliable plates. Broken lines: with pressure compensation.

**Fig.29** Absorber with completely pliable plates damped by a layer of rockwool.

**Fig.30** Frequency response of attenuation for an absorber with resilient plates. Flow velocity: from 50 m/sec upstream to 65 m/sec downstream propagation.

**Fig.31** Phase velocity and attenuation for an absorber consisting of verneer-sheets.

**Fig.32** Absorber consisting of verneer-sheets damped with a layer of rockwool.

**Fig.33** Comparison of the different absorbers.

### Part C

**Fig.34** Sketch of the wind tunnel.

**Fig.35** Turbulence level at the center line of the wind tunnel.

**Fig.36** Flow velocity profiles.  $V_m$  center velocity,  $h/h_0$  wall distance.

**Fig.37** Turbulence profiles.

**Fig.38** Experimental set-up.

**Fig.39** Profiles of the flow distortions in a double-logarithmic scale.

**Fig.40** Amplitude variation of the TSW when the transducer is switched on at  $t_1$  or switched off at  $t_2$ .

- Fig.41 Amplitude exponent  $\alpha$  as a function of the oscillation velocity amplitude.
- Fig.42 Occurrence frequency of the turbulent spots as a function of oscillation velocity amplitude and of position.
- Fig.43 Change of the spot frequency when the transducer is switched on.
- Fig.44 Profiles of mean flow velocity and of turbulence level for several signal amplitudes.
- Fig.45 Shear stress vs. normalised wall distance for the cases of laminar flow, of turbulent spots and of fully developed turbulence and its change by signal irradiation.
- Fig.46 Spectrum of fully developed turbulence with and without signal irradiation.
- Fig.47 Distortion level as a function of the initial distortion.
- Fig.48 Spatial development of the boundary layer with sound superposition.

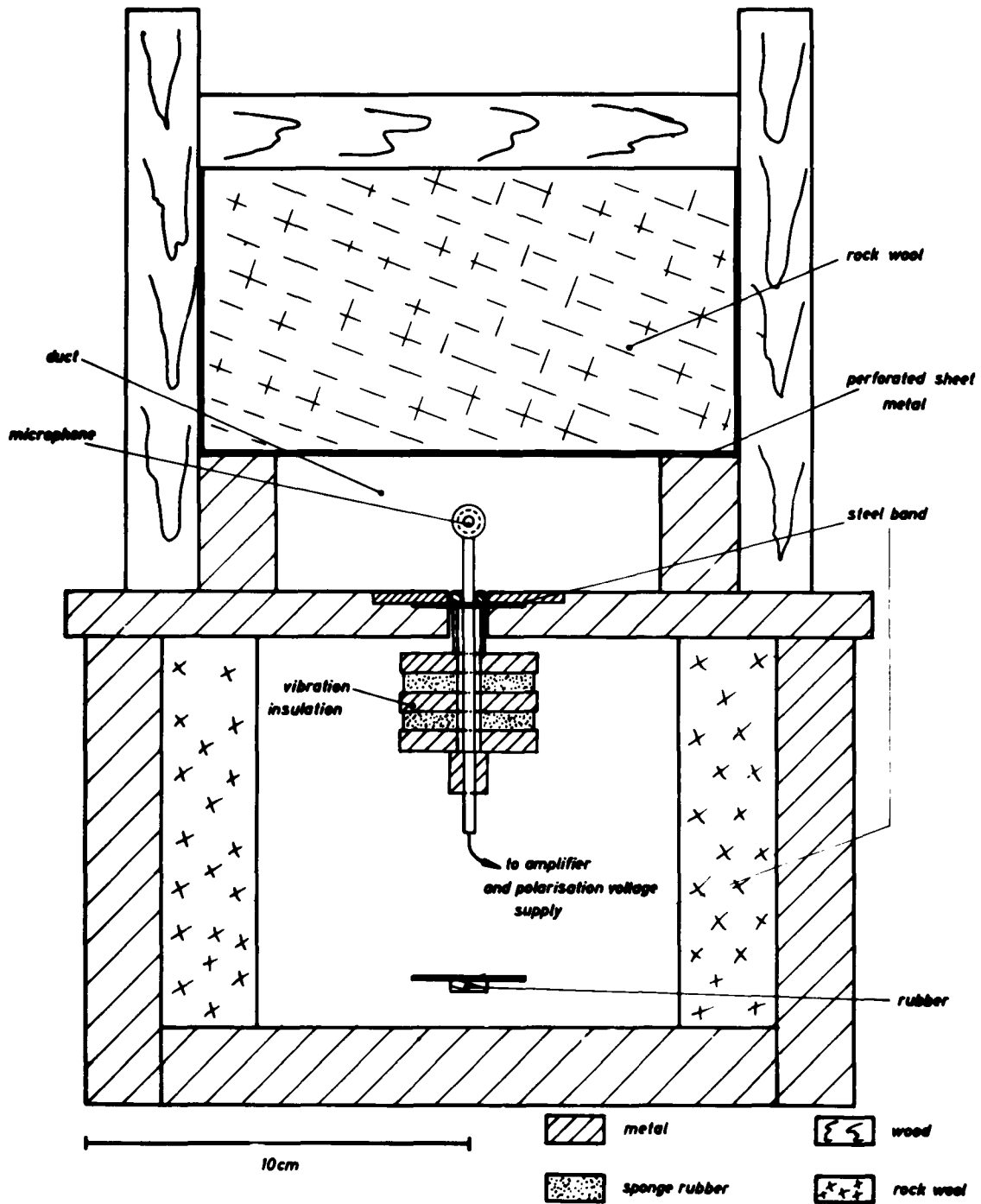


**Fig.1**

**Cross-sectional view of the test section with a rockwool absorber under test.**



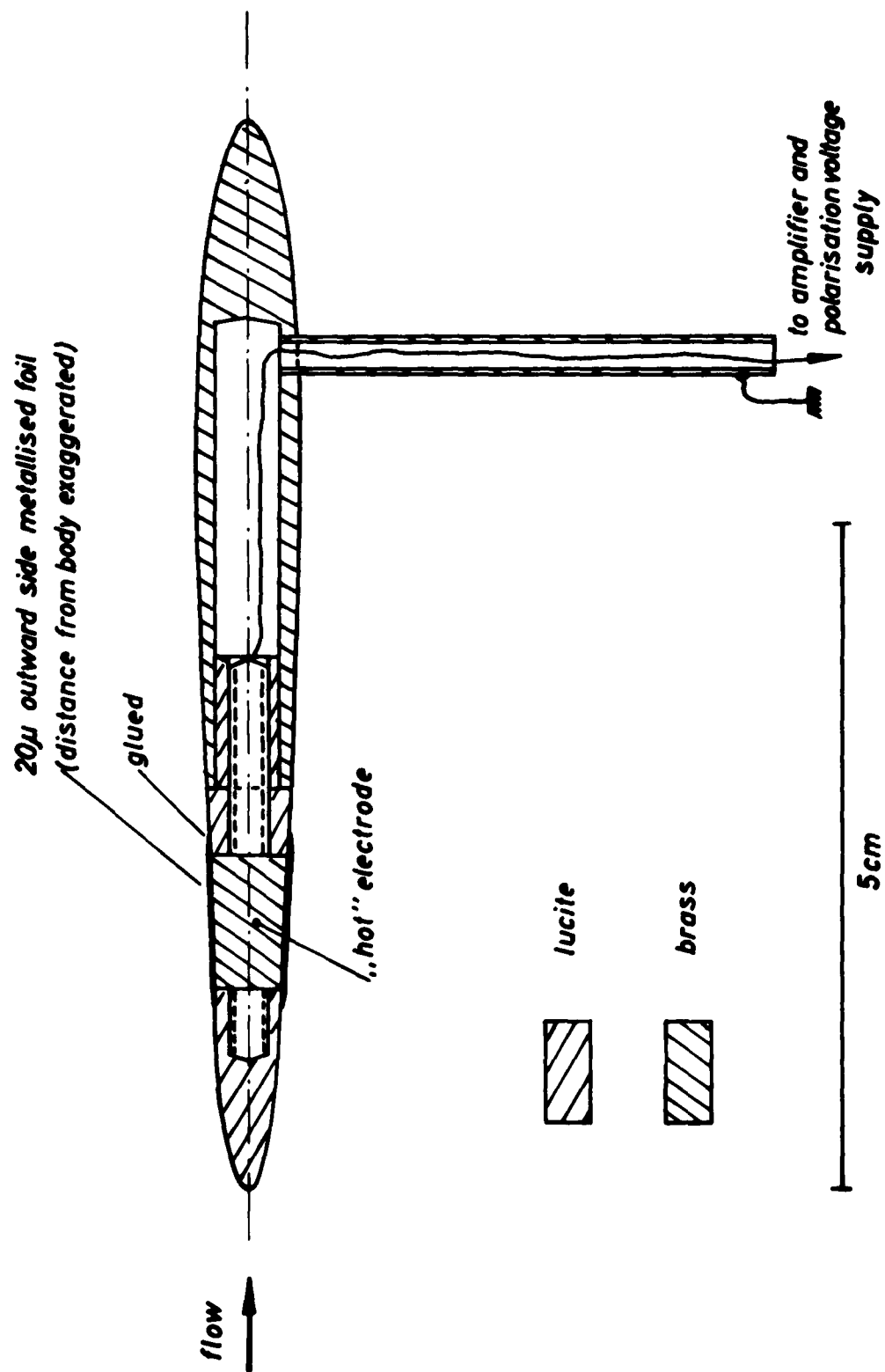


Fig.2 Cross-sectional view of the probe microphone.

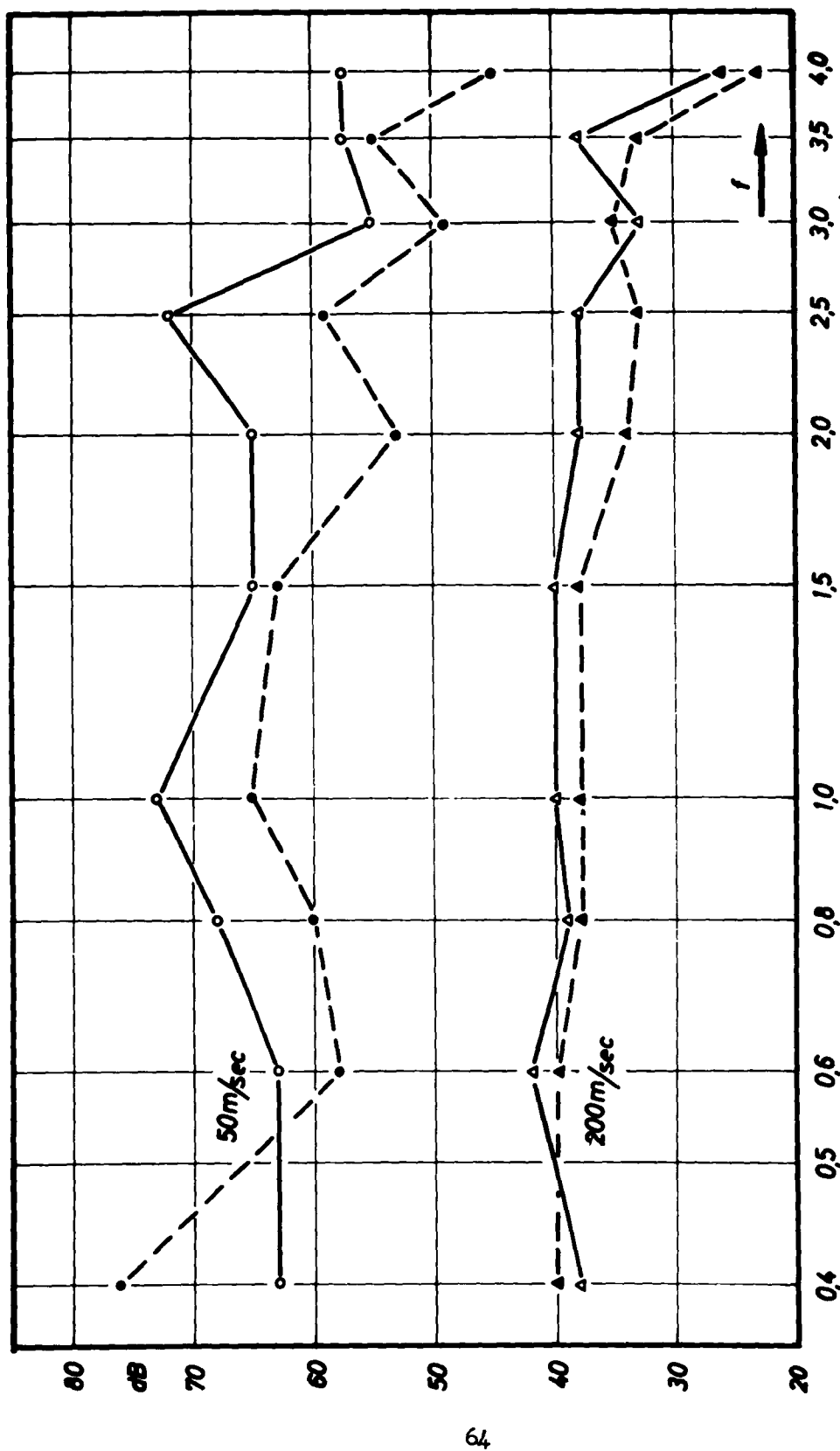
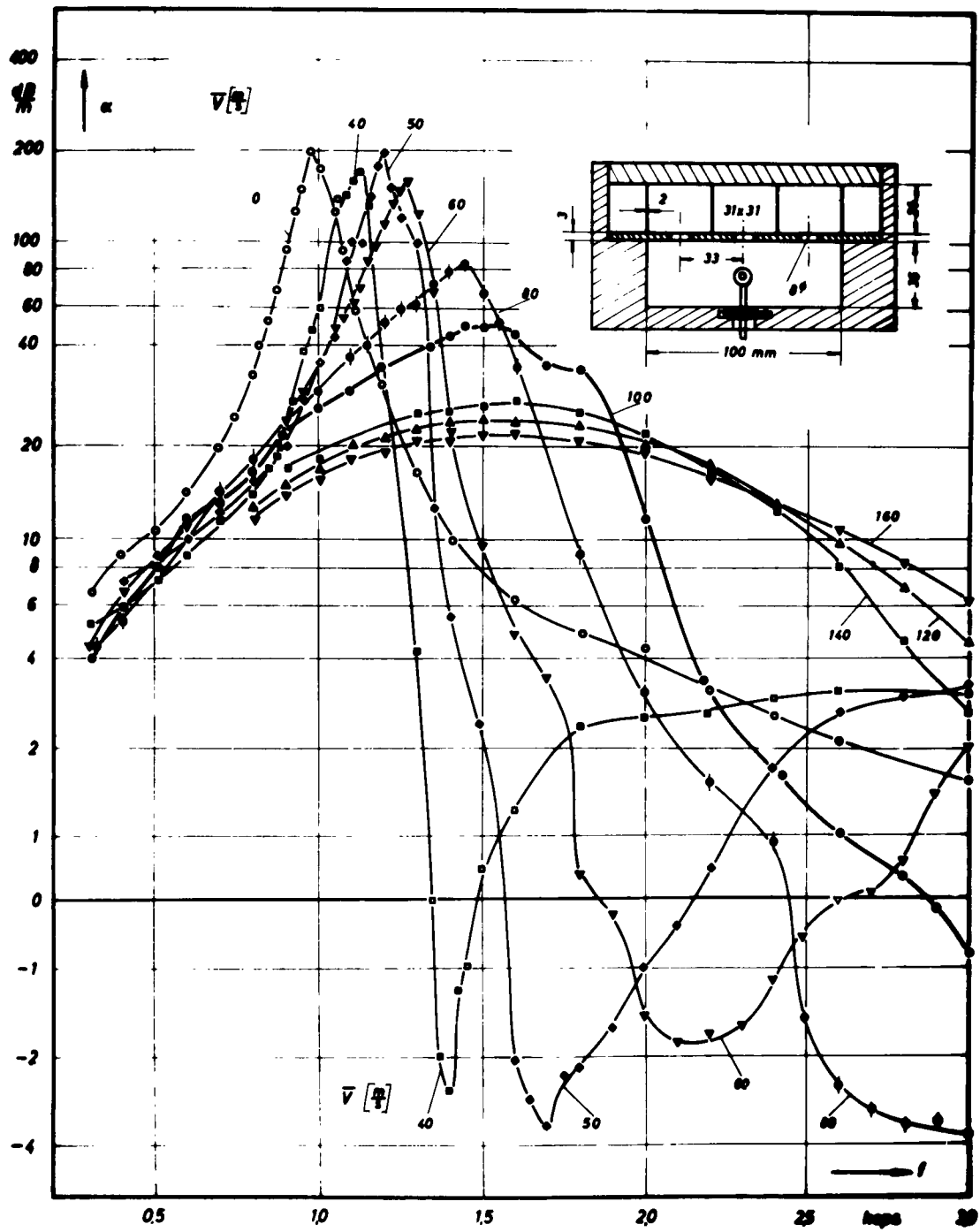
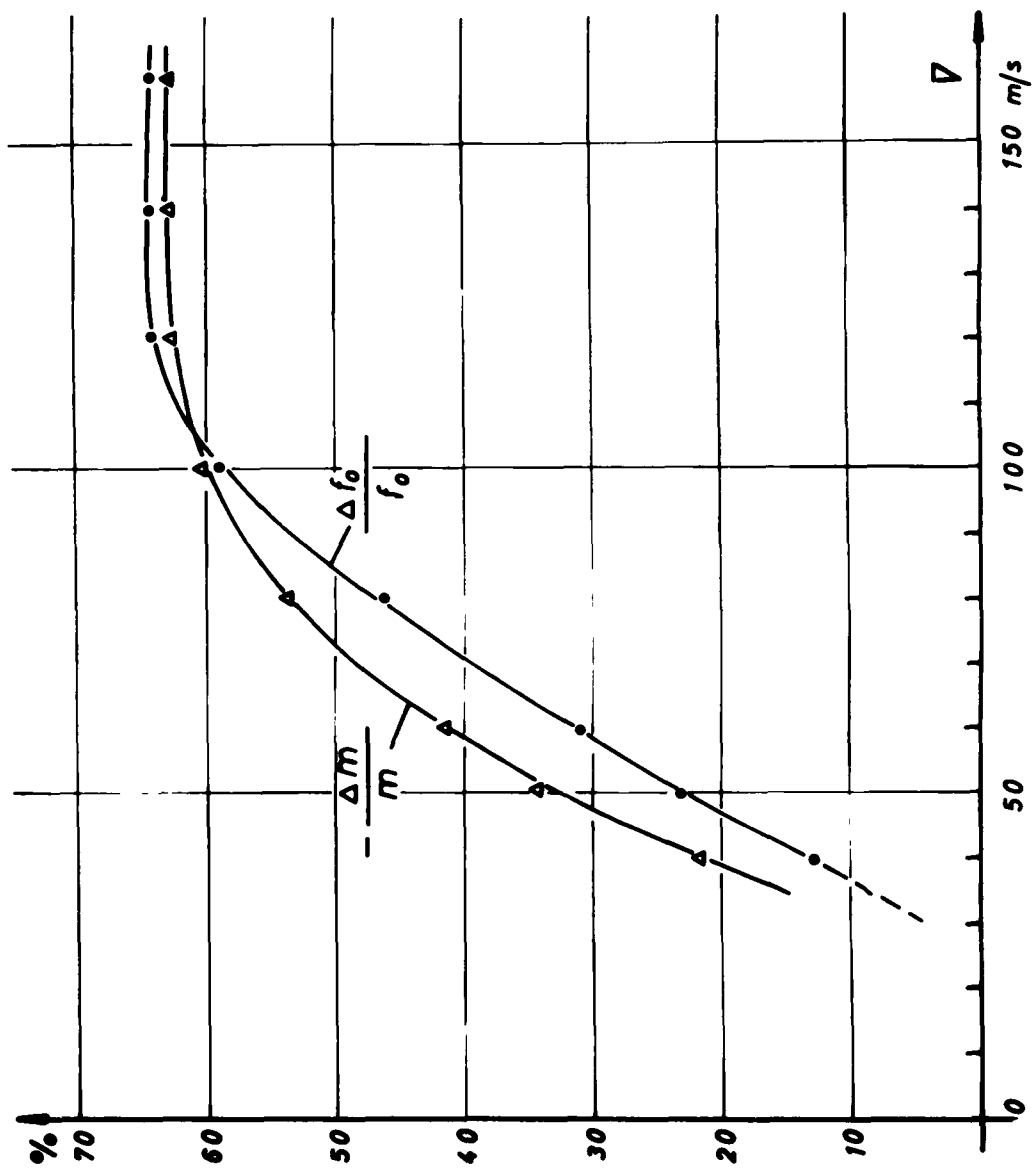


Fig. 3 Signal-to-noise ratio obtained with the microphone from Fig. 2 for 50 Watts loudspeaker input. Dashed curves are valid for the probe used in ref. [1] of Part A.



**Fig.4** Attenuation  $\alpha$  vs. frequency  $f$  for undamped resonators with short circular necks. Parameter: Mean flow velocity  $V \neq 0$ .



**Fig.5** Relative shift of resonance frequency  $f_0$  and oscillating mass  $m$  of a resonator according to Fig.4 as a function of mean flow velocity.

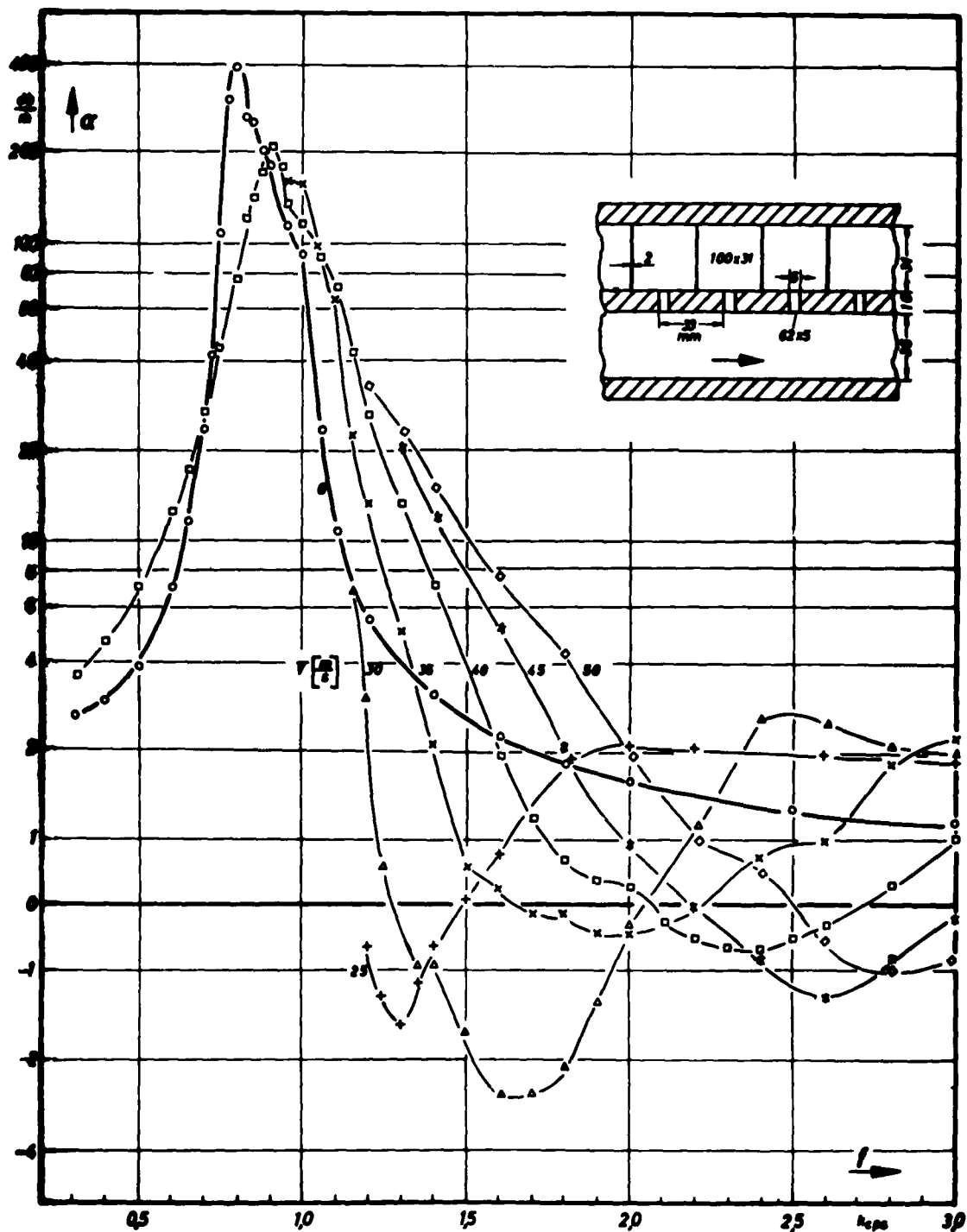


Fig.6 Attenuation vs. frequency  $f$  for undamped slit resonators.  
Parameter: Mean flow velocity  $V \neq 0$ .

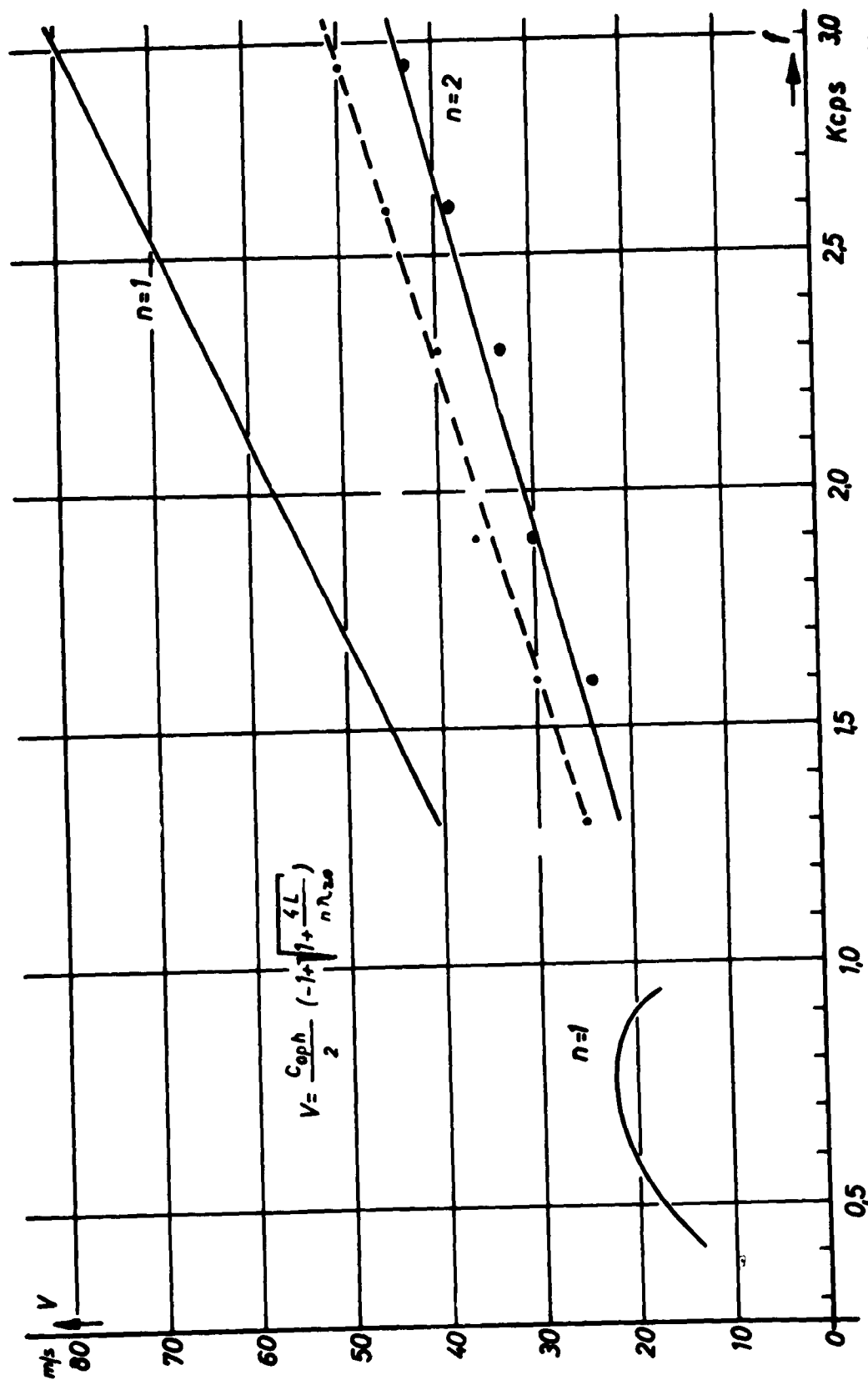


Fig. 7 Comparison of the values of frequency and flow velocity of maximum deattenuation with the dispersion curves of the first and second Hartree harmonic. o---o using the mean flow velocity, ••••• using the local flow velocity near the wall.

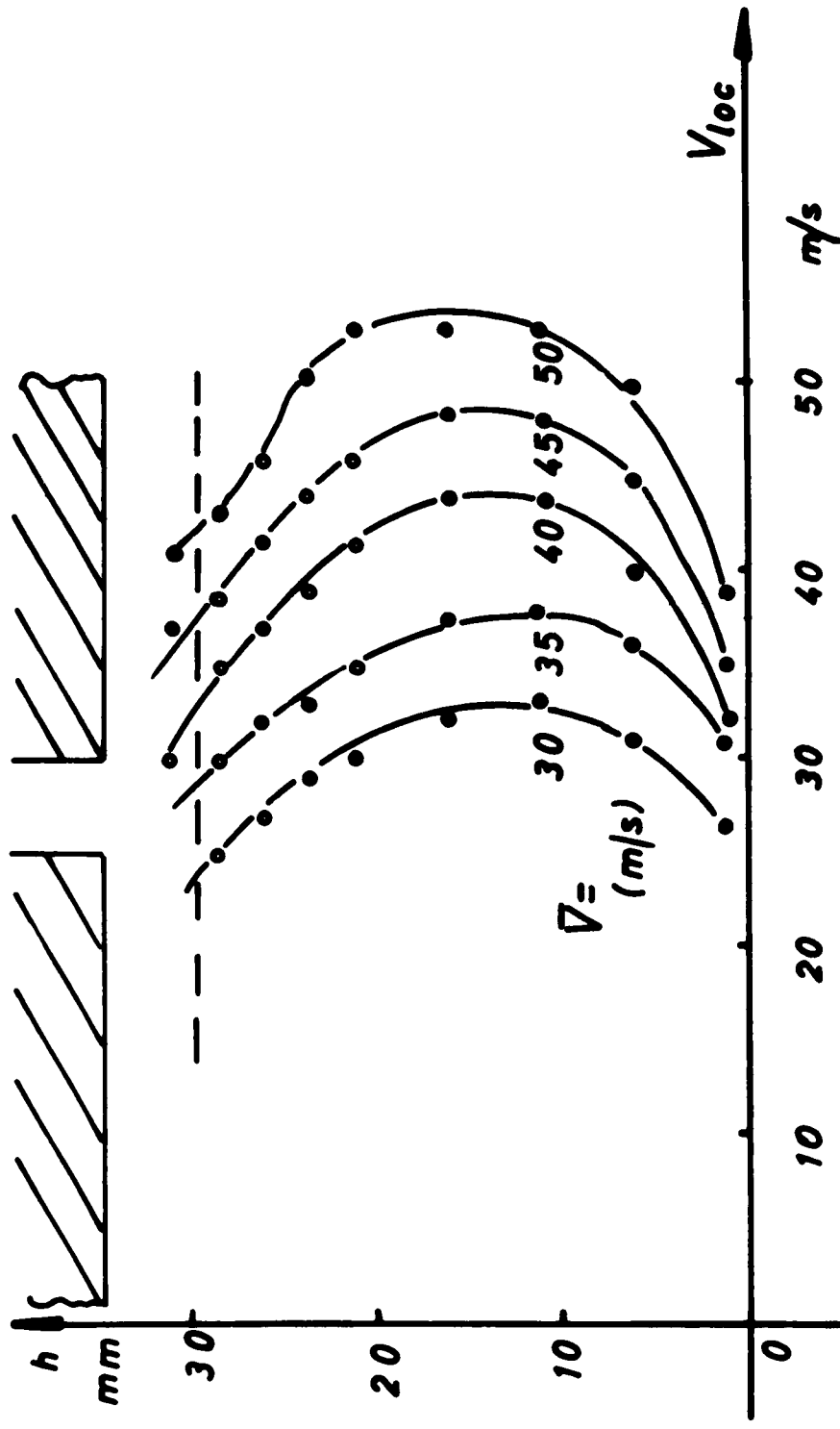
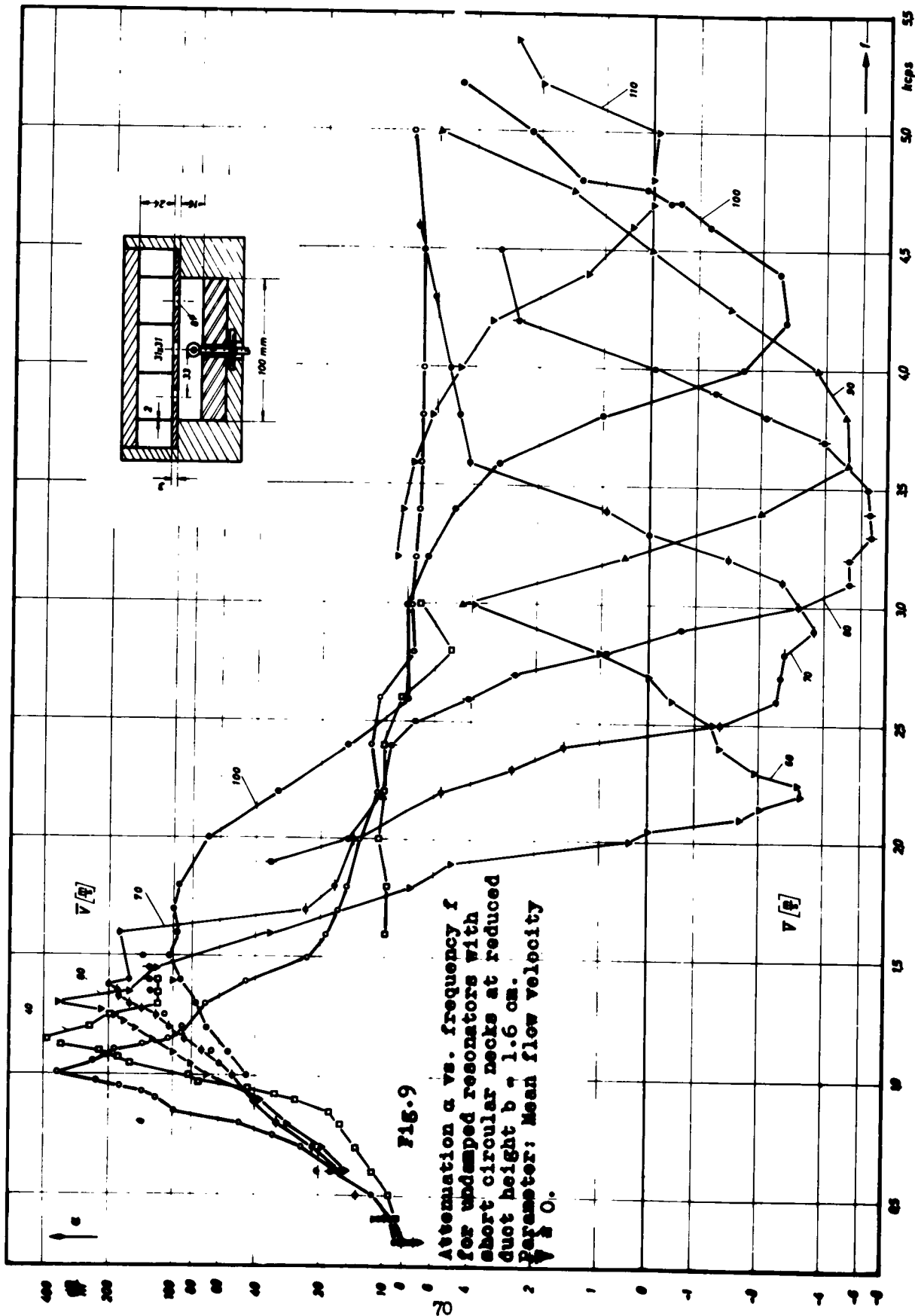


Fig.8 Local flow velocity  $V_{loc}$  vs. wall distance for the resonators of Fig.4 for several mean flow velocities.





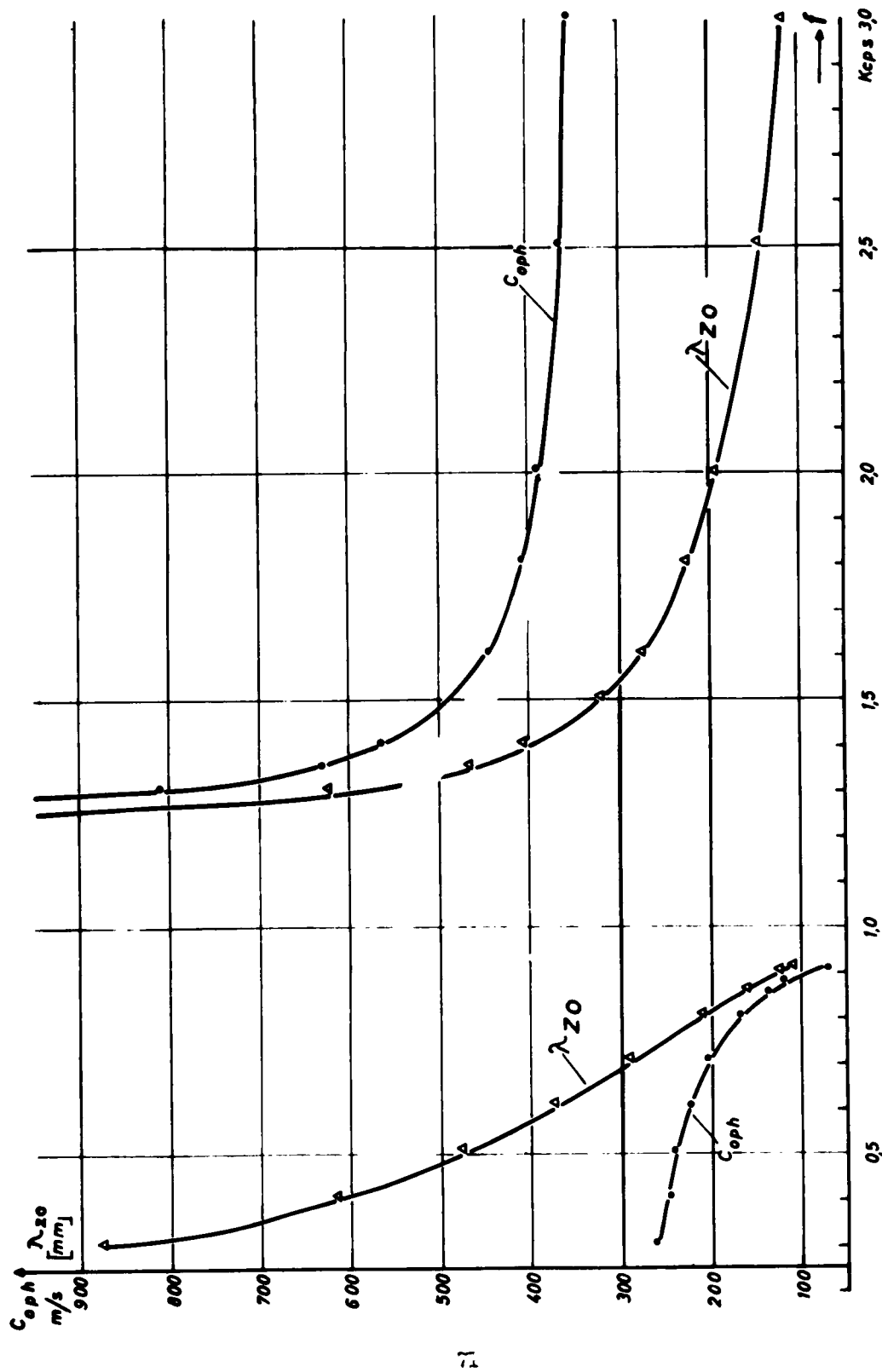


Fig. 10 Wavelength  $\lambda_{z0}$  and phase velocity  $c_{oph}$  in the duct without flow covered with slit resonators with the resonance frequency at 1.0 kc.

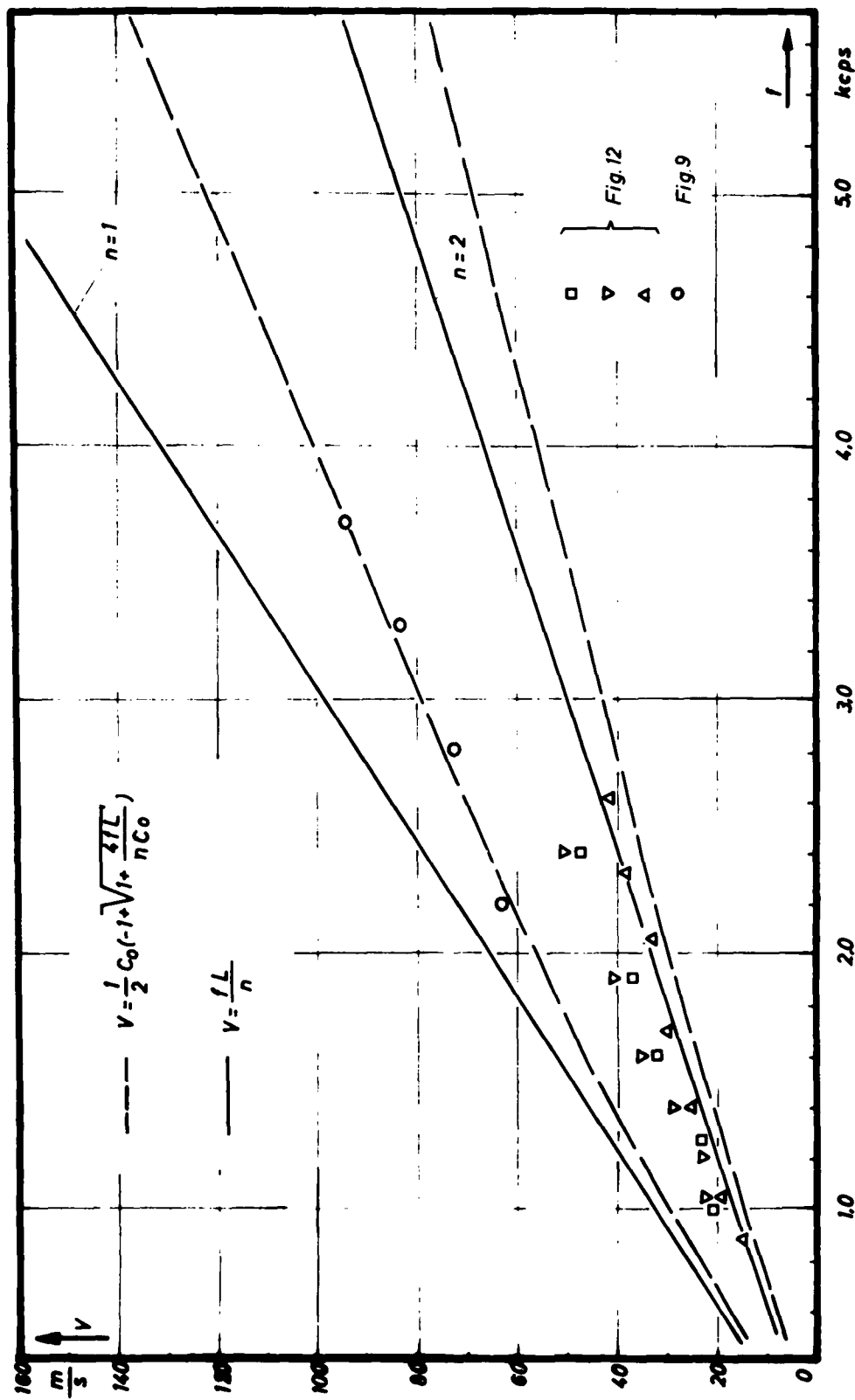
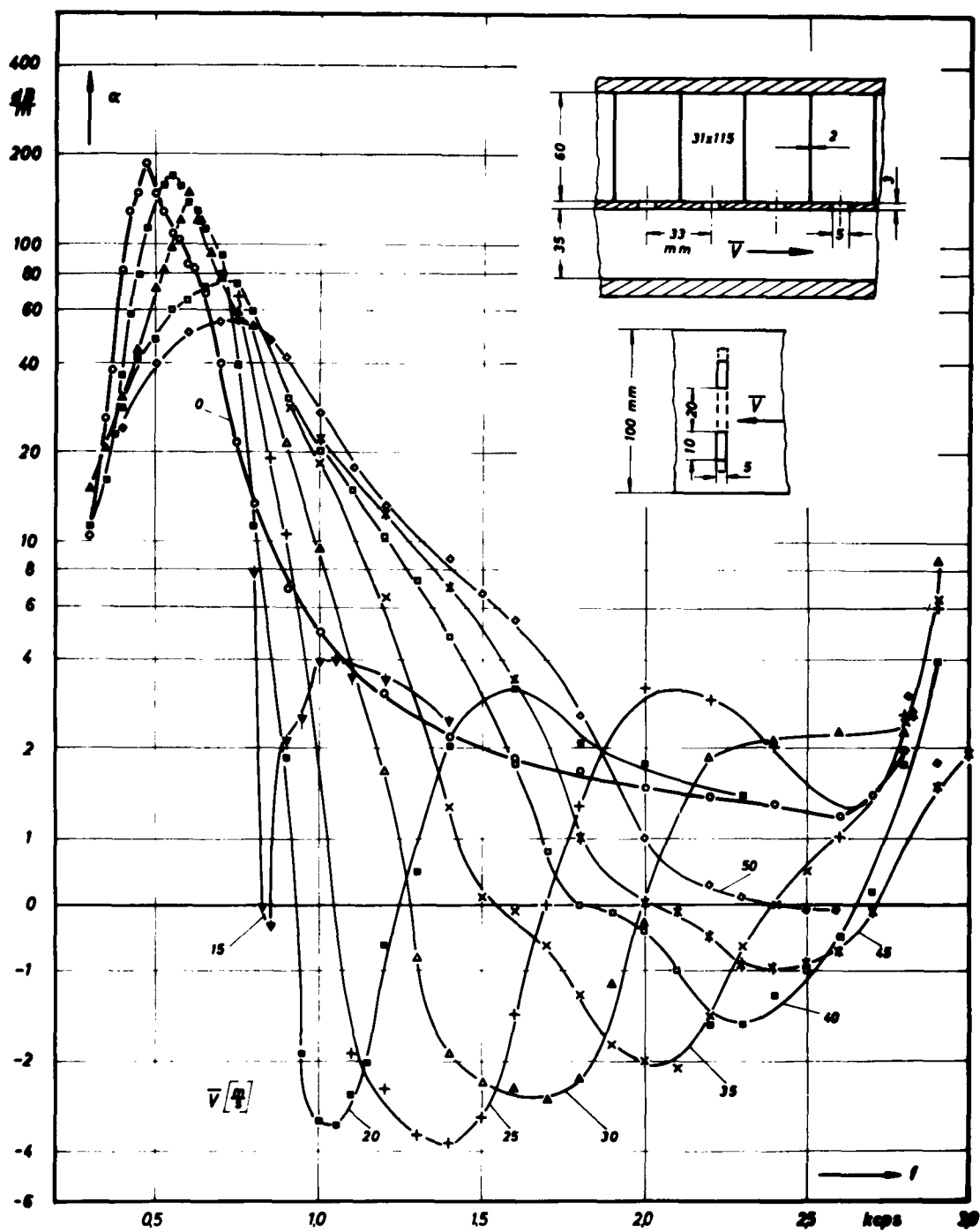
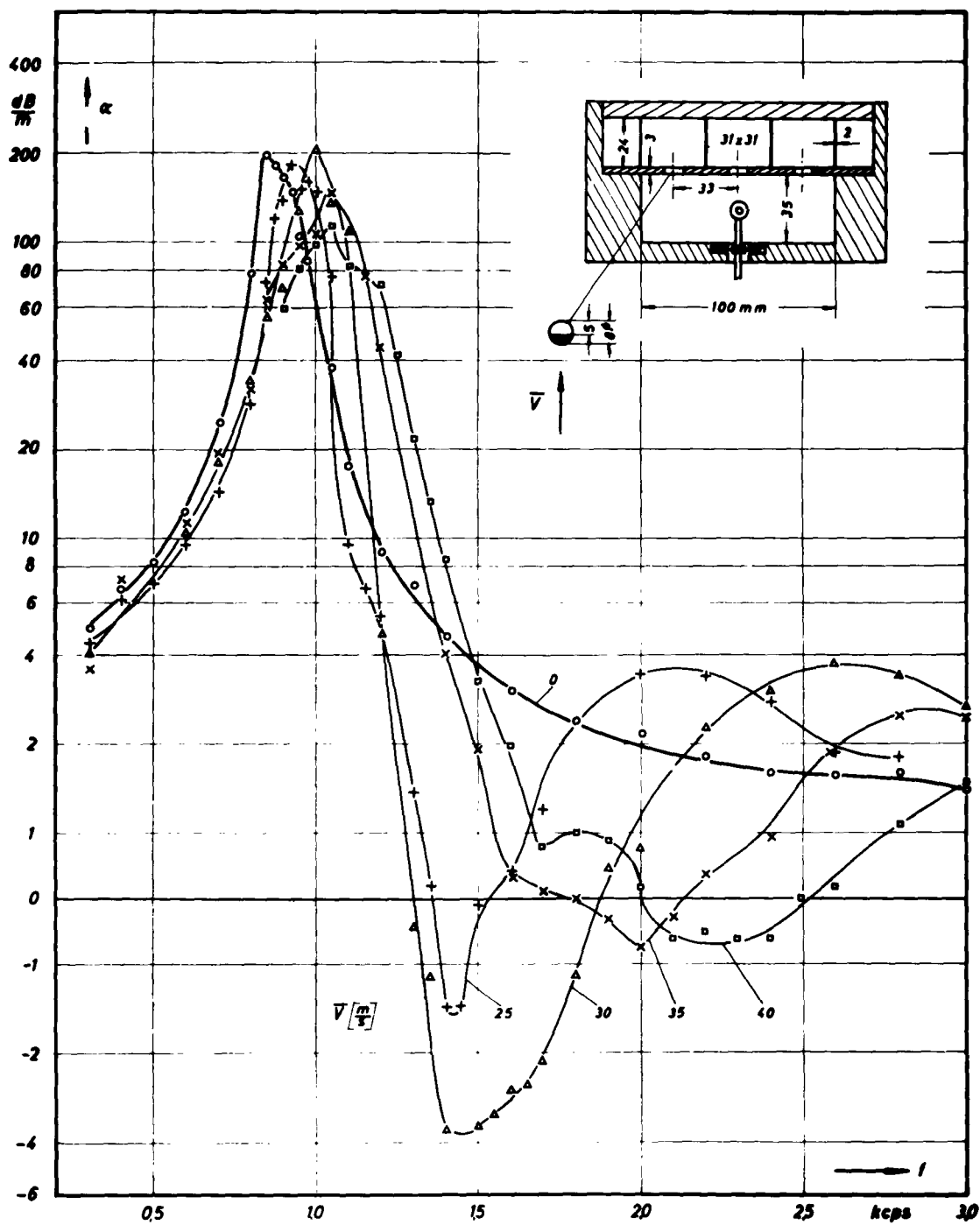


Fig.11 Limits for the position of the dispersion curves of the first and second Hartree harmonics at frequencies above resonance. Measuring points: values of mean flow velocity  $\bar{V}$  and frequency of maximum deattenuation for several resonators.



**Fig.12** Attenuation  $\alpha$  vs. frequency  $f$  for slit resonators with partially covered slits and low resonance frequency. Parameter: Mean flow velocity.



**Fig.13** Attenuation  $\alpha$  vs. frequency  $f$  for undamped resonators with short circular necks as in Fig.4, now partially covered. Parameter: Mean flow velocity  $V \geq 0$ .

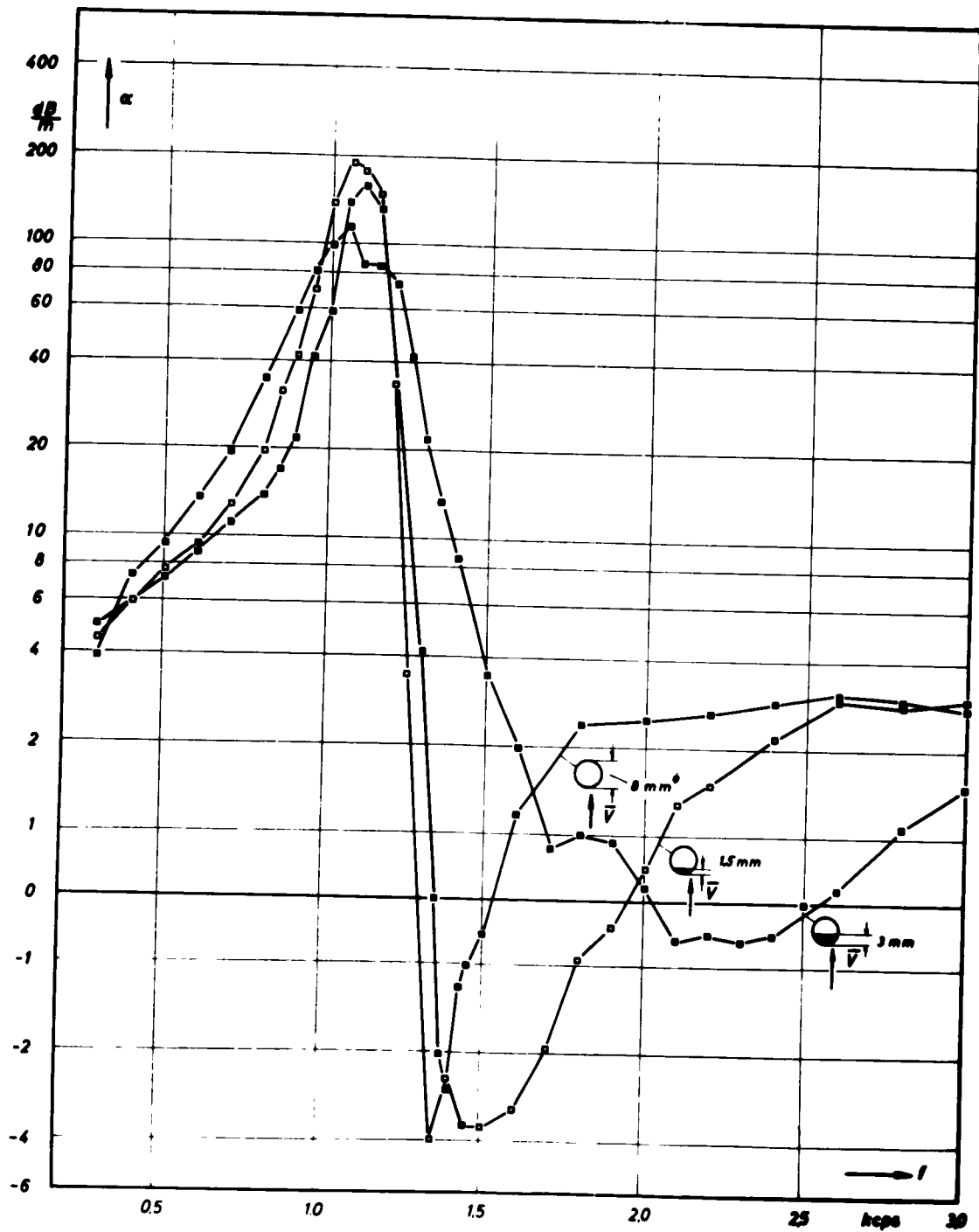


**Fig.14** Comparison of the attenuation curves of undamped resonators with short circular necks for different degrees of covering at a mean flow velocity  $V = 40\text{ m/sec}$ .

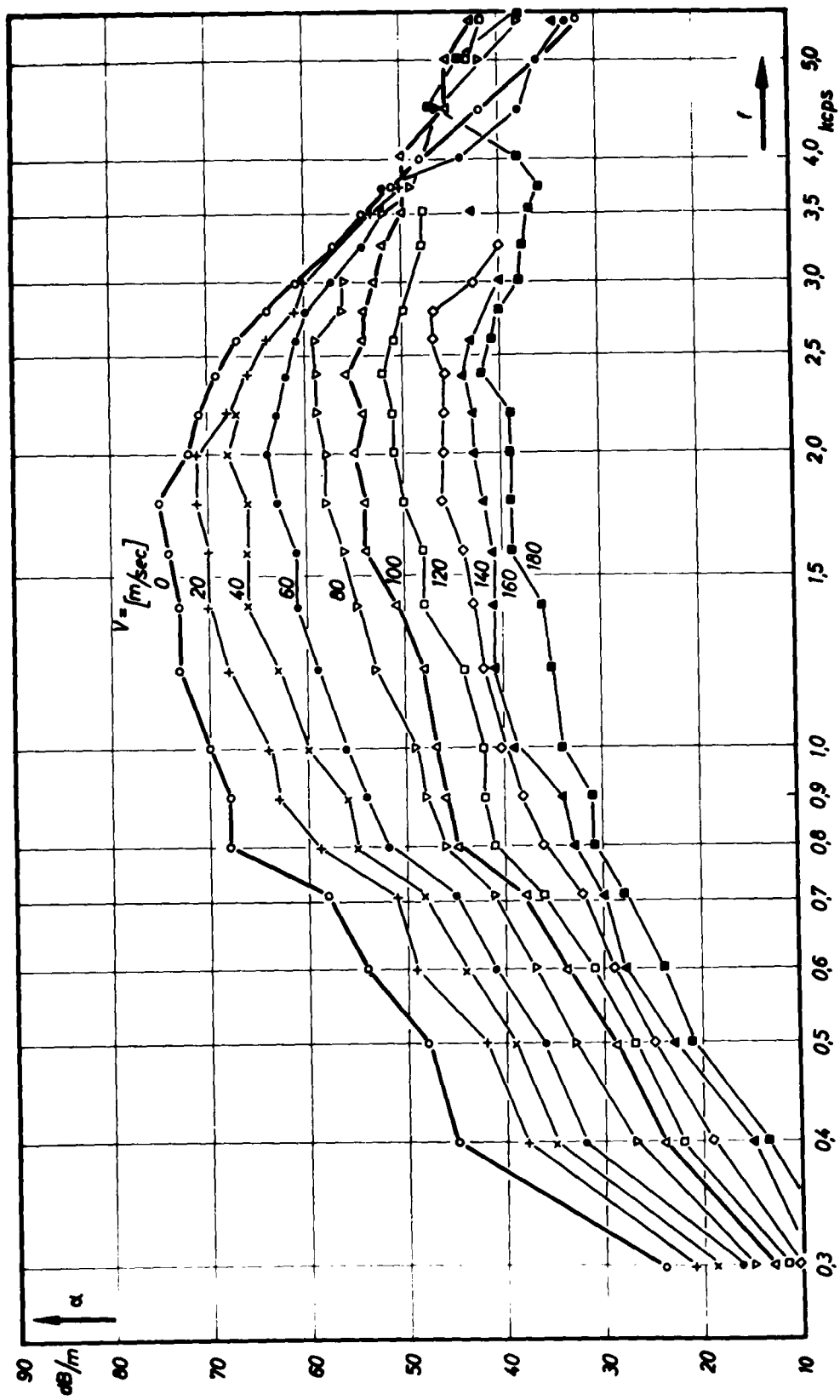


Fig.15 Attenuation  $\alpha$  of a porous absorber (Fig.1) for downstream propagation.

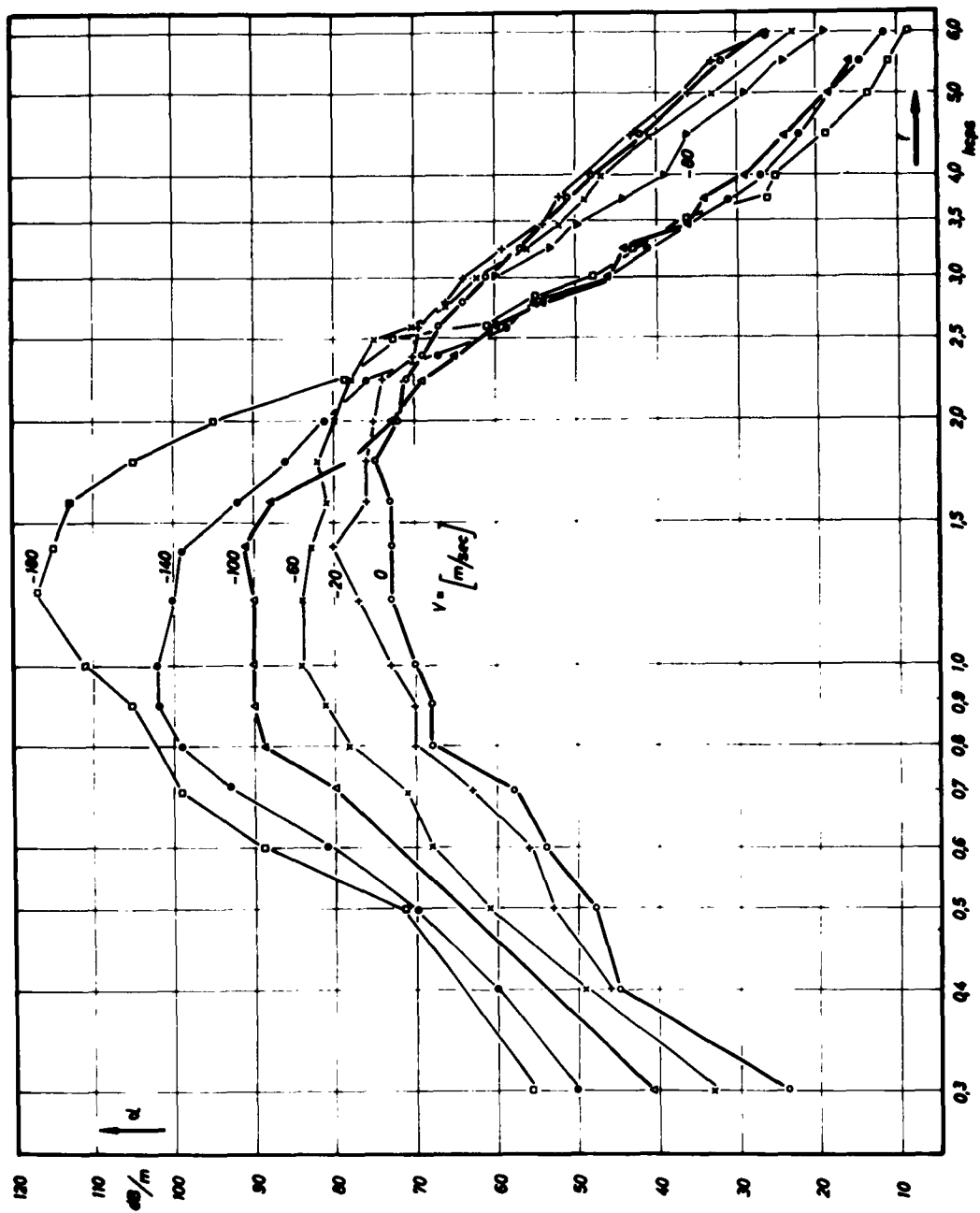


Fig. 16 As in Fig. 15 but for upstream propagation.

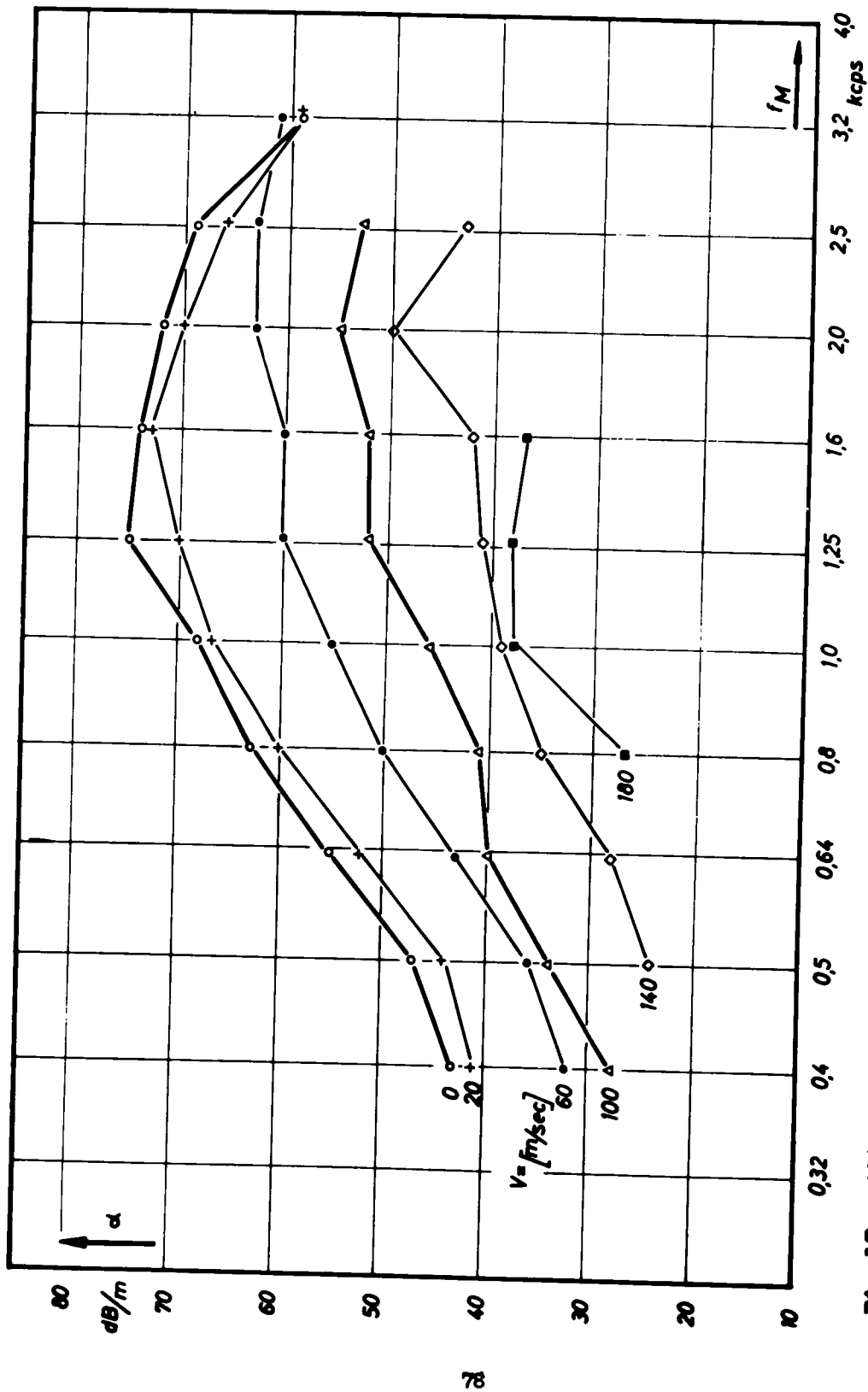


Fig.17 Attenuation for third-octave noise propagating downstream.



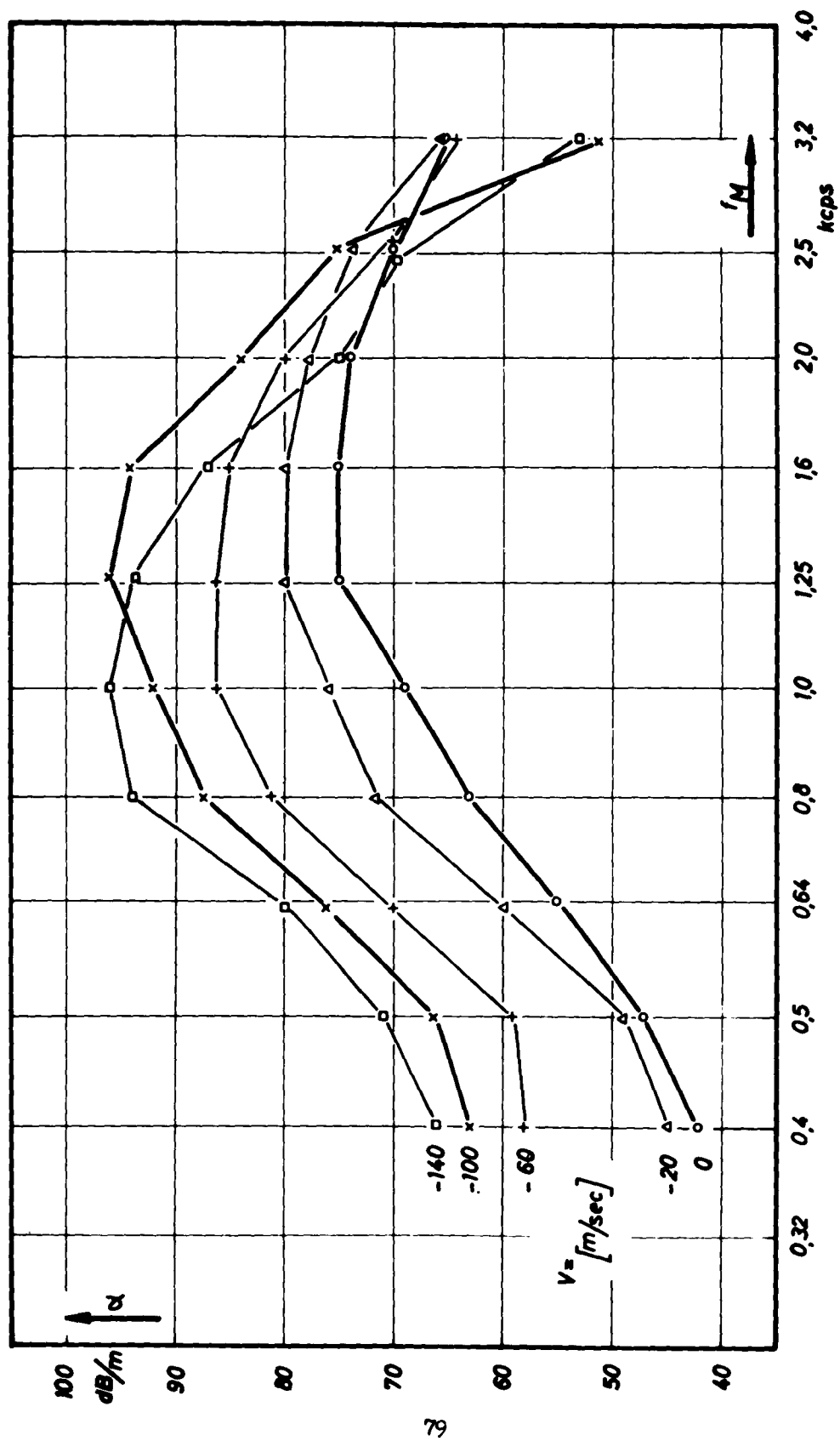


Fig.18 Attenuation for third-octave noise propagating upstream.

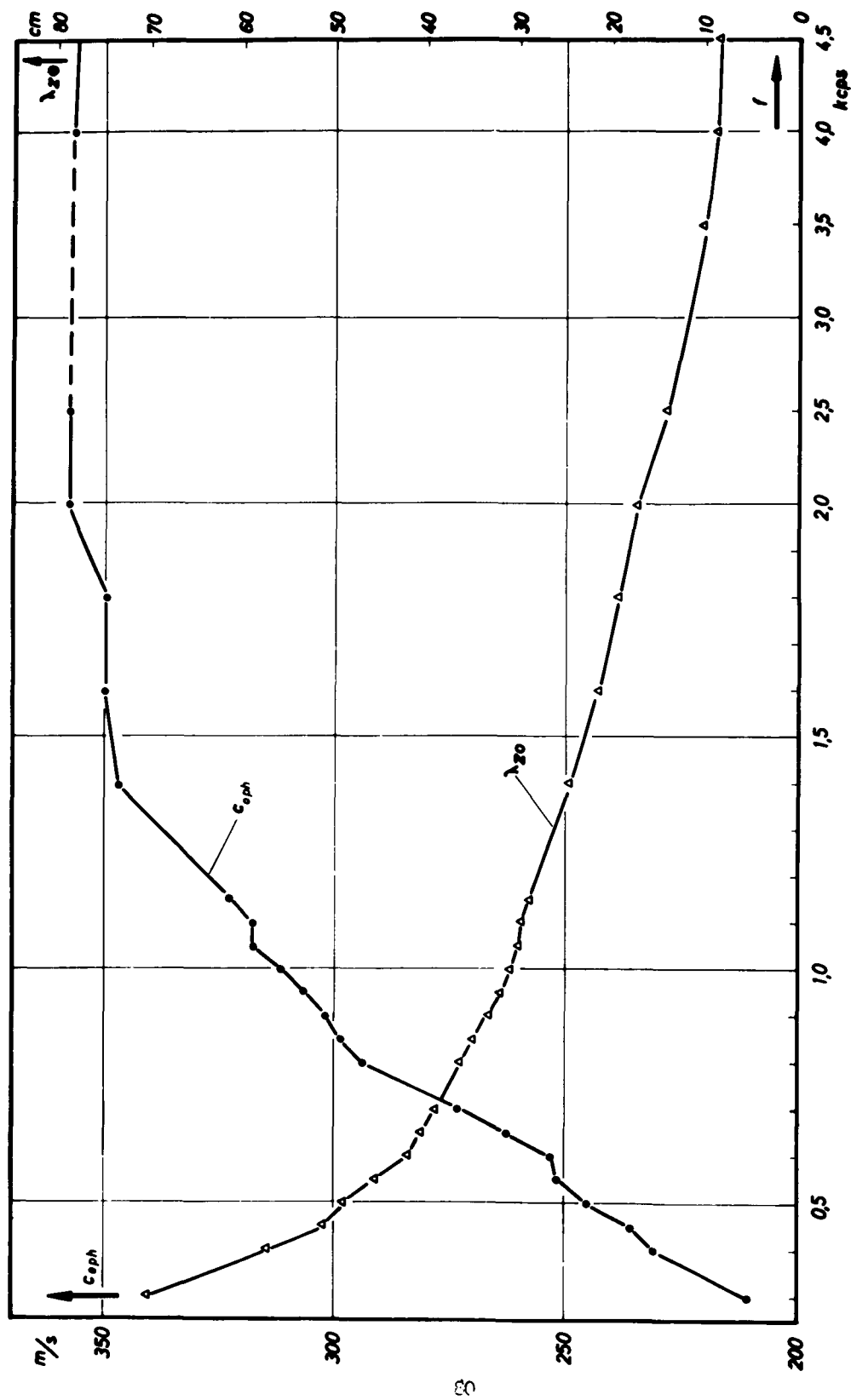


Fig. 1.19 Wavelength and phase velocity in the duct of Fig. 1.1.

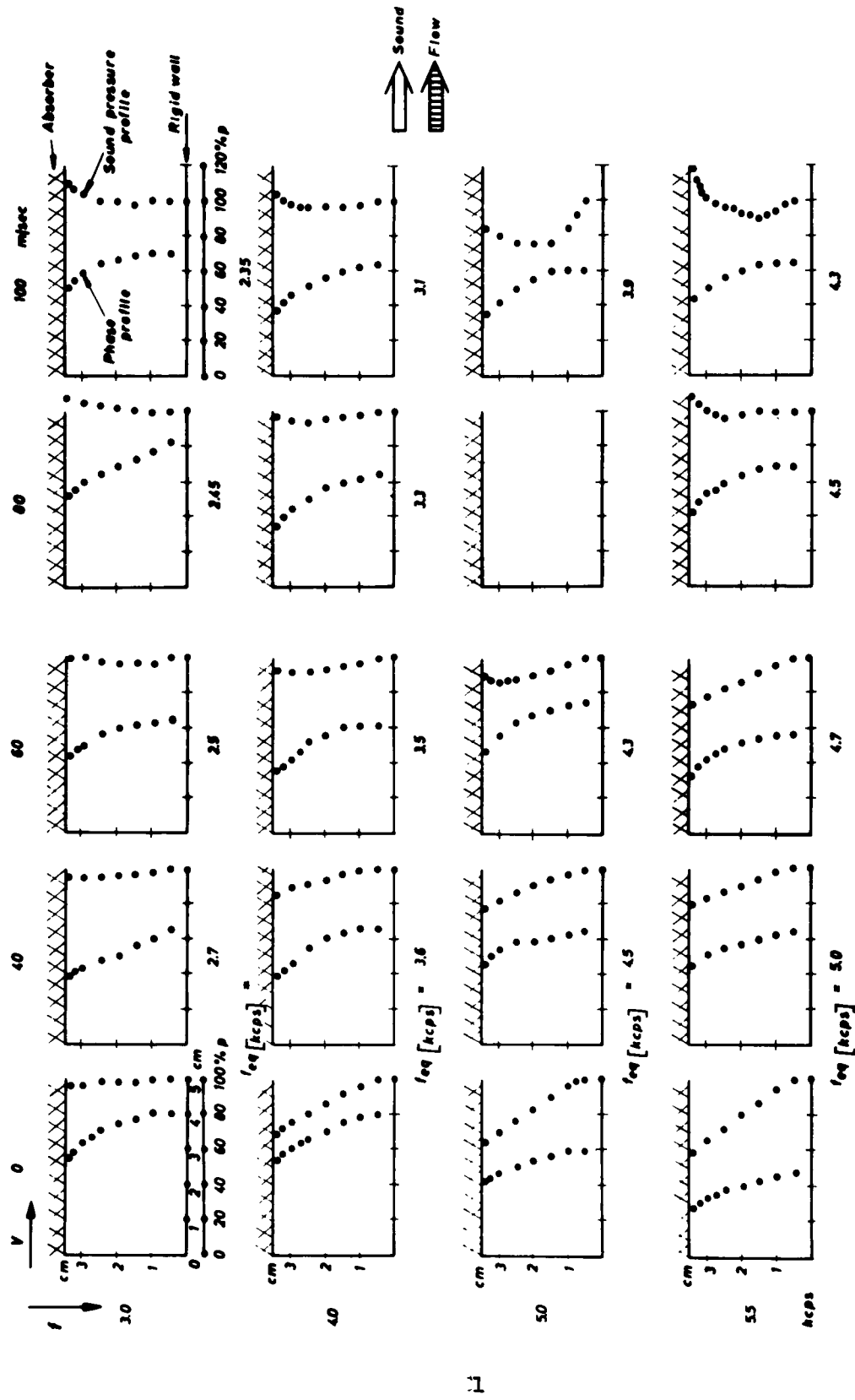
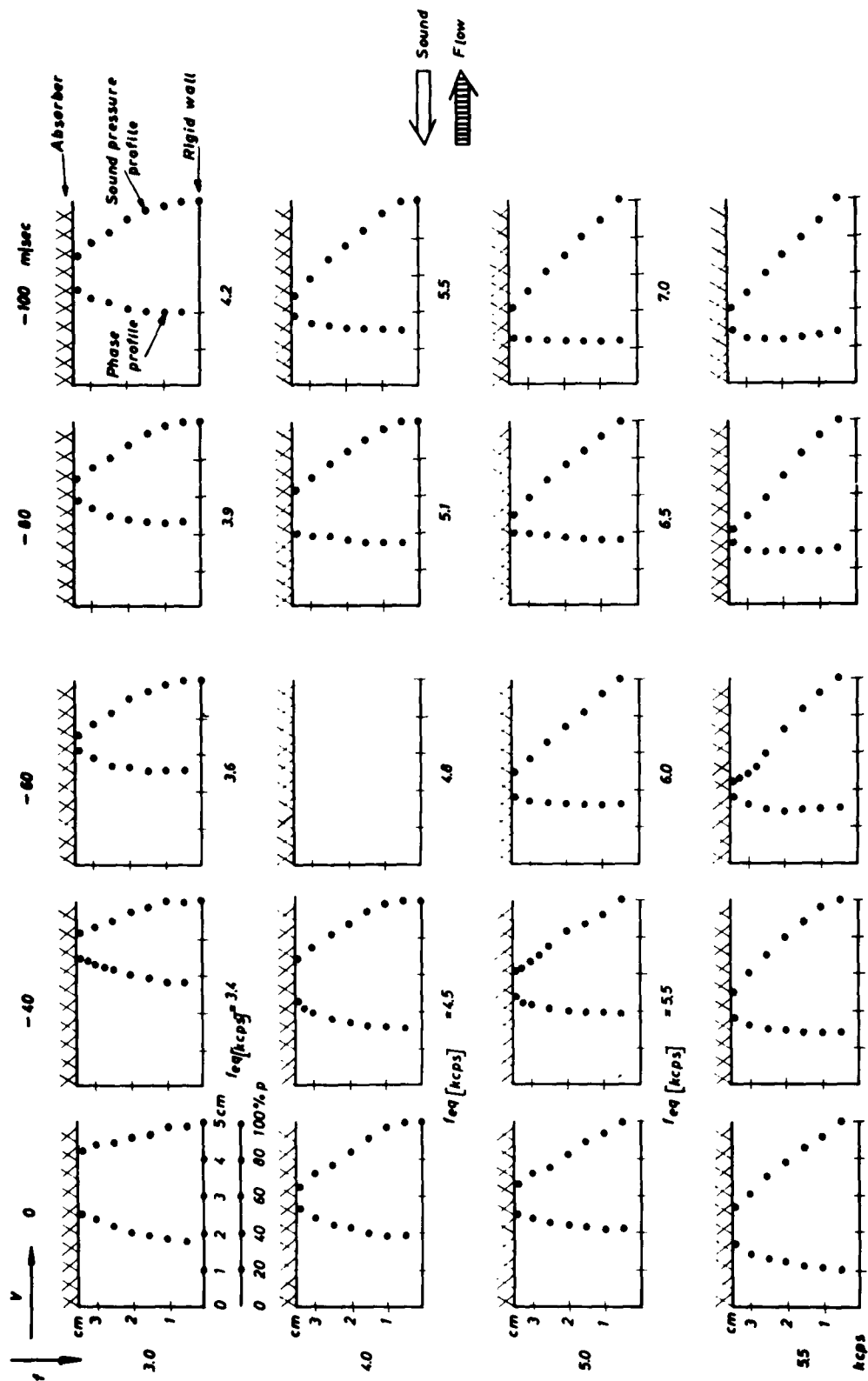
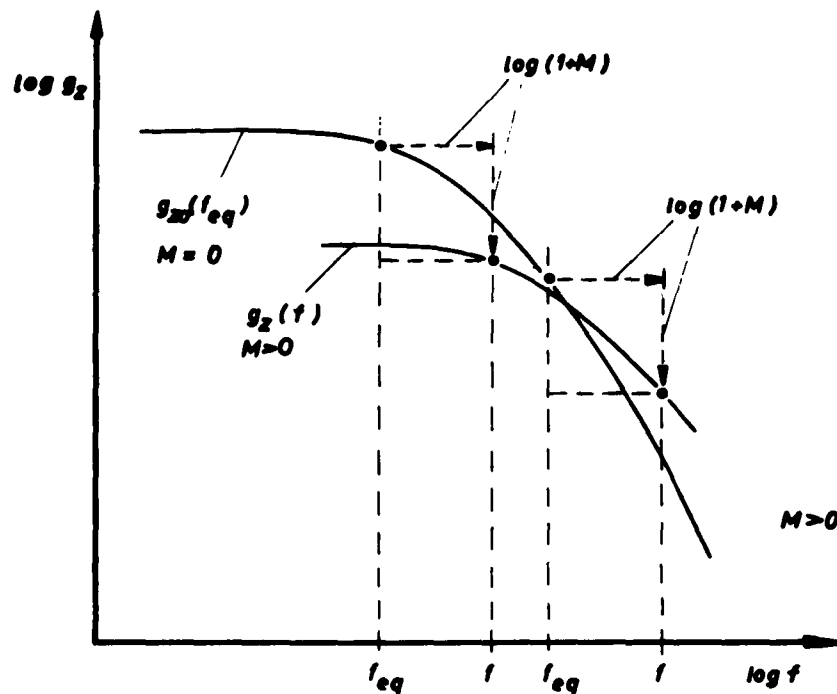


Fig. 20 Profiles of sound pressure and phase in the duct with a porous absorber for several values of signal frequency and flow velocity. Downstream propagation.



**Fig.21** Profiles of sound pressure and phase in the duct with a porous absorber for several values of signal frequency and flow velocity. Upstream propagation.



**Fig.22** Construction of the curve of frequency response of sound attenuation with superimposed flow from the attenuation curve without flow. Downstream propagation.

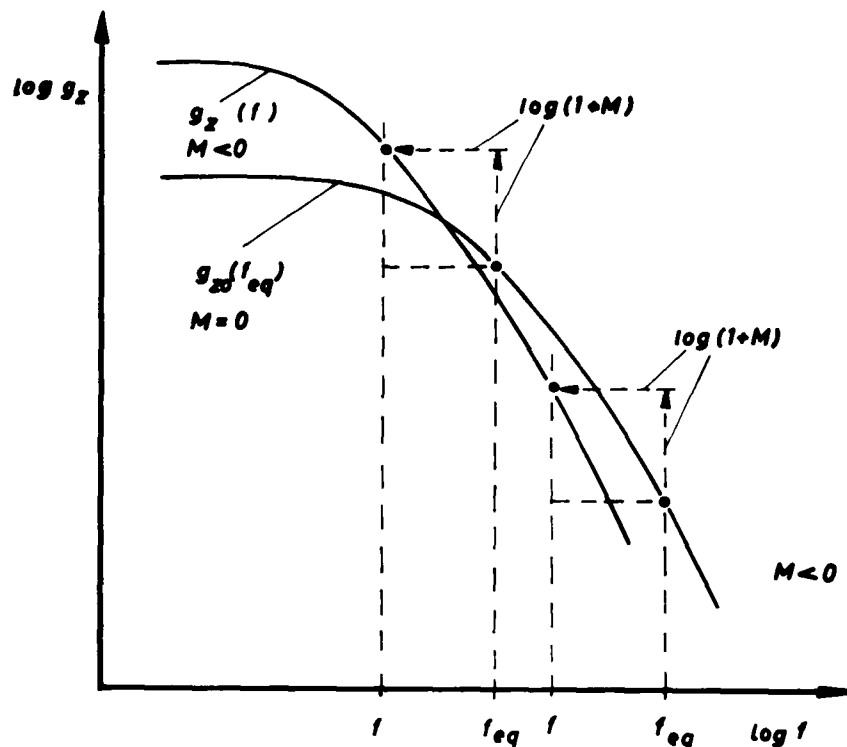


**Fig.23** Construction of the curve of frequency response of sound attenuation with superimposed flow from the attenuation curve without flow. Upstream propagation.

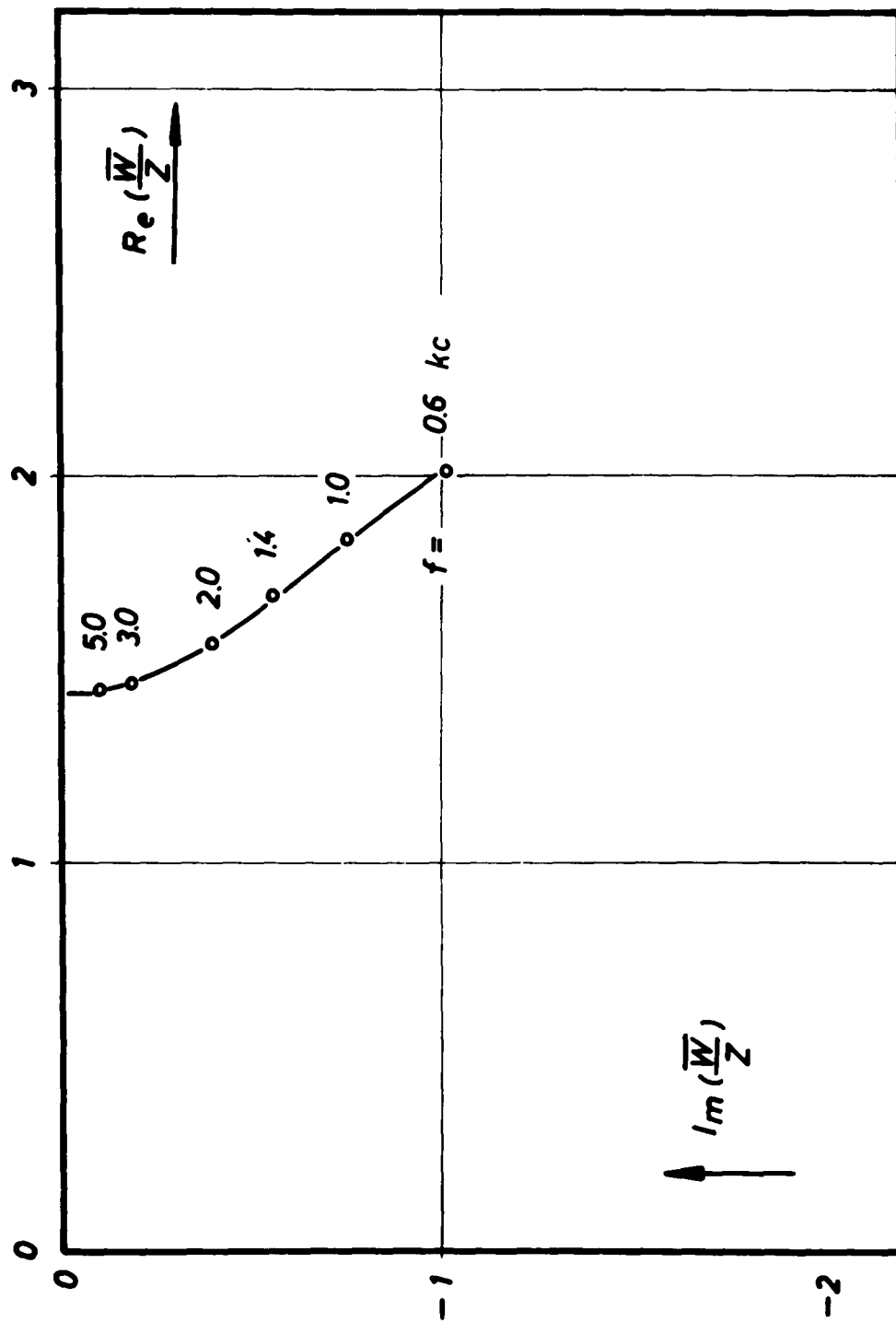


Fig.24 Wall impedance of the porous absorber.

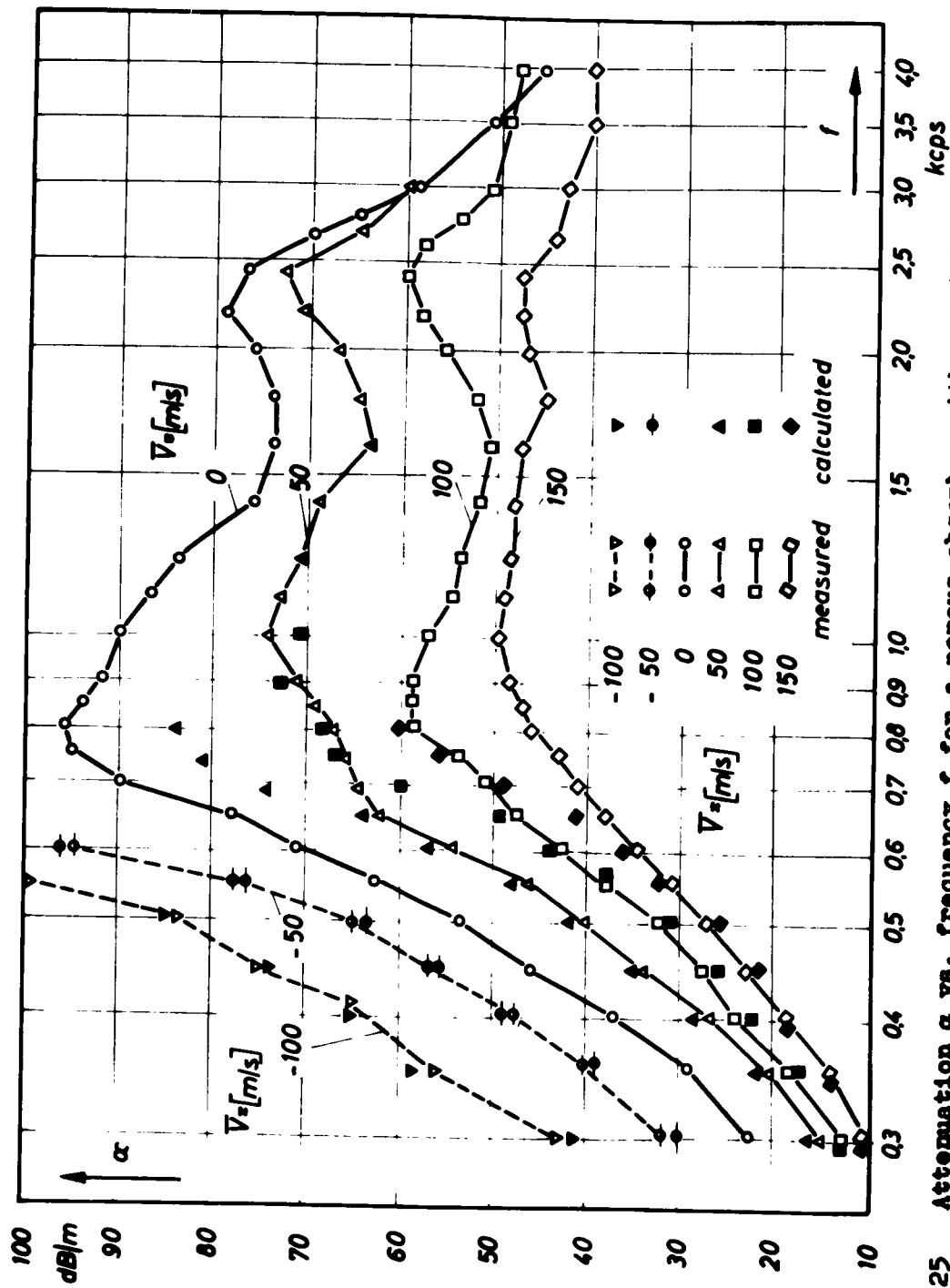
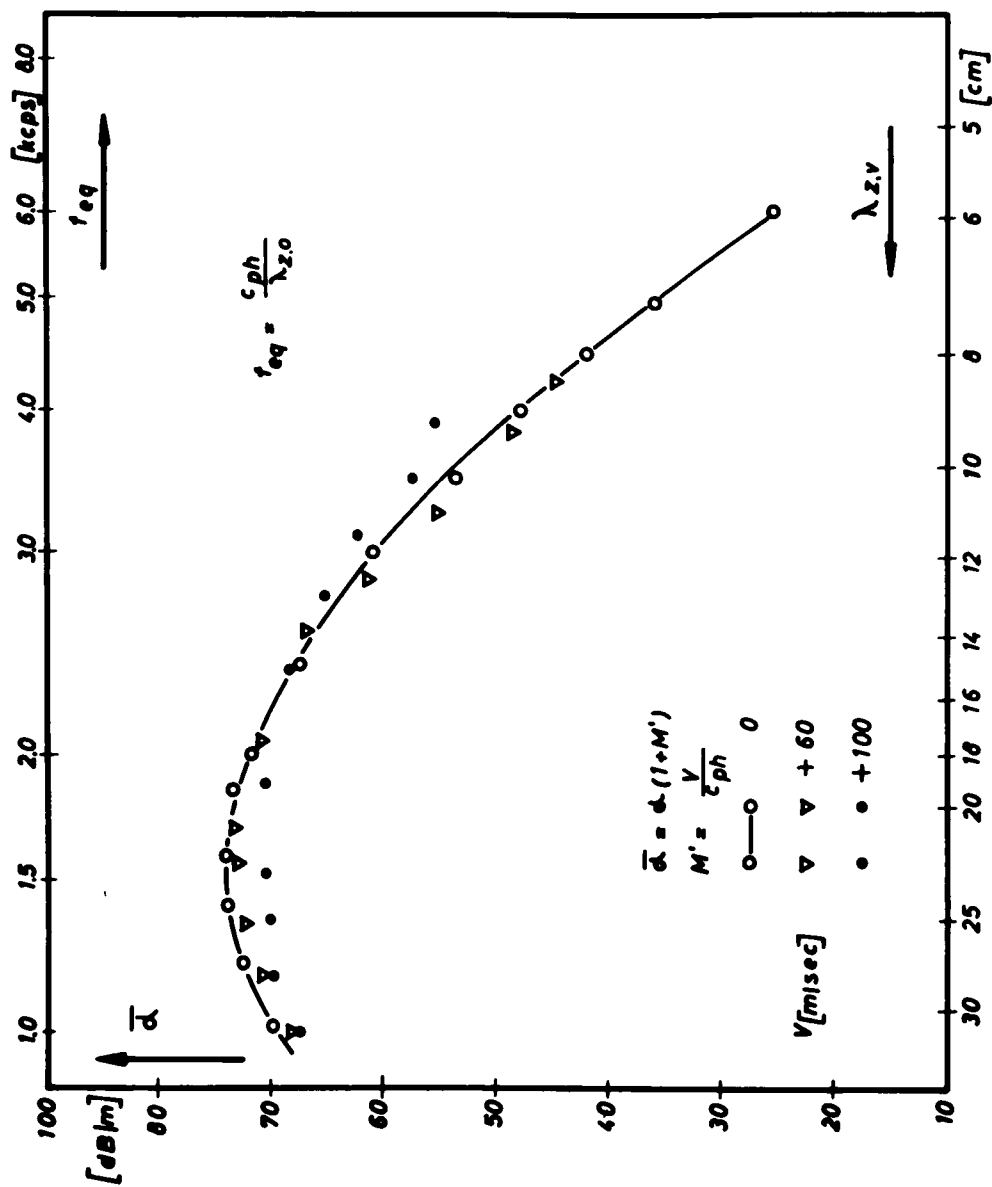


Fig.25 Attenuation  $\alpha$  vs. frequency  $f$  for a porous absorber with partitions. Comparison of the measured values (open points) with the calculated values (full points). Parameter: Mean flow velocity.



**Fig. 26** Measured values of sound attenuation in the sound absorbing duct with superimposed flow multiplied by  $(1 + M')$  vs. signal wavelength in the duct. Downstream propagation.



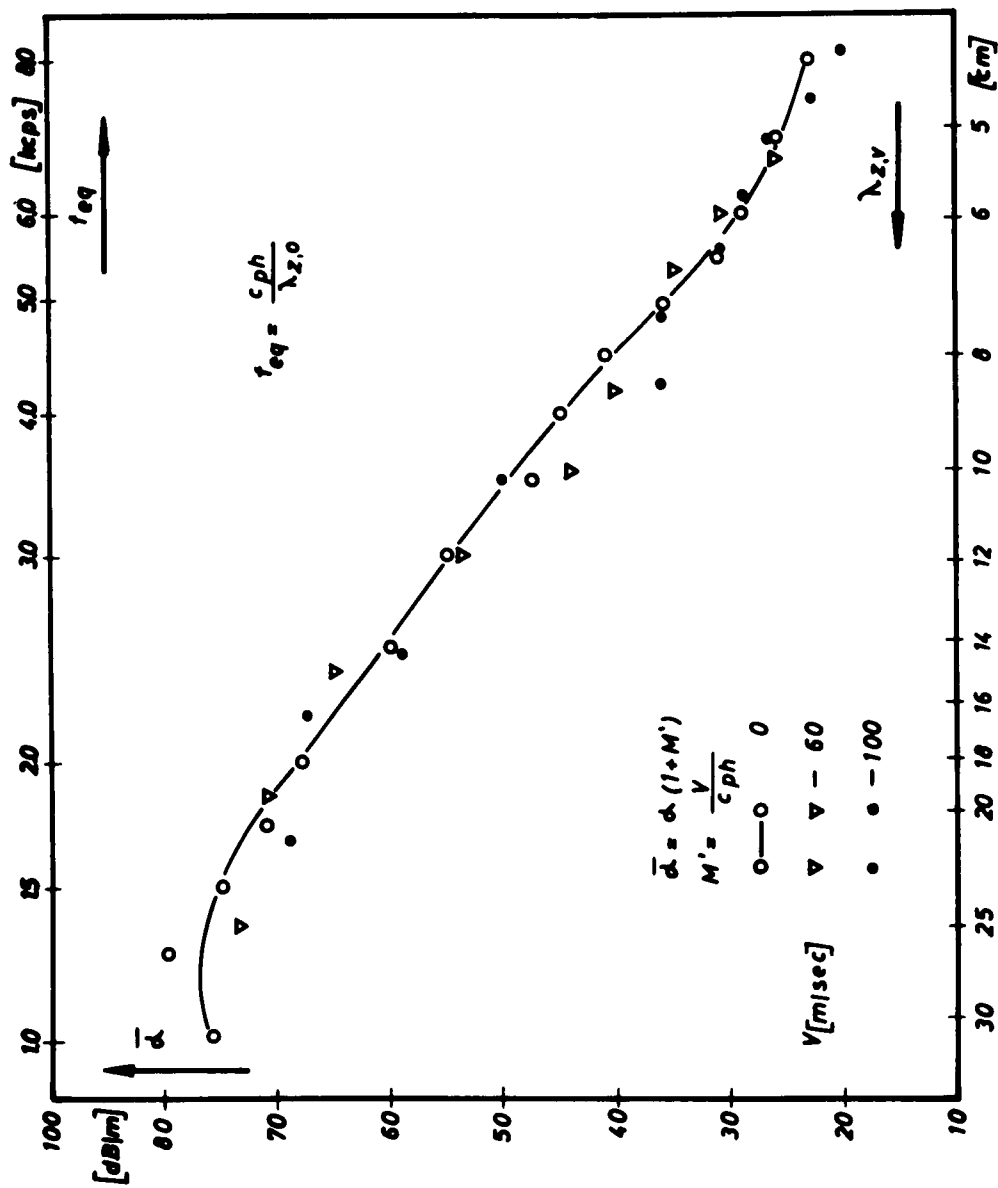


Fig.27 Measured values of sound attenuation in the sound absorbing duct with superimposed flow multiplied by  $(1 + M')$  vs. wavelength in the duct. Upstream propagation.

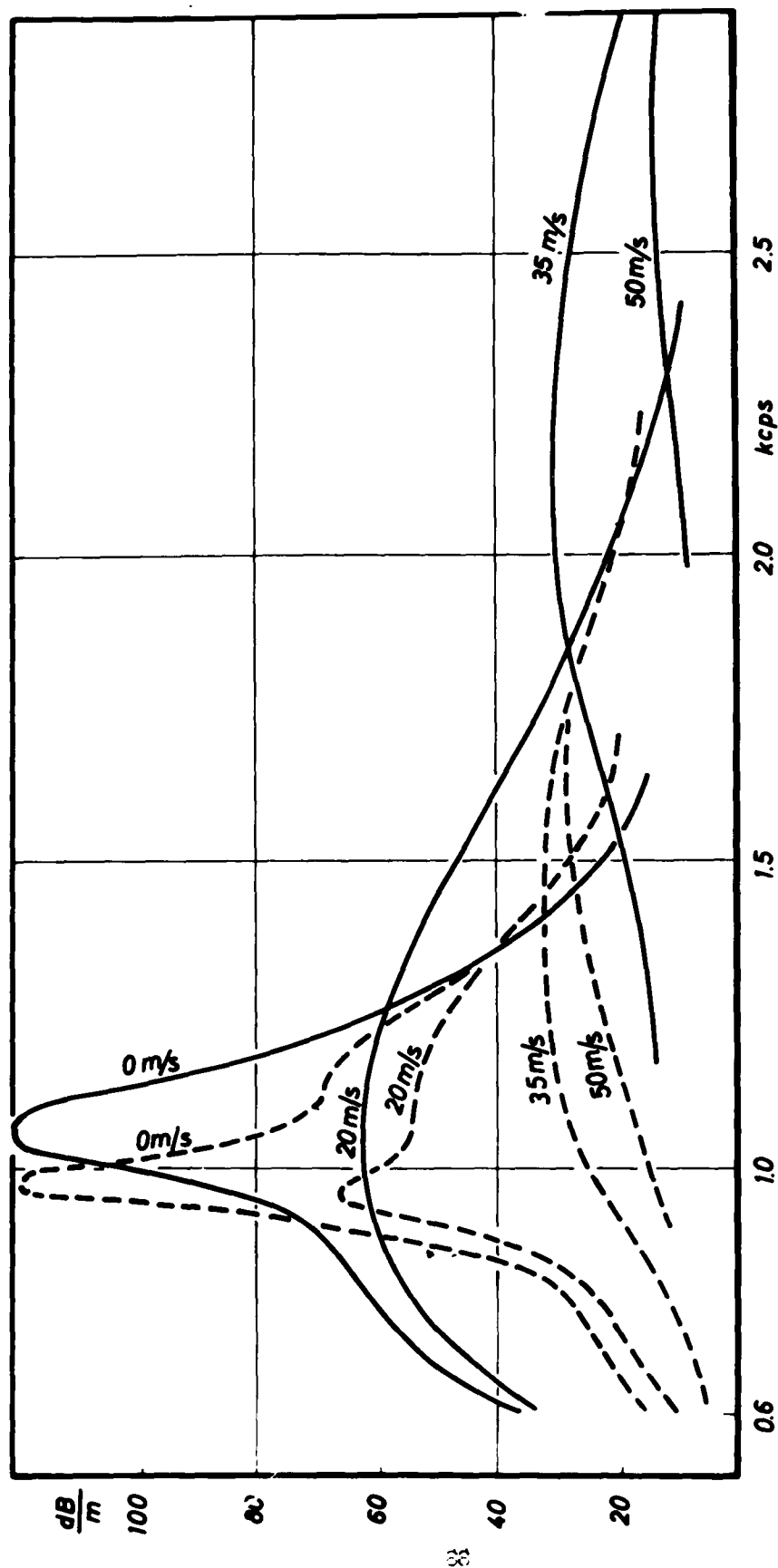


Fig.28 Attenuation vs. frequency for the absorber with completely pliable plates.  
Broken lines: with pressure compensation.

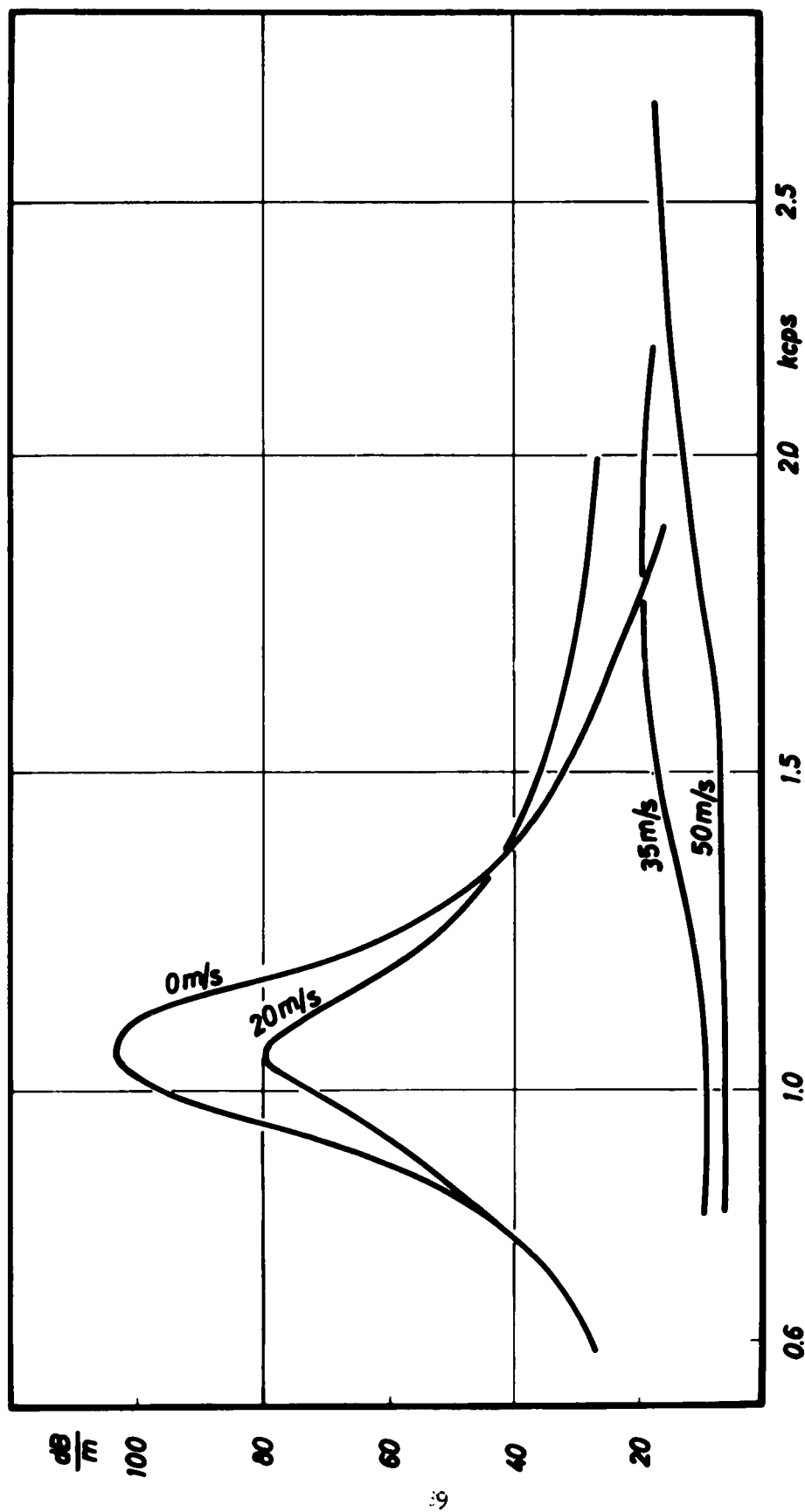


Fig.29 Absorber with completely pliable plates damped by a layer of rockwool.

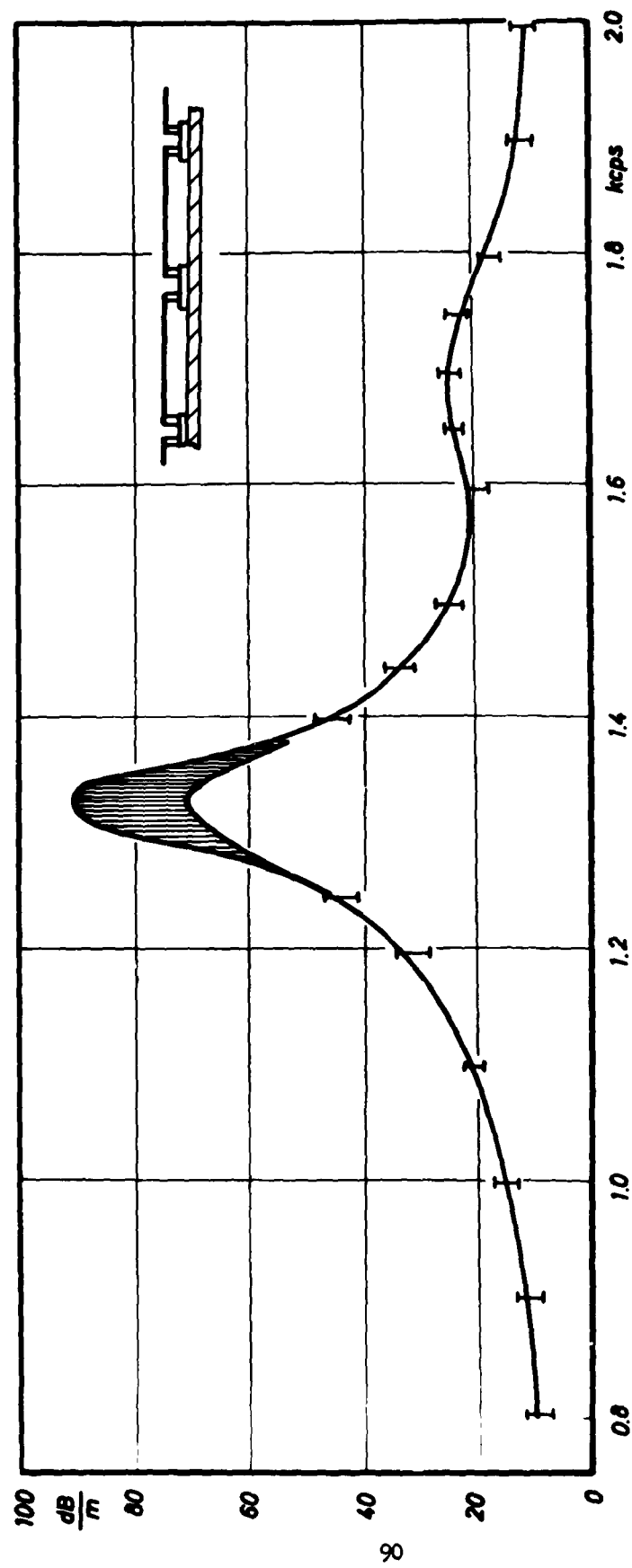


Fig.30 Frequency response of attenuation for an absorber with resilient plates. Flow velocity: from 50 m/sec upstream to 65 m/sec downstream propagation.

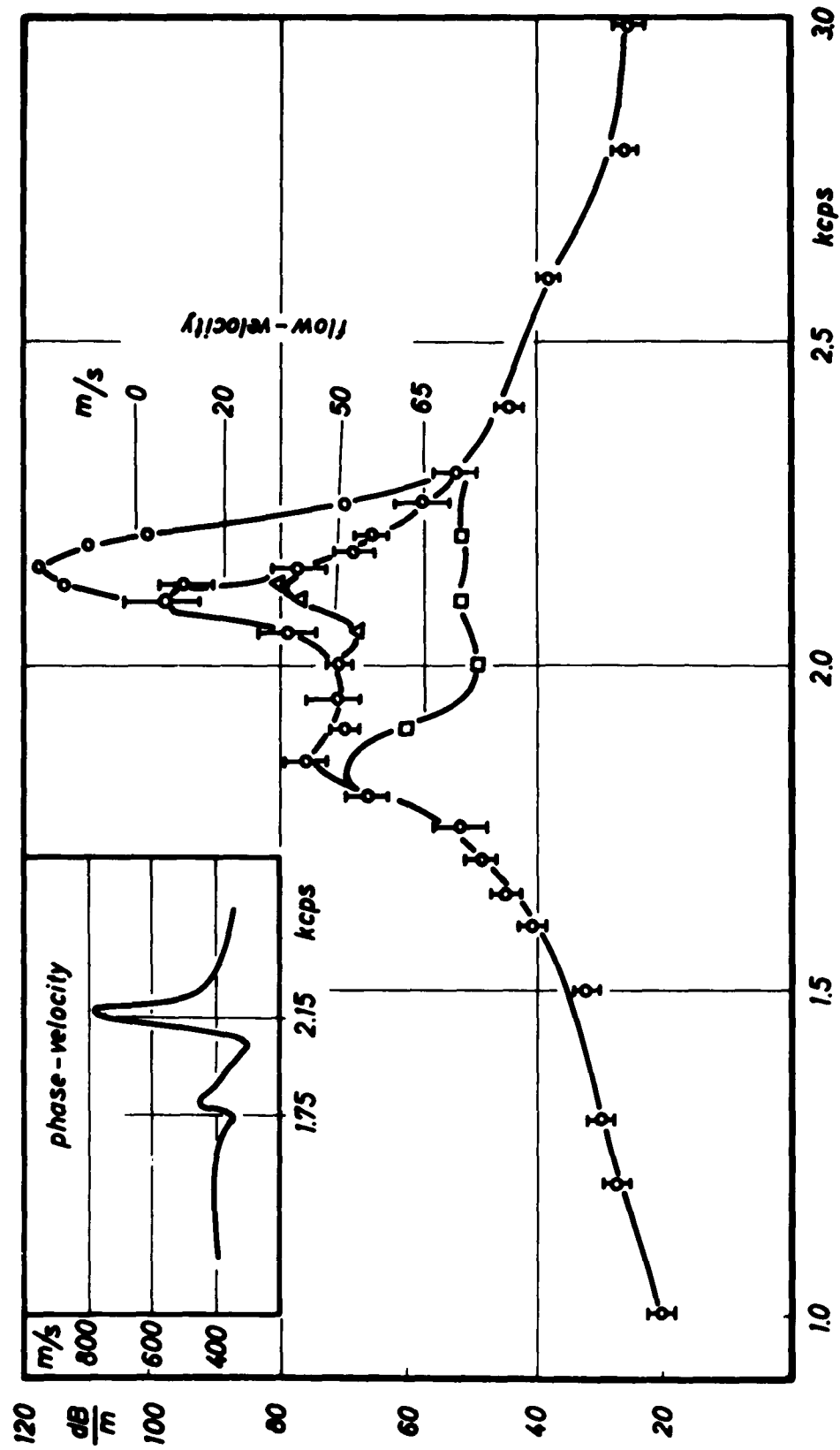


Fig. 31 Phase velocity and attenuation for an absorber consisting of verneer-sheets.

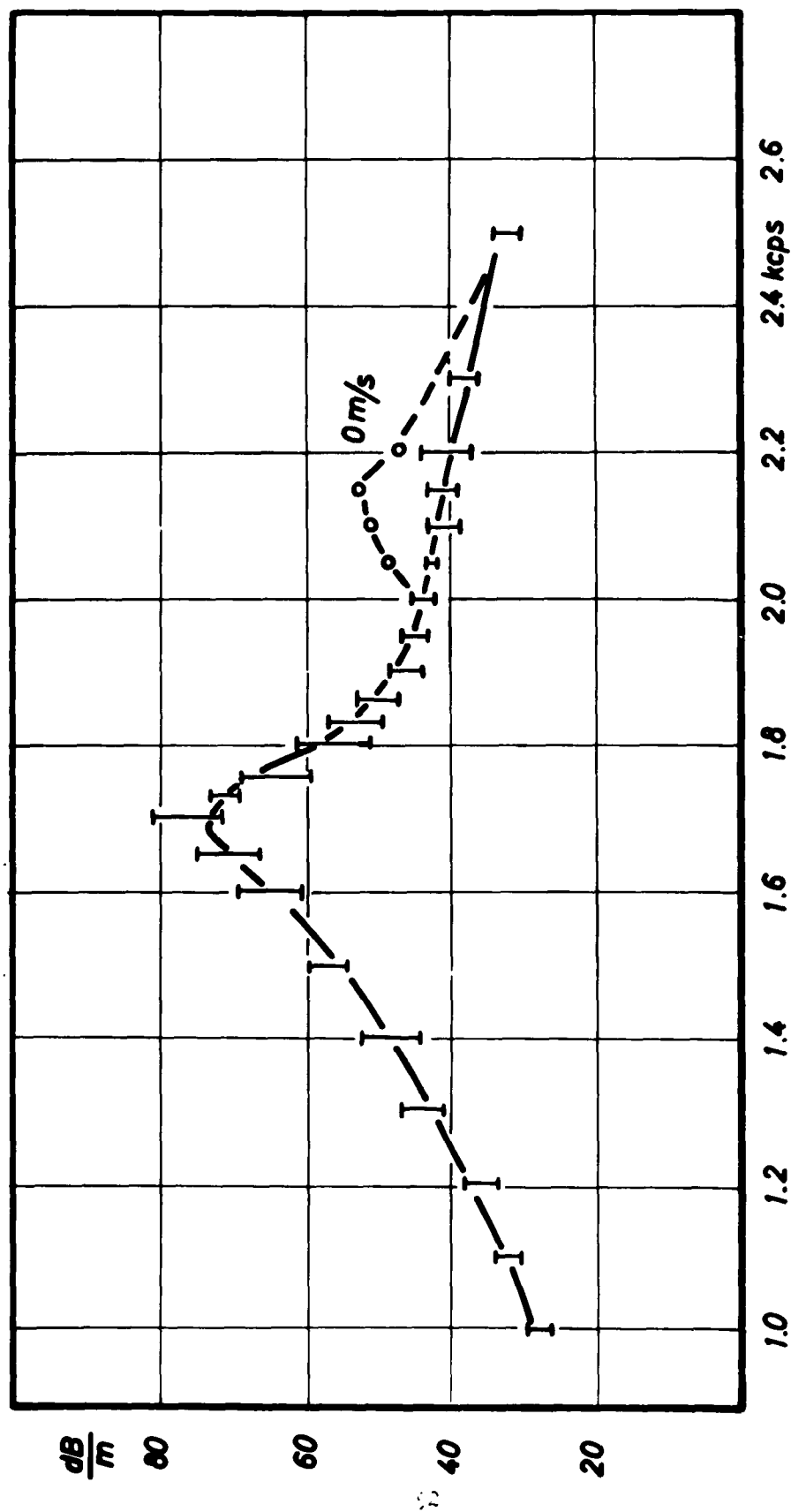


Fig.32 Absorber consisting of verneer-sheets damped with a layer of rockwool.

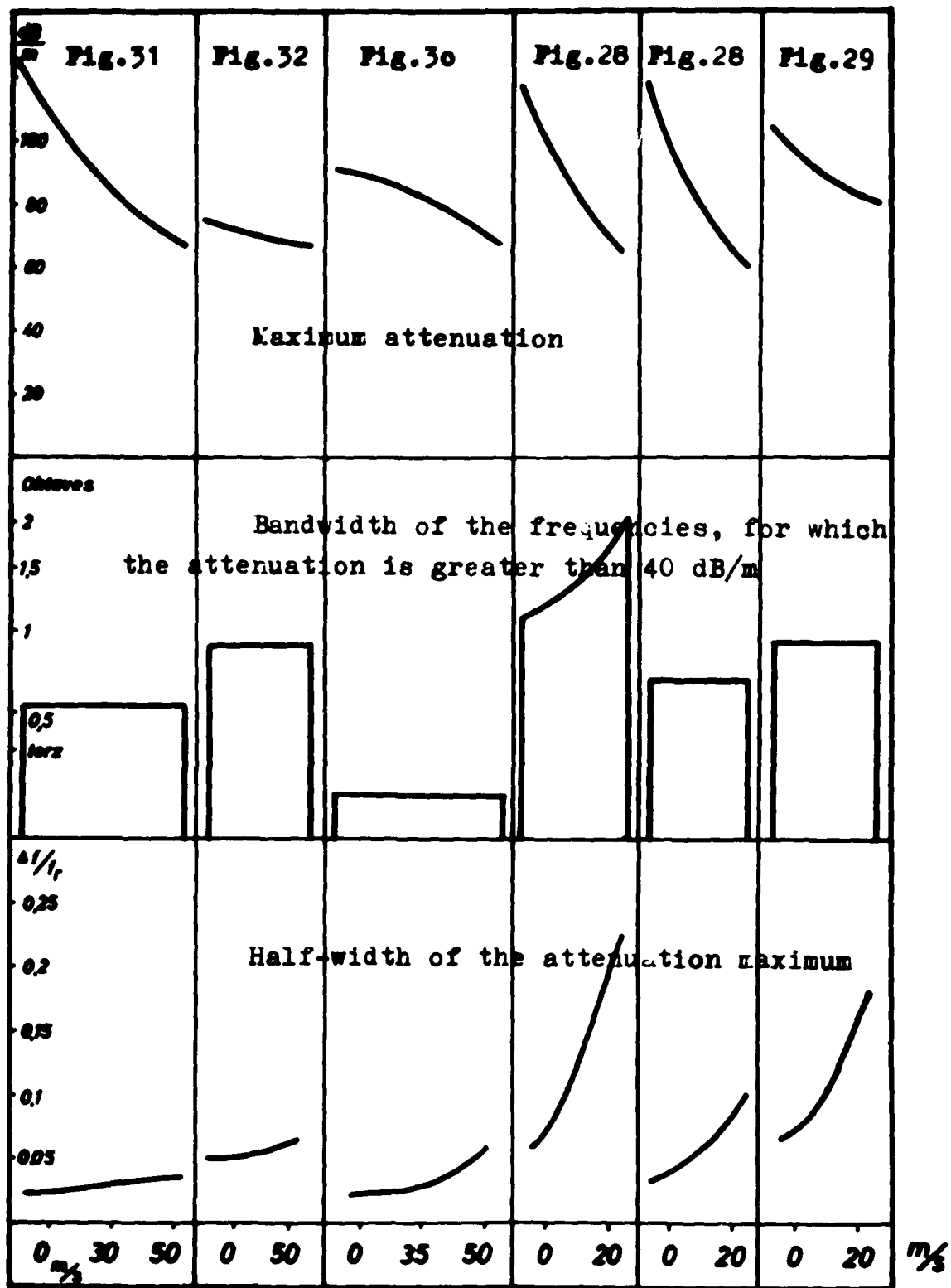


Fig. 33 Comparison of the different absorbers

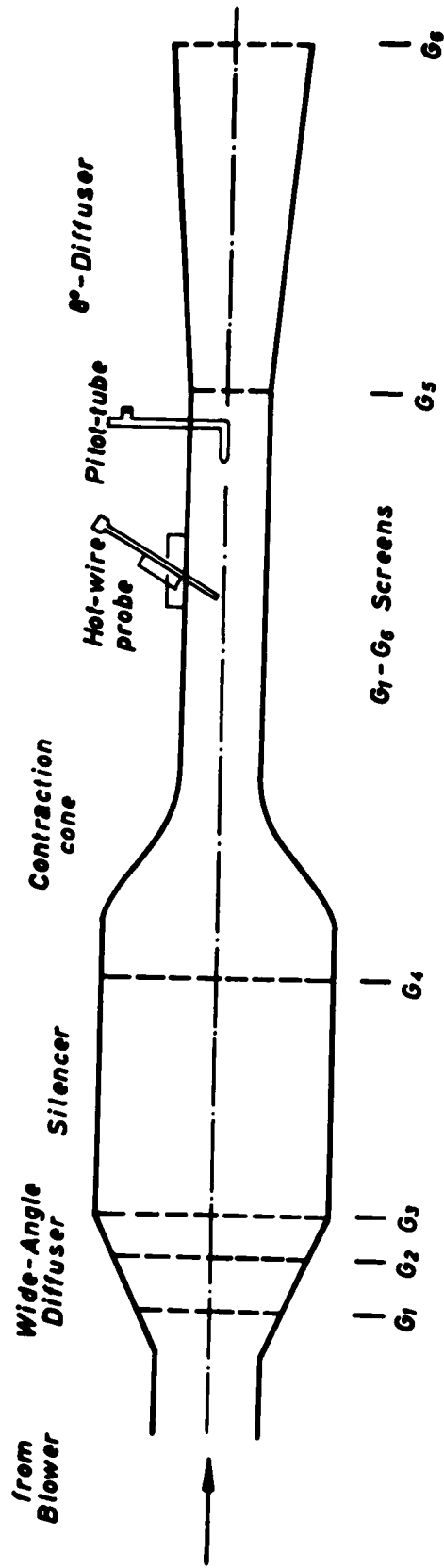


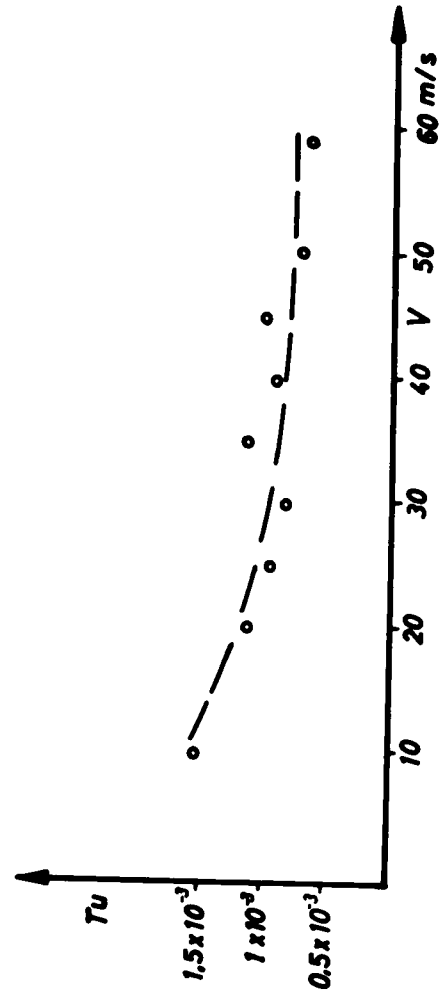
Fig. 34 Sketch of the wind tunnel.

$V = \text{Center-velocity}$

$$Tu = \frac{\sqrt{\overline{v'^2}}}{V}$$

Fig. 35

Turbulence level at the center line of the wind tunnel.





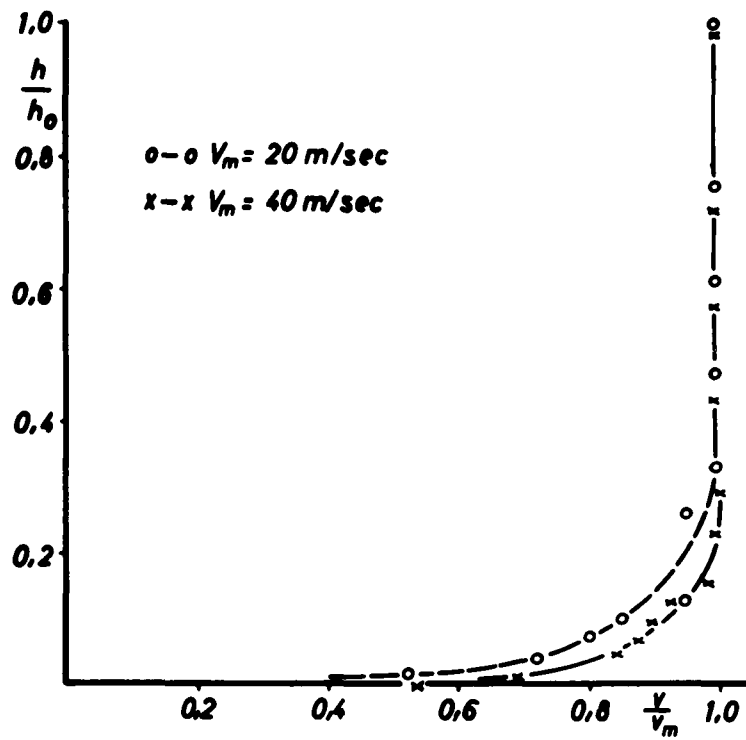


Fig.36 Flow velocity profiles.  $V_m$  center velocity,  $h/h_0$  wall distance.

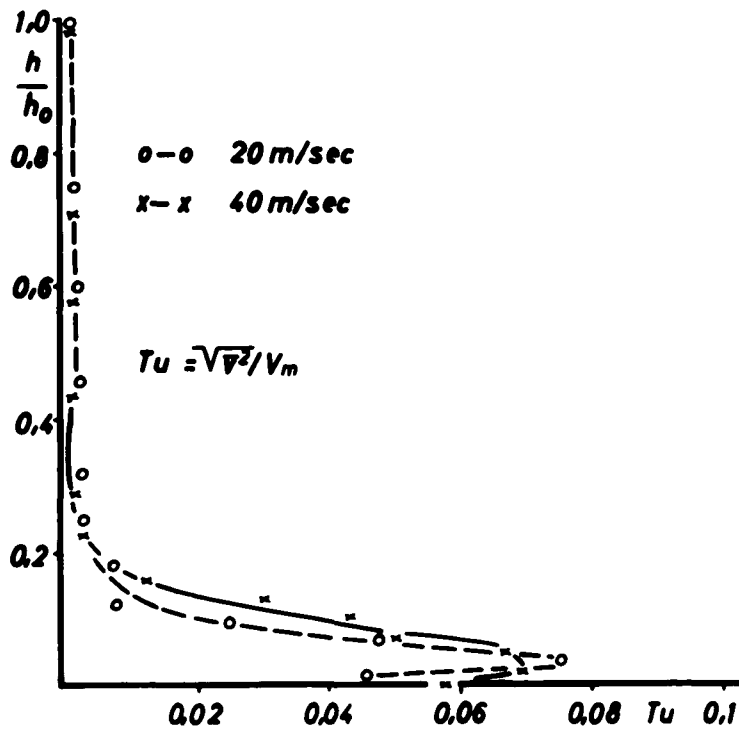


Fig.37 Turbulence profiles.

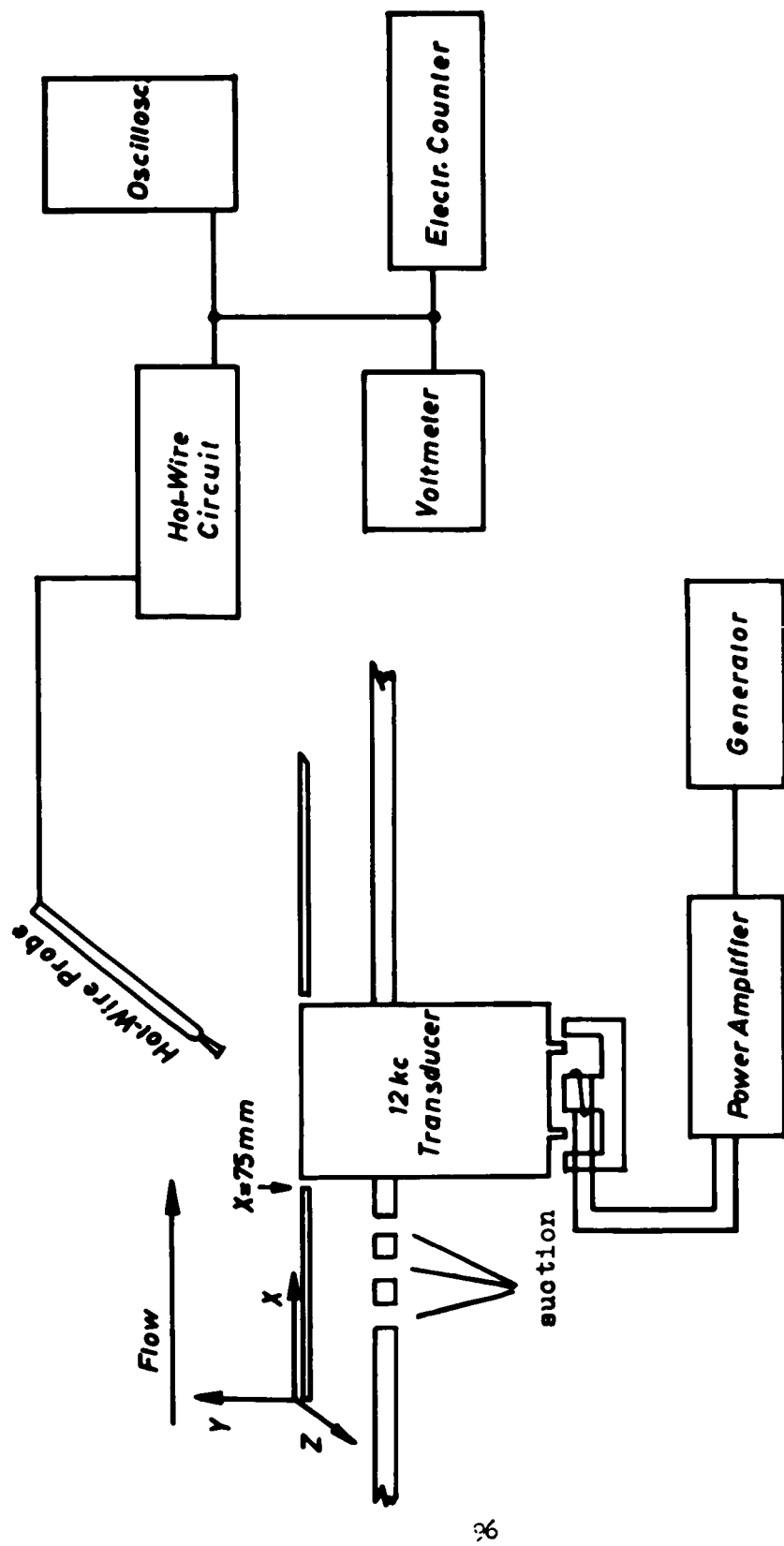


Fig. 38 Experimental set-up.

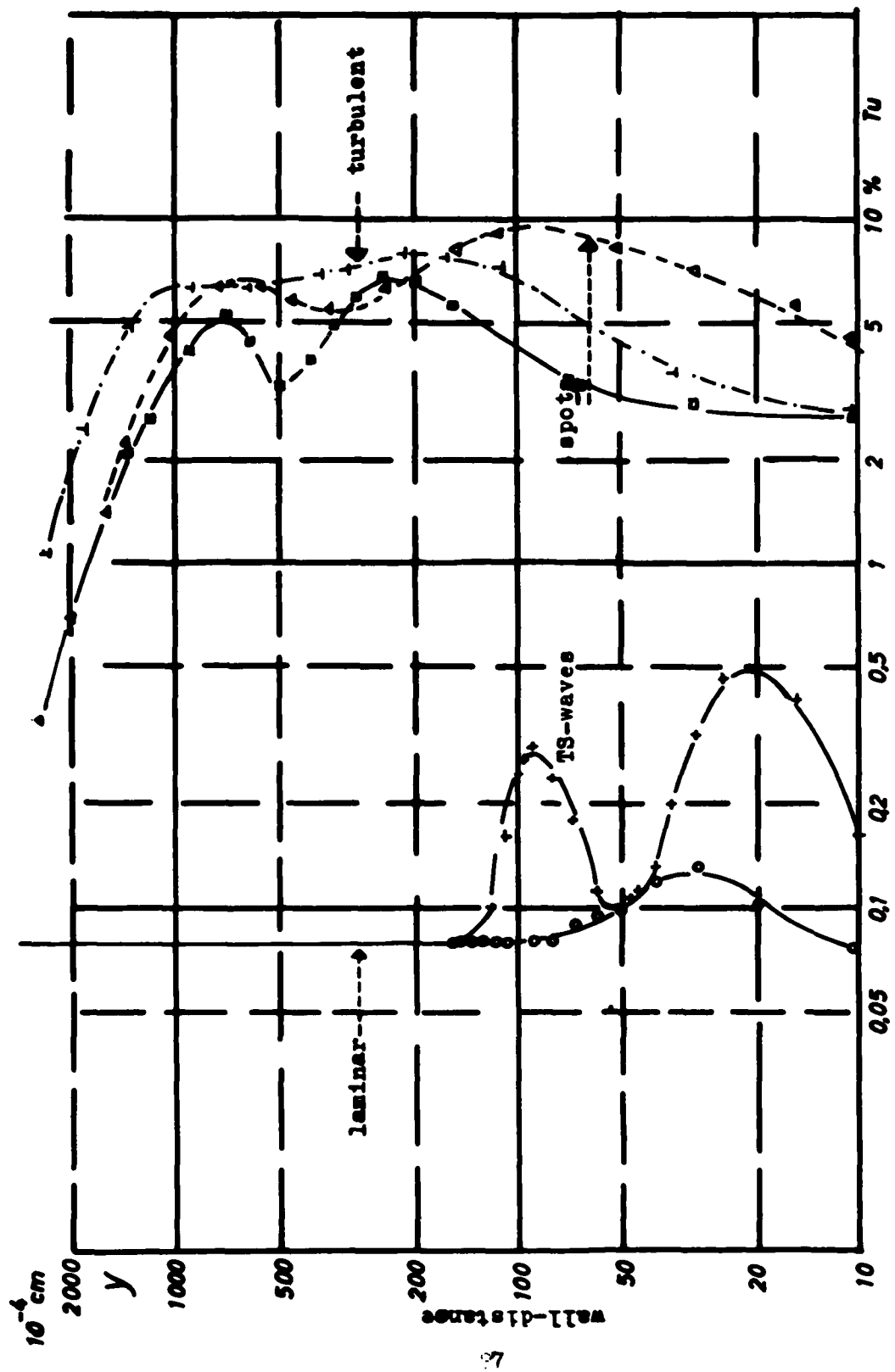
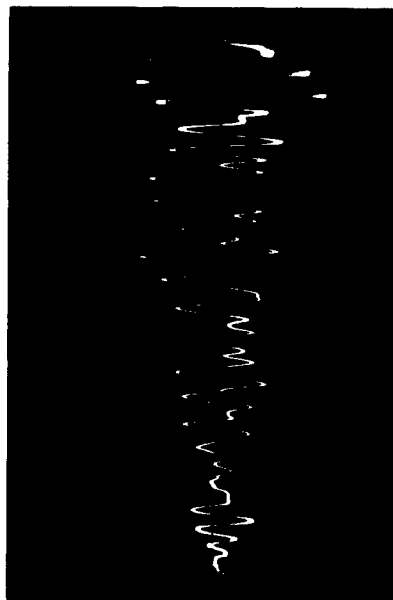


Fig.39 Profiles of the flow distortions in a double-logarithmic scale.



**Fig. 40** Amplitude variation of the TSW when the transducer is switched on at  $t_1$  or switched off at  $t_2$ .

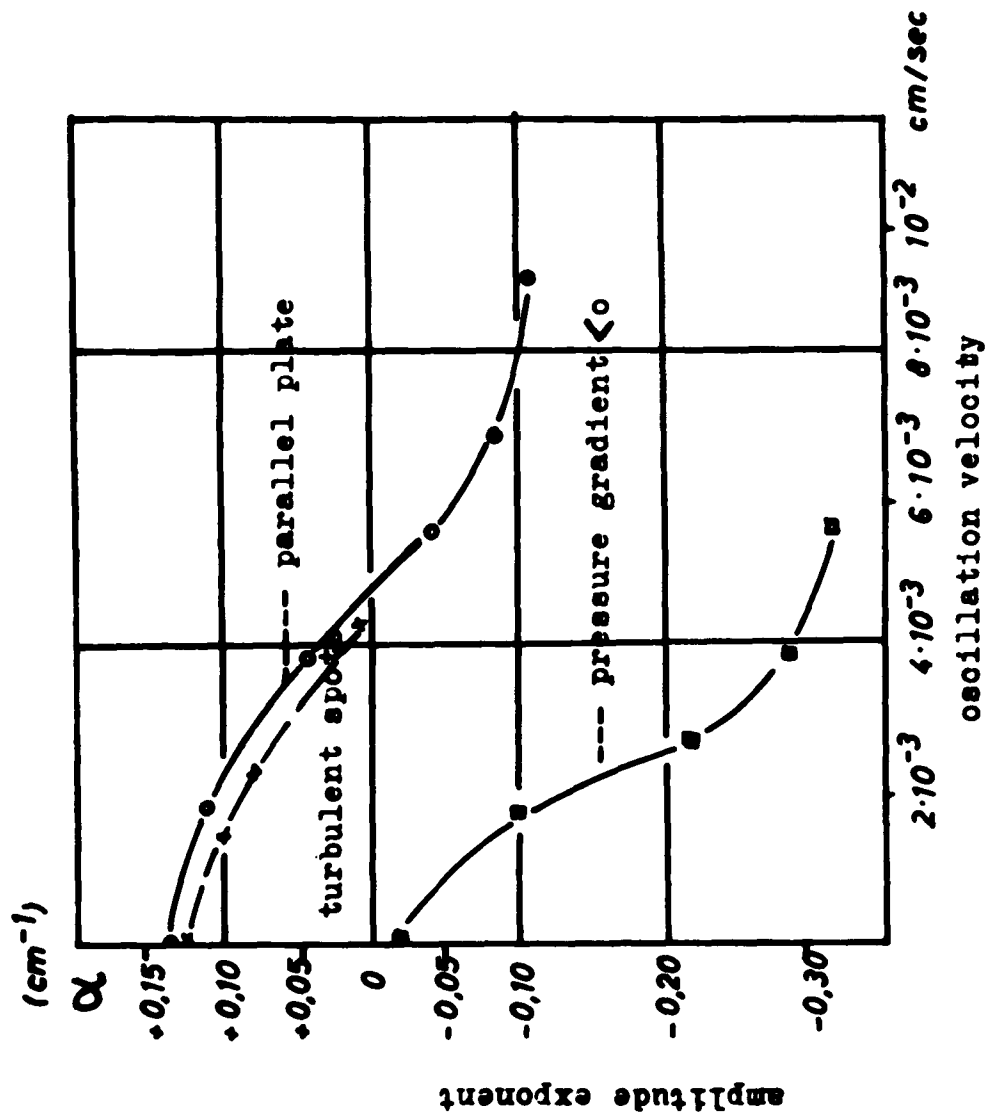


Fig 41 Amplitude exponent  $\alpha$  as a function of the oscillation velocity amplitude.

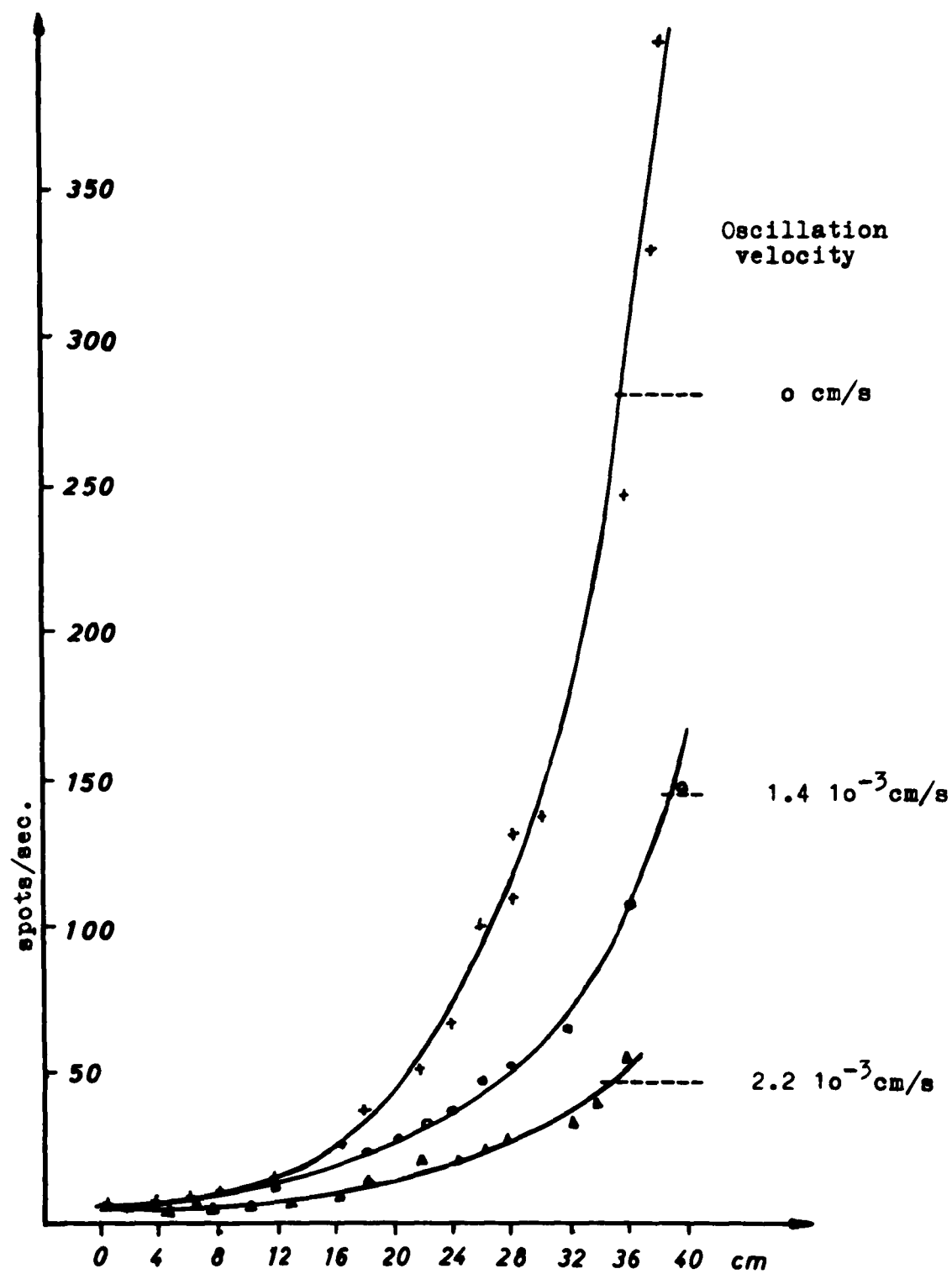
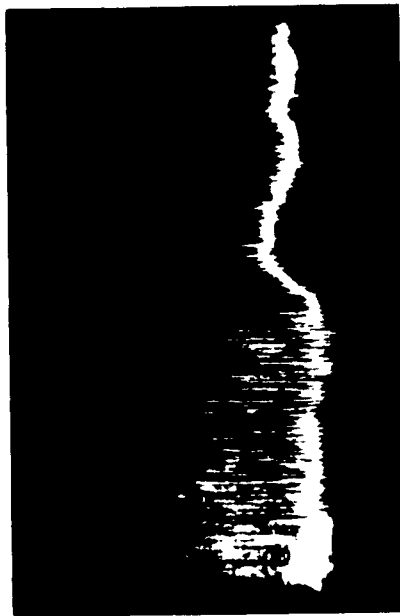


Fig.42 Occurrence frequency of the turbulent spots as a function of oscillation velocity amplitude and of position.



spot frequency  $< 400/s$



spot frequency  $> 400/s$

Fig.43 Change of the spot frequency when the transducer is switched on.

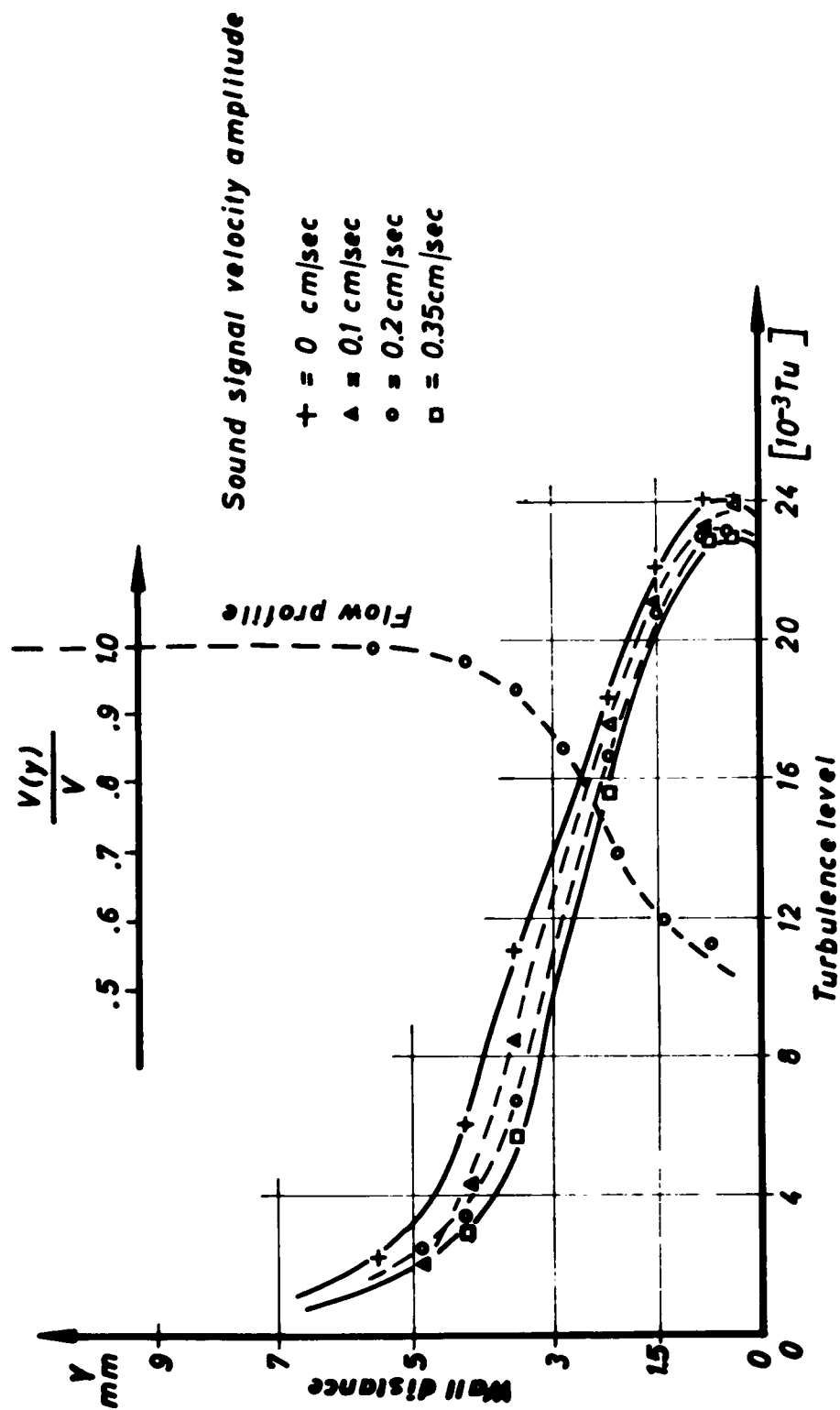


Fig. 44 Profiles of mean flow velocity and of turbulence level for several signal amplitudes.



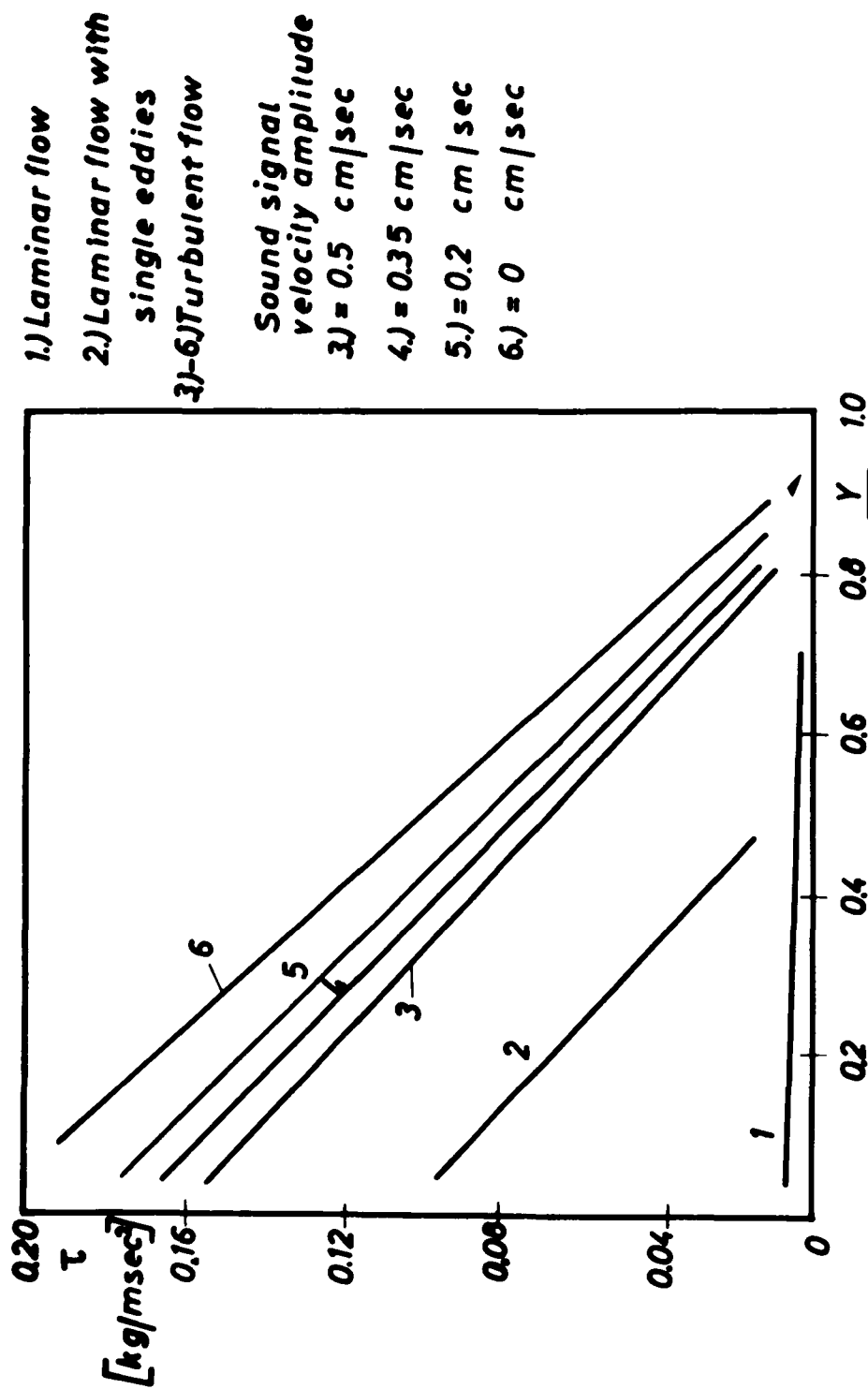


FIG. 45 Shear stress vs. normalized wall distance for the cases of laminar flow, of turbulent spots and of fully developed turbulence and its change by signal irradiation.

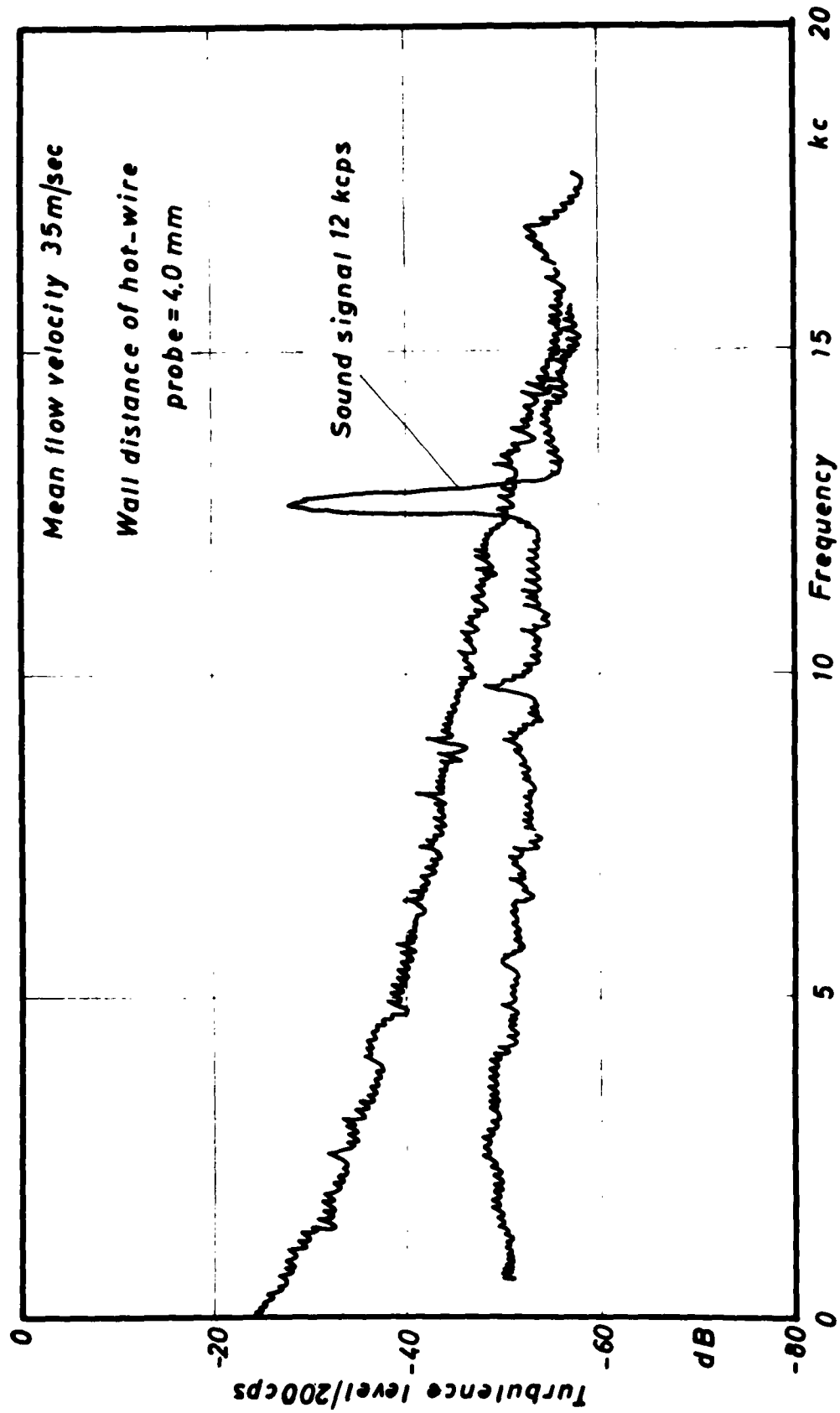


Fig.46 Spectrum of fully developed turbulence with and without signal irradiation.

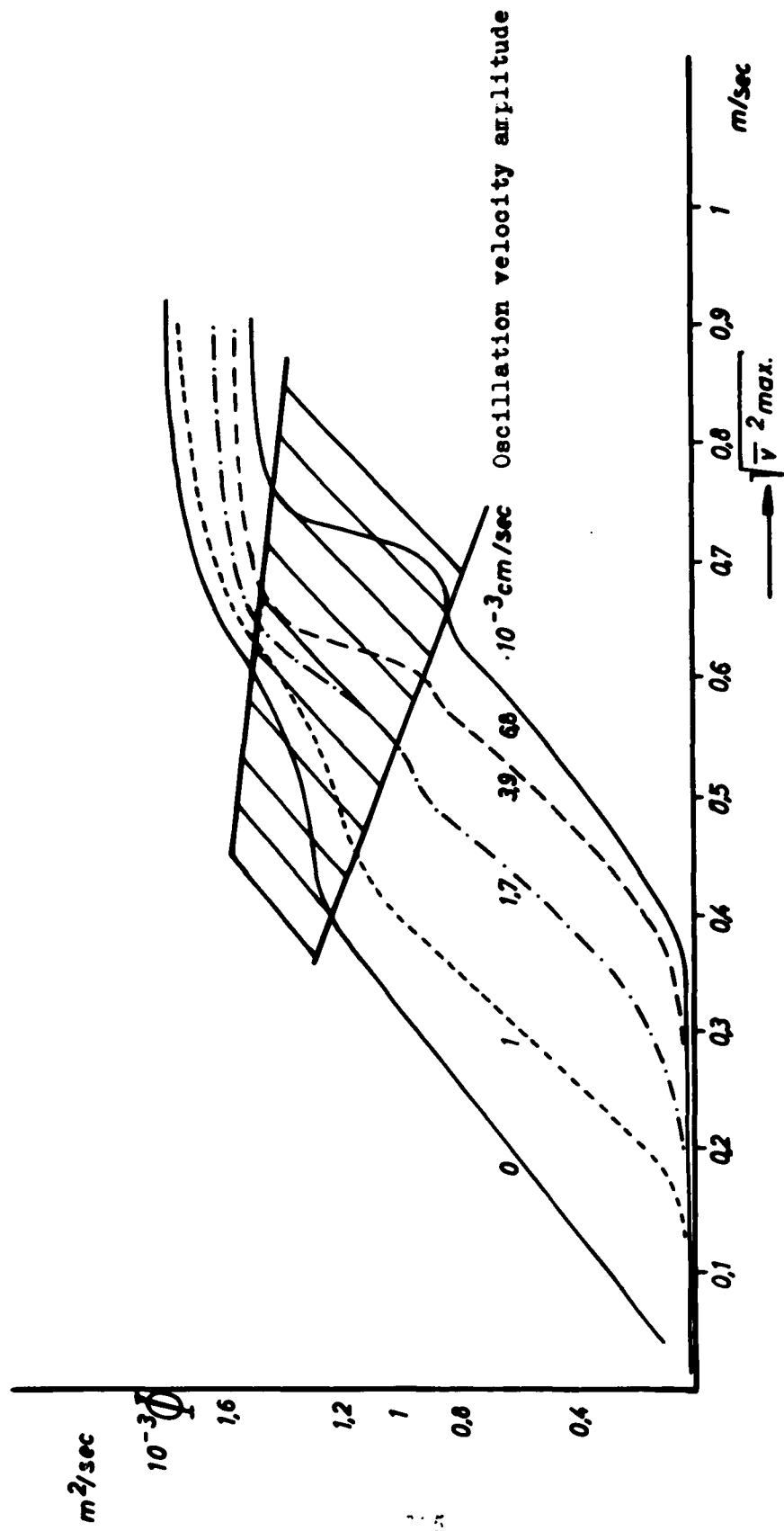


Fig. 4.7 Distortion level as a function of the initial distortion.

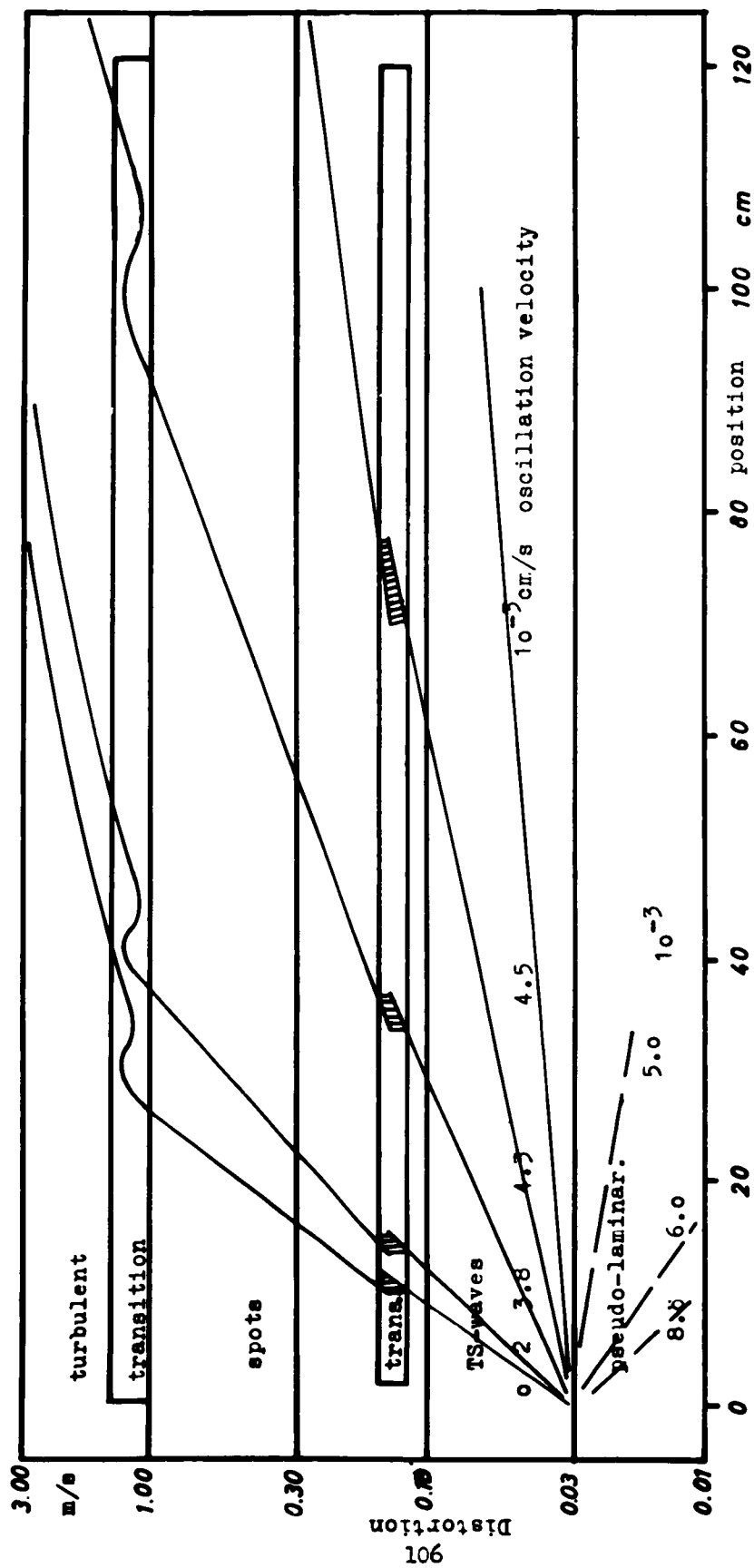


Fig.48 Spatial development of the boundary layer with sound superposition.

<p>Aerospace Medical Division, 6570th Aerospace Medical Research Laboratories, Wright-Patterson AFB, Ohio Rpt. No. AMRL-TDR-62-140 (III). RESEARCH ON SOUND PROPAGATION IN SOUND- ABSORBENT DUCTS WITH SUPERIMPOSED AIR STREAMS. Final report, Dec 62, vii + 106 pp incl. illus. Unclassified Report</p> <p>This report, Volume III, gives theoretical and experimental results on the interaction between sound and air flow in a duct for the following studies: (1) signal amplification as related to size, shape, and position of periodically spaced Helmholtz resonators mounted in the walls of a duct, (2) extension of flow velocity and signal frequency parameters (as employed in Vols. I and II) for a duct coated with a porous absorber ( over )</p>	<p>UNCLASSIFIED</p> <p>1. Attenuation (wave propagation) 2. Sound transmission (sound and acoustics) 3. Acoustics (sound and acoustics)</p> <p>I. AFSC Project 7231, Task 723104 II. Biomedical Laboratory III. Contract AF 61(052)-112 IV. Physikalisches Institut der Universität Göttingen</p> <p>UNCLASSIFIED</p>	<p>UNCLASSIFIED</p> <p>1. Attenuation (wave propagation) 2. Sound transmission (sound and acoustics) 3. Acoustics (sound and acoustics)</p> <p>I. AFSC Project 7231, Task 723104 II. Biomedical Laboratory III. Contract AF 61(052)-112 IV. Physikalisches Institut der Universität Göttingen</p> <p>UNCLASSIFIED</p>
<p>Aerospace Medical Division, 6570th Aerospace Medical Research Laboratories, Wright-Patterson AFB, Ohio Rpt. No. AMRL-TDR-62-140 (III). RESEARCH ON SOUND PROPAGATION IN SOUND- ABSORBENT DUCTS WITH SUPERIMPOSED AIR STREAMS. Final report, Dec 62, vii + 106 pp incl. illus. Unclassified Report</p> <p>This report, Volume III, gives theoretical and experimental results on the interaction between sound and air flow in a duct for the following studies: (1) signal amplification as related to size, shape, and position of periodically spaced Helmholtz resonators mounted in the walls of a duct, (2) extension of flow velocity and signal frequency parameters (as employed in Vols. I and II) for a duct coated with a porous absorber ( over )</p>	<p>UNCLASSIFIED</p> <p>1. Attenuation (wave propagation) 2. Sound transmission (sound and acoustics) 3. Acoustics (sound and acoustics)</p> <p>I. AFSC Project 7231, Task 723104 II. Biomedical Laboratory III. Contract AF 61(052)-112 IV. Physikalisches Institut der Universität Göttingen</p> <p>UNCLASSIFIED</p>	<p>UNCLASSIFIED</p> <p>1. Attenuation (wave propagation) 2. Sound transmission (sound and acoustics) 3. Acoustics (sound and acoustics)</p> <p>I. AFSC Project 7231, Task 723104 II. Biomedical Laboratory III. Contract AF 61(052)-112 IV. Physikalisches Institut der Universität Göttingen</p> <p>UNCLASSIFIED</p>